Fall 2014

High-throughput identification and characterization of novel inhibitors of Regulator of G Protein Signaling 17 as pretherapeutic leads for the treatment of lung and prostate cancers

Duncan Ian Mackie
University of Iowa

HIGH-THROUGHPUT IDENTIFICATION AND CHARACTERIZATION OF NOVEL INHIBITORS OF REGULATOR OF G PROTEIN SIGNALING 17 AS PRETHERAPEUTIC LEADS FOR THE TREATMENT OF LUNG AND PROSTATE CANCERS

by

Duncan Ian Mackie

A thesis submitted in partial fulfillment
of the requirements for the Doctor of
Philosophy degree in Pharmacy (Medicinal and Natural Products Chemistry)
in the Graduate College of
The University of Iowa

December 2014

Thesis Supervisor: Associate Professor David L. Roman

Graduate College
The University of Iowa
Iowa City, Iowa

CERTIFICATE OF APPROVAL

_____

PH.D. THESIS

_____

This is to certify that the Ph.D. thesis of

Duncan Ian Mackie

has been approved by the Examining Committee
for the thesis requirement for the Doctor of Philosophy
degree in Pharmacy (Medicinal and Natural Products Chemistry) at the December 2014 graduation.

Thesis Committee: _____
David L. Roman, Thesis Supervisor

_____
Robert J. Kerns

_____
Michael W. Duffel

_____
Michael A. Spies

_____
Michael D. Henry

I would like to dedication my thesis to my family, Mom, Dad, Felicia, Cara, Vern, Shaun and Nicole, as well as those grandparents who could not be with us for this occasion. Thank you for your love and support through the years

ACKNOWLEDGMENTS

None of this work would have been possible without the instruction and guidance of Dr. David L. Roman. My sincerest thanks go to him for accepting me into his lab and helping me develop into a confident and independent scientist. I would also like to thank the members of my committee: Dr. Robert Kerns, Dr. Michael Duffel, Dr. M. Ashley Spies, and Dr. Michael Henry. The guidance and assistance provided from the rest of the MNPC faculty has also not gone unappreciated; thank you to Dr. Horacio Olivo, Dr. Zhendong Jin, Dr. Meng Wu, Ms. Kelly Walsh, Ms. Patricia Sadowski, and Ms. Kellie Northup. Finally, special thanks go to Dr. Kevin Rice, who was instrumental in my choosing The University of Iowa and the MNPC program.

I owe a debt of gratitude to our collaborators, Dr. Heather Bartlett, Dr. Elesa Wedemeyer, Dr. Dawn E. Quelle, Dr. Ernesto Fuentes, and Mr. Xu Liu. Their contributions too many of my research projects and guidance have been greatly appreciated.

I would also like to thank all of the members of the Roman lab for supporting me when research was not going well and for celebrating with me when it was. A special thanks to Tyrell Towle, Benjamin Williamson, Ioana Craciun, and Edwin Squirewell for supporting me during graduate school and for their constant encouragement to help me to always be my best.

Finally, I would never have made it this far without the love and support of my family; mom, dad, Felicia, Care, Vern and Nicole. I would also like to thank Justine Delgado for her support during my graduate research and for always listening. Thank you to everyone for always pushing me to achieve my full potential and for your undying support.

ABSTRACT

G-Protein Coupled Receptors are one of the most important targets in drug development, making up over 60% of drug targets. Recent studies have implicated a role of Regulator of G-Protein Signaling (RGS) proteins in the development and progression of pathologies, including some cancers. RGS17, the most-recently identified family member of the RZ family of RGS proteins, has been implicated in the growth, proliferation, metastasis and migration of prostate tumors as well as small-cell and non-small cell lung cancers. In neoplastic tumor tissues RGS17 is up-regulated 13 fold over patient-matched normal tissues in prostate cancer. Studies have shown that RGS17 RNAi knockdown inhibits colony formation and decreases tumorigenesis in nude mice. Based on these findings, this thesis explores the research undertaken to develop small molecule inhibitors of the RGS17: $G\alpha_o$ protein: protein interaction.

In this thesis, we implemented AlphaScreen® technology to develop a high-throughput screening method for interrogating small molecule libraries for inhibitors of RGS17. Chapter 3 focuses on the initial results of the AlphaScreen® in 384-well format. The screen utilizes a measurement of the Gα: RGS17 protein: protein interaction (PPI) and with an excellent Z-score exceeding 0.73, a signal to noise ratio >70 and a screening time of 1,100 compounds per hour. Chapter 3 presents the development, validation and initial high-throughput screening for inhibitors of Gα: RGS17 interaction as well as preliminary characterization of the RL series of hits. In this pilot screen the NCI Diversity Set II was interrogated, yielding 35 initial hits of which 16 were confirmed after screening against controls. The 16 compounds exhibited IC50 <10 μM in dose-response experiments for inhibiting the Gα: RGS17 interaction. Four exhibited IC50 values <6 μM while inhibiting the Gα: RGS17 interaction >50% when compared to a biotinylated GST control (TrueHits). Compounds RL-1 and RL-2 were confirmed by flow cytometry protein interaction assay (FCPIA) while RL-3 and RL-4 were unable to

disrupt this PPI in FCPIA. All four compounds were tested using the differential scanning fluorimetry (DSF) method, which is based on energetic coupling between ligand binding and protein unfolding, and found compounds RL-1 to RL-4 all slightly increased protein stability upon ligand binding.

Chapter 4 focuses on the miniaturization and optimization of AlphaScreen® to a 1536-well format and screening of the MicroSource SPECTRUM and NDL3000 small molecule libraries. This increased throughput 11-fold and decreased our working volumes from 45 μL to 10 μL, which reduced reagent cost. After optimization, we retained an excellent Z-factor ≥0.65 with S/N >28 and increased the screening rate to more than 12,000 compounds per hour. In this format, the initial screening of the SPECTRUM and NDL3000 libraries was completed and filtered the initial hits by counter screening and PAINs filtering as well as developing four powerful orthogonal assays for the characterization of potential lead molecules.

Chapter 6 focuses on the future directions, which include screening the in-house 50,000 compound library in the University of Iowa HTS Core facility as well as the development of cell based assays to determine the activity of these leads in the cellular milieu. These screens are the first step to developing novel pharmacophores for further optimization of structure with the focus on RGS17 activity in enzymatic, whole cell, xenograft and whole animal models as well as providing new avenues for the development of anticancer therapies.

Table of Contents

LIST OF TABLES

LIST OF FIGURES

LIST OF ABBREVIATIONS

AC Adenyl Cyclase

AD Adenocarcinoma

AMF A mixture of $AlCl_3$, $MgCl_2$, NaF

AMP Adenosine Monophosphate

ASB AlphaScreen Buffer

ATP Adenosine Triphosphate

AVP Vasopressin

CPS Counts Per Second

CREB cAMP response element-binding protein

DAG Diacylglycerol

DEP Disheveled/Egl-10/Pleckstrin

DH Dbl Homology

DMR Dynamic Mass Redistribution

DMSO Dimethyl sulfoxide

DRC Dose Response Curve

DS Developing Solution

DSF Differential Scanning Fluorimetry

DTT Dithiothreitol

FCPIA Flow Cytometry Protein Interaction Assay

FPLC Fast Protein Liquid Chromatography

GAIP Gα-interacting protein

GAP GTPase-Activating Proteins

GDP Guanosine Diphosphate

GEF Guanine Nucleotide-Exchange Factor

GGL G-Gamma-Like Domain

GoLoco $G\alpha_{i/o}$-Loco Intraction Domain

GPCR G Protein Coupled Receptor

GST Glutatione S-Transferase

GTP Guanosine Triphosphate

GWAS Genome-Wide Association Study

HSP90 Heat Shock Protein 90

HTS High Throughput Screening

IC_{50} Half Maximal Inhibitory Concentration

IP_3 Inositol Trisphosphate

ITC Isothermal Titration Calorimetry

K_d Dissociation Constant

LCC Large Cell Carcinoma

LCNC Large Cell Neuroendocrine

LH Luteinizing Hormone

MGB Malachite Green Buffer

MTT 3-(4,5-dimethylthiazol-2-yl)-2,5-diphenyltetrazolium bromide

NAD(P)H Nicotinamide Adenine Dinucleotide Phosphate

NCI National Cancer Institute

NEM N-Ethylmaleimide

PDZ PSD-95/Dlg/ZO-1 Domain

PH Pleckstrin Homology Domain

PIP_2 Phosphatidylinositol 4,5-bisphosphate

PKA Protein Kinase A

ppi protein: protein interaction

PSA Prostate-Specific Antigen

PTB Phosphotyrosine Binding Domain

qRT-PCR Quantitative Reverse Transcription Polymerase Chain Reaction

R7BP R7 Family-Binding Protein

RBD Ras-binding Domain

RGS Regulator of G protein Signaling

RH RGS Homology Domain

ROS Reactive Oxygen Species

RWG Resonant Waveguide Grating

SCC Squamous Cell Carcinoma

SH2 Src Homology 2 Domain

SPR Surface Plasmon Resonance

Sst2 Yeast RGS protein

STAT Signal Transducer and Activator of Transcription

T4 Thyroxine

TCEP Tris-(2-Carboxyethyl)phosphine

TM Trans membrane

TR-FRET Time-Resolved Forester Resonance Energy Transfer

TSH Thyroid-Stimulating Hormone

β2AR Beta-2 Adrenergic Receptor

CHAPTER I: INTRODUCTION: GPCRS AND THE ROLE OF RGS17 IN THE DEVELOPMENT AND PROGRESSION OF METASTATIC LUNG AND PROSTATE CANCERS

Abstract

Ligands for G-protein-coupled receptors (GPCRs) represent approximately 50% of currently marketed drugs. Regulators of G Protein Signaling (RGS) proteins modulate heterotrimeric G proteins and, thus, GPCR signaling, by accelerating the intrinsic GTPase activity of the Gα subunit. Given the prevalence of GPCR targeted therapeutics and the role RGS proteins play in G protein signaling, some RGS proteins are emerging as targets in their own right. One such RGS protein is RGS17. Increased RGS17 expression in some prostate and lung cancers has been demonstrated to support cancer progression, while reduced expression of RGS17 can lead to development of chemotherapeutic resistance in ovarian cancer. High-throughput screening is a powerful tool for lead compound identification, and utilization of high-throughput technologies has led to the discovery of several RGS inhibitors, thus far. As screening technologies advance, the identification of novel lead compounds and the subsequent development of targeted therapeutics appears promising.

Introduction

Every cell maintains homeostasis and communicates with the surrounding environment. This often occurs through complex signaling pathways involving specific protein: protein interactions (ppi). These signaling cascades are often initiated by membrane bound receptors. One of the most important classes of these cellular receptors are the GPCRs. GPCRs are delimited by seven trans-membrane helices, an N-terminus extending into the extracellular environment, and a C-terminus in the intracellular milieu. Members of this family include receptors for many hormones, neurotransmitters,

chemokines, and calcium ions [1]. Since their discovery, GPCRs have become the target for 50-60% of all currently marketed therapeutics [2].

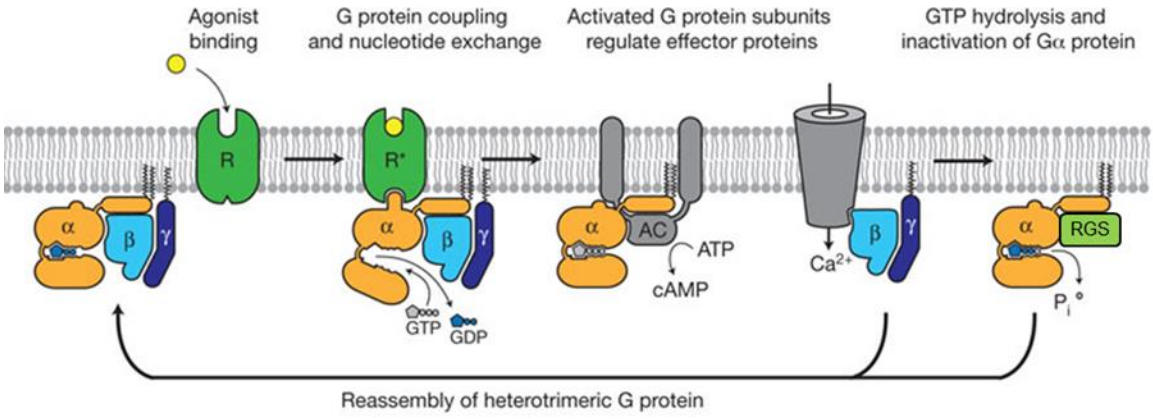

Figure 1. Extracellular agonist binding to the β_2AR leads to conformational rearrangements of the cytoplasmic ends of transmembrane segments that enable the G protein heterotrimer (α, β, and γ) to bind the receptor. GDP is released from the α subunit upon formation of GPCR–G protein complex. The GTP binds to the nucleotide-free α subunit resulting in dissociation of α and βγ subunits from the receptor. The subunits regulate their respective effector proteins (example: adenylyl cyclase (AC) and Ca^{2+} channels). The G protein heterotrimer reassembles from α and βγ subunits following hydrolysis of GTP to GDP in the Gα subunit which is regulated by the family of RGS proteins (Figure adapted from SG Rasmussen et al. Nature. 2011 Jul 19;477(7366):549-55) [3].

GPCRs couple to heterotrimeric G proteins that consist of a Gα subunit and a βγ heterodimer [4]. The Gα subunit of the G protein binds guanosine-5'-diphosphate (GDP) in the basal, inactive state. Activation of the GPCR by an extracellular ligand initiates a series of coupled conformational changes, first in the GPCR and then the Gα subunit, releasing GDP and allowing GTP to bind—causing the Gα and βγ heterodimer to dissociate and signal through their respective intracellular effectors (Figure 1) [5]. Hydrolysis of the bound GTP to GDP by the intrinsic GTPase activity of the Gα subunit induces the re-association of the α and βγ subunits, terminating the signaling cascade [6].

RGS proteins temporally regulate these signaling events, serving as GTPase accelerating proteins (GAPs)—increasing the intrinsic rate of hydrolysis of G proteins and acting to terminate GPCR signaling much more rapidly. RGS proteins are a diverse protein family with unique tissue distributions for each member [7]. The first of this unique family of proteins was discovered in yeast genetic studies of GPCR signaling and later members identified by using sequence homology searching within a conserved 120-amino acid domain, known as the RGS Homology (RH) domain or RGS box identified from the founding member [8-11]. Since these early discoveries ~30 members of the RGS superfamily have been characterized. Many RGS proteins contain multiple functional motifs and domains by which they mediate cross talk between GPCR-dependent and –independent signaling pathways [12]. These accessory domains further divide RGS proteins into sub-families.

Studies of GPCR signaling pathways have implicated these signaling cascades in multiple disease states that range from cancer and heart disease to immunological and neurological pathologies [13-18]. Furthermore, successful targeting of GPCRs is still just a small fraction of the possible therapeutic potential of the GPCR pathway rich in other targets. Because of their ability to regulate multiple signaling events in a temporally and tissue specific manner, RGS proteins present a unique opportunity for drug discovery. Targeting RGS ppis that govern select signals downstream of GPCRs is challenging but expands the number of potential targets and allows exploitation of the discrete roles that specific interactions may play within cellular signaling cascades [6].

Discovery of the GPCR signaling pathway

The discovery of G protein signaling began in the early 1970s when Dr. Alfred G. Gilman made the first observation of the norepinephrine stimulated increase of cyclic AMP levels in developing mouse brain cell cultures [19]. It would take nearly 10 years for his research team to purify and characterize the regulatory component of adenylate

cyclase [20-21]. The regulatory component of adenylate cyclase, which was purified, contains three putative subunits with molecular weights of 52,000, 45,000, and 35,000. This was the first identification of the guanosine nucleotide-binding proteins, later called G proteins. They consist of the Gα and the tightly associated Gβγ subunits. This discovery opened the door for the discovery and characterization of several sub-families of G proteins, which fall into one of four different classes, $G\alpha_s$ (G stimulatory), $G\alpha_i$ (G inhibitory), $G\alpha_o$ (G other), $G\alpha_{q/11}$, and $G\alpha_{12/13}$. These observed G proteins possessed a major discrepancy when comparing *in vivo* GTPase activity with their *in vitro* GTPase rates. It would take almost another 10 years before the next component of the signaling pathway would be revealed.

In 1988, Dietzel and Kurjan [22-23], used the yeast two-hybrid system to identify and clone the *SST2* gene. This led to the model for pheromone desensitization by the regulation of the yeast G protein signaling cascade. Sst2 is the first regulator of G protein signaling discovered and paved the way for the discovery of homologs in humans. In 1995, Farquhar and colleagues identified the founding member of the human homolog of the RGS proteins using the yeast two-hybrid system [24]. They named this new protein GAIP (G Alpha Interacting Protein), later named RGS19, because it specifically interacted with the heterotrimeric GTP binding protein $G\alpha_{i3}$. The discovery of the RGS proteins explained the differences between observed rates of intrinsic GTP hydrolysis by Gα subunits *in vitro* and *in vivo*. Further research has elucidated a very complex and diverse signaling cascade that the scientific community is still investigating to this day.

G Protein diversity and complexity of signaling

The term “G protein” can refer to two distinct families of proteins. The first family is the heterotrimeric G proteins. These are sometimes referred to as the "large" G proteins and were previously mentioned. These heterotrimeric G proteins are activated by GPCRs and are comprised of three subunits known as alpha (α), beta (β), and gamma (γ).

There are also "small" G proteins (20-25kDa) that belong to the Ras superfamily of small GTPases [25-26]. These proteins are homologous to the alpha (α) subunit found in heterotrimers, and are in fact monomeric. The focus of my research is on the heterotrimeric G proteins and their regulation by the family of proteins, Regulators of G protein Signaling (RGS) proteins. The heterotrimeric G proteins have a complex and diverse signaling cascade that is regulated by the GPCR, RGS and arrestin proteins, which all serve to modulate the strength and duration of the signaling cascade as well as which downstream effectors are activated/inhibited.

The $G\alpha_s$ protein activates the cAMP-dependent pathway by stimulating the production of cAMP from ATP [27]. This is accomplished by direct stimulation of the membrane-associated enzyme adenylate cyclase. cAMP acts as a second messenger that activates protein kinase A (PKA) [28-30]. PKA can then phosphorylate a myriad of downstream targets. The cAMP dependent pathway is used as a signal transduction pathway for many hormones. A few examples of these $G\alpha_s$ stimulated hormones include thyroid-stimulating hormone (TSH or hTSH), a hormone that stimulates the thyroid gland to produce thyroxine (T4) [31-32], luteinizing hormone (LH), which stimulates follicular maturation and ovulation in women and stimulates testosterone production and spermatogenesis in men, and glucagon, a peptide hormone, produced by alpha cells of the pancreas, that raises the concentration of glucose in the bloodstream [33-35].

In comparison, the $G\alpha_{i/o}$ proteins act in the opposite fashion as the $G\alpha_s$ protein, as $G\alpha_{i/o}$ activation leads to inhibition of adenylate cyclase and a decrease in the concentration of the second messenger cAMP [27]. $G\alpha_{i/o}$ proteins play major roles in signaling by coupling to a multitude of receptors such as the acetylcholine M2 & M4 receptors [36], adrenergic α2A, α2B, & α2C receptors [37-38], cannabinoid receptors CB1 & CB2 [39-40], dopamine D2, D3 & D4 [41] and the metabotropic glutamate mGluR2, mGluR3, mGluR4, mGluR6, mGluR7, & mGluR8 receptors [42-43], just to name a few.

Next, $G\alpha_{q/11}$ proteins stimulate membrane-bound phospholipase C beta, which then cleaves phosphatidylinositol 4,5-bisphosphate (PIP_2) (a minor membrane phosphoinositol) into two second messengers, inositol trisphosphate (IP_3) and diacylglycerol (DAG) [44-46]. The inositol phospholipid dependent pathway is used as a signal transduction pathway for many hormones including vasopressin (AVP) and angiotensin [47-49]. AVP is a hormone that is found in most mammals. Its two primary functions are to retain water in the body and to constrict blood vessels [50]. Angiotensin is a peptide hormone that causes vasoconstriction and a subsequent increase in blood pressure [51]. It is part of the renin-angiotensin system, which is a major target for drugs that lower blood pressure.

Finally, the $G\alpha_{12/13}$ protein is involved in Rho family GTPase signaling and control cell cytoskeleton remodeling, thus regulating cell migration [52]. $G\alpha_{13}$ is also essential for receptor tyrosine kinase-induced migration of fibroblast and endothelial cells [53]. These pathways have become of greater importance for the drug discovery community for the possibility of blocking cell migration and treating metastatic cancers.

G proteins are controlled by the GPCRs to which they couple but they are further regulated by the RGS family of proteins. These RGS proteins are the regulatory protein of interest to my work. These proteins are multi-functional, GTPase-accelerating proteins that promote GTP hydrolysis by the alpha subunit of heterotrimeric G proteins; thereby inactivating the G protein and rapidly switching off G protein-coupled receptor signaling pathways [54].

RGS proteins: families and structure

Since their discovery in the mid-1990s, the RGS superfamily of proteins has grown to contain eight subfamilies. These subfamilies all contain the RGS homology (RH) domain but are classified based on a diverse array of accessory domains. The classical RGS proteins fall into one of four groups: A/RZ, B/R4, C/R7, and D/R12

(Figure 2) [55]. These four subfamilies differ drastically in accessory domains present while still maintaining GAP-competent RH domains. The B (or R4) family is the largest; this group consists of nine RGS proteins that feature only the RH domain with an N-terminal amphipathic alpha-helical region [56]. The C (or R7) subfamily has four members that are larger due to the presence of N-terminal disheveled/Egl-10/pleckstrin (DEP) and G-protein gamma subunit like (GGL) domains [57-61]. These two accessory domains contribute to membrane localization by binding R7 binding proteins and stability through binding the Gβ protein, Gβ5, respectively [57-60, 62]. The D (or R12) subfamily of RGS proteins contains the largest classical RGS proteins discovered to date. These large proteins contain multiple accessory domains like the PSD-95/Dlg/ZO-1 (PDZ), phosphotyrosine-binding (PTB), Ras-binding domain (RBD) and the $G\alpha_{i/o}$-Loco interaction (GoLoco) domains [63-65]. Each of these domains contributes to the multiple functions and downstream signaling interactions of the R12 subfamily of RGS proteins. The A (or RZ) subfamily, made up of four RGS proteins, are classified by an N-terminal cysteine-rich cluster or "cysteine string" (Cys) [56]. This motif is believed to be heavily palmitoylated, leading to tight membrane association [66].

The founding member of the RZ subfamily is G Alpha-Interacting Protein (GAIP), known as RGS19. RGS19 was the first mammalian RGS protein identified via the yeast two-hybrid system, with $G\alpha_{i3}$ serving as "bait" [24]. Additionally, two more members of this family (RGS17/RGSZ2 and RGS20/RGSZ1) were isolated by yeast two-hybrid screens using $G\alpha_z$ and $G\alpha_o$ as bait [67-68]. RGSZ2 (RGS17) was discovered using $G\alpha_o$ as bait in a screen of chick dorsal root ganglion neuron cDNA [68]. The last member of the RZ family is Ret-RGS, which is a splice variant of RGS20 and was originally discovered as a GAP for transducin ($G\alpha_t$) in the retina [69].

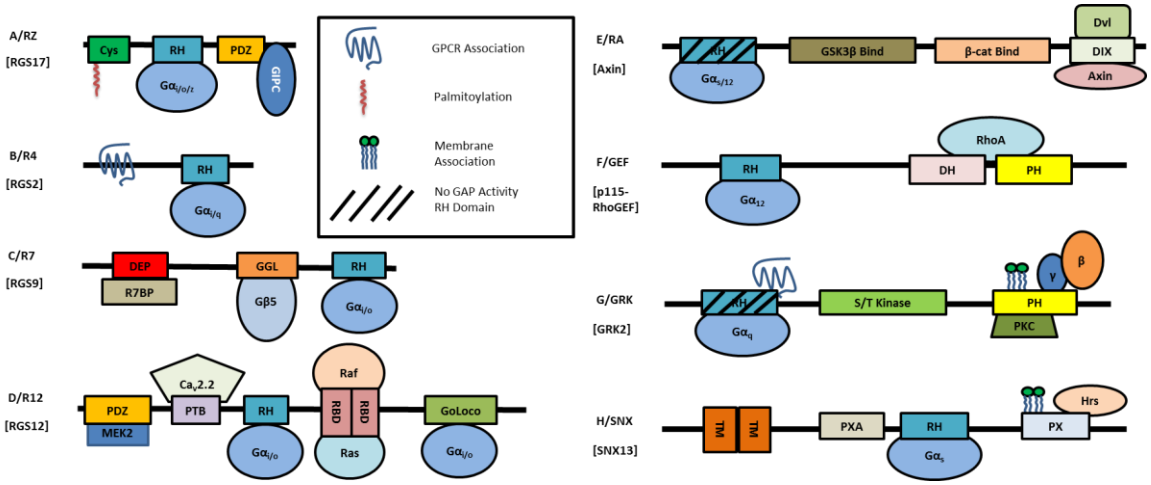

Figure 2. RGS subfamilies and common interacting proteins. RGS proteins are divided into eight subfamilies based on RGS domain homology and accessory domains as well as domains protein interactions and intracellular localization. The first four groups are part of the canonical RGS proteins.The A/RZ family contains a poly-Cys sting in the N-terminus that is palmitoylated and directs these RGS proteins to the cellular membrane. Furthermore, the scaffolding protein GIPC binds RGS19 at the C-terminus though its PDZ domain. The B/R4 family contains the simplest RGS proteins with a short N-terminal region that is required for receptor co-localization. C/R7 family members are characterized by Dishevelled/Egl-10/Pleckstrin (DEP) domains, which bind syntaxin-like proteins such as R7 binding protein (R7BP) to mediate intracellular localization, and Gγ-like (GGL) domains which bind Gβ5-subunits. The D/R12 family varies greatly and is home to some of the largest RGS proteins. The second four groups represent the non-canonical RGS protein families. Members of the E/RA family are negative regulators of the Wnt signaling pathway. The F/GEF family RGS proteins are RhoA specific guanine nucleotide exchange factors (GEFs) with canonical Dbl homology (DH) and Pleckstrin homology (PH) domains. The G/GRK family consists of the G-protein coupled receptor kinases, each with an N-terminal RGS domain that binds $G\alpha_q$. The serine/threonine kinase domain (S/T kinase) phosphorylates GPCRs to initiate internalization. Three sorting nexins make up the H/SNX family and are characterized by an RGS domain located between phosphatidylinositol-binding (PX) and PX-associated (PXA) domains. The PXA, PX, and transmembrane domains (TM) mediate membrane association, and binding to hepatocyte growth factor-regulated tyrosine kinase substrate (Hrs) links SNX to the endocytic machinery. (Figure adapted from J. Hurst and SB. Hooks Biochem Pharmacol. 2009 [55])

RGS17, the focus of my research, is conserved between species, the human protein having greater than 90% similarity to rat, chicken, and mouse [70-71]. This similarity increases when comparing the RH domain of RGS17 with other RZ members. More recently it has been hypothesized that the cysteine string undergoes multiple post-translational modifications to regulate subcellular localization.

RGS17's role in cancer

In early 2009, RGS17, through microarray and gene expression analysis, was determined to be up-regulated in 80% of lung tumors, and also up-regulated in prostate tumors [72]. This finding was not surprising as other RGS proteins had recently been discovered as either being up or down regulated in cancer diseases states [55] (Table 1). In the work by James and colleagues, it was confirmed through the knockdown and overexpression of RGS17 in tumor cells, RGS17 confers a proliferative phenotype and is required for the maintenance of the proliferative potential of tumor cells [72-73]. The researchers showed through exon microarray analysis of four published data sets representing 161 lung tumors that RGS17 was up-regulated in oncogenic lung tissues when compared to patient matched normal tissues [72]. Furthermore, one published data set was examined that represented 13 prostate tumors and 6 controls. In this data set, RGS17 displayed increased expression in tumors compared with normal tissues. RGS17 transcript was increased in 80% of lung tumors by an average of 8.3-fold ($P = 1.36x10^{-9}$) over matched normal lung tissue and was increased in all of 5 prostate tumors tested by an average of 7.5-fold ($P < 0.02$) [72].

Table 1. RGS proteins are emerging as a family of proteins that are linked to the initiation and progression of cancer.

Family A/RZ	
RGS17/RGSZ2	↑ in prostate cancer [72-73]; ↑ in lung cancer [72-73]
RGS19/GAIP	↑ in ovarian cancer [15]; regulates wnt/β-catenin signaling [74]; binding partner GIPC down-regulated in primary kidney tumors, colorectal tumors, gastric cancer, and prostate cancer [75]
RGS20/RGSZ1	↑ in melanoma [76]
Family B/R4	
RGS1	↑ in melanoma [14]; ↑ in head and neck squamous cell carcinoma [77]; ↑ in adult T-cell leukemia [78]; ↑ in renal cell carcinoma [13]; ↑ in ovarian cancer [13]; ↑ in cervical cancer [79]; ↑ in mantle cell lymphoma [80]
RGS2	↓ in ovarian cancer [15]; ↑ in breast cancer [81]; ↑ in fibrolamellar carcinoma [82]; ↓ in prostate cancer [83]; ↓ in acute myeloid leukemia [84]; ↑ in mantle cell lymphoma [80]
RGS3	↑ in docetaxel resistant breast cancers [85]; ↑ associated with enhanced glioma cell motility [86]; ↑ in soft tissue sarcomas [87]
RGS4	↑ associated with enhanced glioma cell motility [86]; ↑ in thyroid carcinoma [88]; ↓ in ovarian cancer [15]
RGS5	↑ in hepatocellular carcinoma [89]; ↑ in breast cancer, melanoma, multiple myeloma, ovarian cancer, and acute myeloid leukemia [90]; ↑ in fibrolamellar carcinoma [82]
RGS13	↓ in mantle cell lymphoma [91]; ↑ in B- and T-cell lymphoma [92]
RGS16	↑ in pediatric high hyperdiploid acute lymphoblastic leukemias [93]; ↑ in pineal parenchymal tumors [94]; p53 target gene in colorectal cancer [95]
Family C/R7	
RGS6	↑ in ovarian cancer [15]; SNPs associated with bladder cancer risk [96]
RGS11	Increased associated w/ Oxaliplatin resistance in colorectal cancer [97]
Family E/RA	
Axin 1/Axin 2	Mutations associated with gastric cancer [98], renal cell carcinoma [99], intrahepatic cholangiocarcinomas [100], adenoid cystic carcinoma [101], cerebellar medulloblastomas [102], oral squamous cell carcinoma [103]; colorectal cancer [104]; ↓ in colorectal cancer [105]; ↓ in non-small cell lung cancer [106]; ↓ in ovarian endometroid adenocarcinoma [107]; ↓ in breast cancer [108]; ↓in sporadic medulloblastomas [109]

[a]Reports from the literature of changes in RGS transcript expression that have been linked to specific types of cancer. (Table Adapted from J. Hurst amd SB. Hooks Biochem Pharmacol. 2009 [55])

Next, You and colleagues used stable shRNA lentiviral vectors directed toward two different RGS17 target sequences (shRGS-1 and shRGS-2) to knockdown RGS17 expression in tumor cell lines from multiple tissue types, including H1299 and A549 lung tumor cells, HeLa cervical tumor cells, Hct116 colon tumor cells, and DU145 prostate tumor cells [73]. The successful knockdown of RGS17 was confirmed in H1299, Hct116 and DU145 cell lines. This effective knockdown yielded a significant phenotypic change determined by the usage of two different methods. The first method was the 3-(4,5-dimethylthiazol-2-yl)-2,5-diphenyltetrazolium bromide (MTT) assay. This is a colorimetric assay used for assessing cell viability. NAD(P)H-dependent cellular oxidoreductase enzymes are used to reflect the number of viable cells present. The second method used was a clonogenic assay. This is a technique used for studying the survival and proliferation of cells.

Upon successful knockdown of RGS17 in H1299 lung cancer cells, it was discovered that there was a marked reduction in cell viability after 10 days of growth [73]. Further examination of the knockdown of RGS17 in H1299 cells lead to the discovery of a decreased proliferative capacity of these cells, as shown by their inability to form colonies [73]. Similarly, knockdown of RGS17 in cancer cell lines Hct116 (colon carcinoma) and DU145 (prostate carcinoma) also resulted in decreased proliferative rates in both cell lines.

Finally, the *in vivo* significance of the proliferative effects of RGS17 knockdown was further established using an athymic nude mouse tumorigenesis assay [73]. This was completed using an *ex vivo*/*in vivo* approach where mice were injected subcutaneously with H1299 human lung tumor cells stably expressing shRNA directed towards *RGS17*. The knockdown with the shRNAs was conducted in an *ex vivo* manner and then the effects of the knockdown were monitored *in vivo* for tumor growth over a 4 week period. The rate of growth and tumor load was decreased significantly by RGS17 knockdown

[73]. Average tumor weights were reduced from 148 mg to 23 mg ($P = 0.03$), and average tumor volumes were reduced from 385 mm^3 to 47 mm^3 ($P < 0.01$) [73].

These significant reductions in volume and weight led investigators to further elucidate the pathway through which RGS17 is exerting these growth and proliferative effects. This was determined by studying cAMP and cAMP responsive proteins such as cyclic AMP (cAMP) responsive element binding protein (CREB), which has been shown to have oncogenic properties when over activated. James et. al. showed that RGS17 promotes CREB-responsive gene expression, increases cAMP levels, and enhances forskolin mediated cAMP production [72]. Furthermore, inhibition of cAMP-dependent kinase prevents tumor cell proliferation, and proliferation is partially rescued by RGS17 overexpression [72]. These findings confirm that RGS17 in both lung and prostate cancers induces tumor proliferation through the cAMP-PKA-CREB signaling pathway.

CHAPTER II: STATEMENT OF PURPOSE

Cancer is a major public health problem in the United States and many other parts of the world. One in four deaths in the United States is due to cancer. The American Cancer Society estimates that there will be 1,665,540 new cases of invasive cancer expected among men and women in the United States in 2014 [110]. This is the equivalent of more than 4,500 new cancer diagnoses each day. Among men, cancers of the prostate, lung and bronchus, and colorectum will account for about 50% of all newly diagnosed cancers (Table 2). Prostate cancer alone will account for 27% (233,000) of incident cases in men. In women, the 3 most commonly diagnosed types of cancer in 2014 will be breast, lung and bronchus, and colorectum, accounting for one-half of all cases in women [110]. Of that total, lung and bronchus cancer makes up 13% (Table 2). The expected numbers of deaths from cancer in 2014 is estimated to be about 585,720. This corresponds to about 1,600 deaths per day. In cancer related deaths, the most important cancers are those of the lung and bronchus, prostate, and colorectum in men and cancers of the lung and bronchus, breast, and colorectum in women. These four cancers account for almost half of the total cancer deaths among men and women Table 2), with lung cancer in both men and women as the leading cause of deaths at 28 and 26% for men and women, respectively. Many drugs used to treat these different cancers are typically indiscriminant, while exhibiting unwanted side effects due to off target effects and the targeting of processes in actively dividing cells. Furthermore, in many cases the cancers become resistant to treatment, as in the case with relapse occurrences of castration-resistant prostate cancer.

Table 2. The estimated new cancer cases and deaths by sex in the United States for 2014.

Estimated New Cancer Cases

Males			Females		
Site	Cases	Percentage	Site	Cases	Percentage
Prostate	233,000	27%	Breast	232,670	29%
Lung & bronchus	116,000	14%	Lung & bronchus	108,210	13%
Colorectum	71,830	8%	Colorectum	65,000	8%
Urinary bladder	56,390	7%	Uterine corpus	52,630	6%
Melanoma of the skin	43,890	5%	Thyroid	47,790	6%
Kidney & renal pelvis	39,140	5%	Non-Hodgkin lymphoma	32,530	4%
Non-Hodgkin lymphoma	38,270	4%	Melanoma of the skin	32,210	4%
Oral cavity & pharynx	30,220	4%	Kidney & renal pelvis	24,780	3%
Leukemia	30,100	4%	Pancreas	22,890	3%
Liver & intrahepatic bile duct	24,600	3%	Leukemia	22,280	3%
All Sites	**855,220**	**100%**	**All Sites**	**810,320**	**100%**

Estimated Cancer Related Deaths

Males			Females		
Site	Cases	Percentage	Site	Cases	Percentage
Lung & bronchus	86,930	28%	Lung & bronchus	72,330	26%
Prostate	29,480	10%	Breast	40,000	15%
Colorectum	26,270	8%	Colorectum	24,040	9%
Pancreas	20,170	7%	Pancreas	19,420	7%
Liver & intrahepatic bile duct	15,870	5%	Ovary	14,270	5%
Leukemia	14,040	5%	Leukemia	10,050	4%
Esophagus	12,450	4%	Uterine corpus	8,590	3%
Urinary bladder	11,170	4%	Non-Hodgkin lymphoma	8,520	3%
Non-Hodgkin lymphoma	10,470	3%	Liver & intrahepatic bile duct	7,130	3%
Kidney & renal pelvis	8,900	3%	Brain & other nervous system	6,230	2%
All Sites	**310,010**	**100%**	**All Sites**	**275,710**	**100%**

[a]Prostate, lung and colorectal cancers are the leading estimated deaths as well as new cases.

[b]For men prostate, lung, and colorectal are the top three estimated new cases as well as the leading cause of deaths.

[c]For women breast, lung, and colorectal are the top three estimated new cases as well as the leading cause of deaths.

To treat these cancers, my work capitalizes on recent research that has demonstrated the protein RGS17 as a powerful mediator for metastatic lung and prostate tumorigensis [72-73]. While other RGS proteins are implicated in cancer progression through other domains, RGS17s cancer activity is demonstrated through its RGS homology (RH) domain (Figure 3).

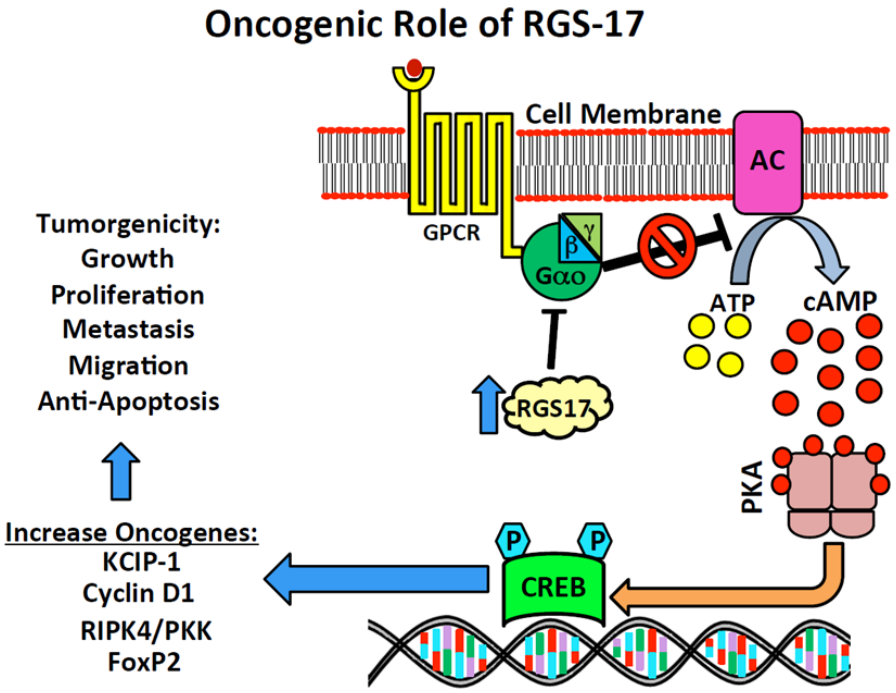

Figure 3. Activation of a GPCR promotes dissociation of the heterotrimeric G protein from the receptor, and simultaneous exchange of GDP for GTP in the Gα subunit active site. $G\alpha_{i/o}$ and $G\alpha_z$ inhibit AC and downregulate cAMP formation. RGS17 regulates $G\alpha_{i/o}$ and $G\alpha_z$ (as well as $G\alpha_q$) by accelerating the rate of GTPase activity of the Gα subunit and returning the α subunit to its inactive, GDP-bound conformation. In response to elevated levels of cAMP, PKA phosphorylates the CREB and promotes DNA transcription. Normal levels of RGS17 will modulate this cAMP-PKA–CREB signaling cascade. In lung and prostate cancers, RGS17 transcripts are increased by an average of 8.3- and 7.5-fold, respectively, over patient matched tissues, which lead to increased transcription via CREB. Several proteins are upregulated due to this increased CREB activation, including KCIP-1, cyclin D1 and RIPK4/PKK, which leads to increased tumorgenicity via increased activity of growth, proliferative, metastasis, migratory and anti-apoptosis pathways.

This activity allows for the targeting of RGS17s RH domain for inhibition leading to the restoration of the G protein ($G\alpha_{i/o}$) signaling cascade to normal levels and reducing tumor cell proliferation (Figure 4).

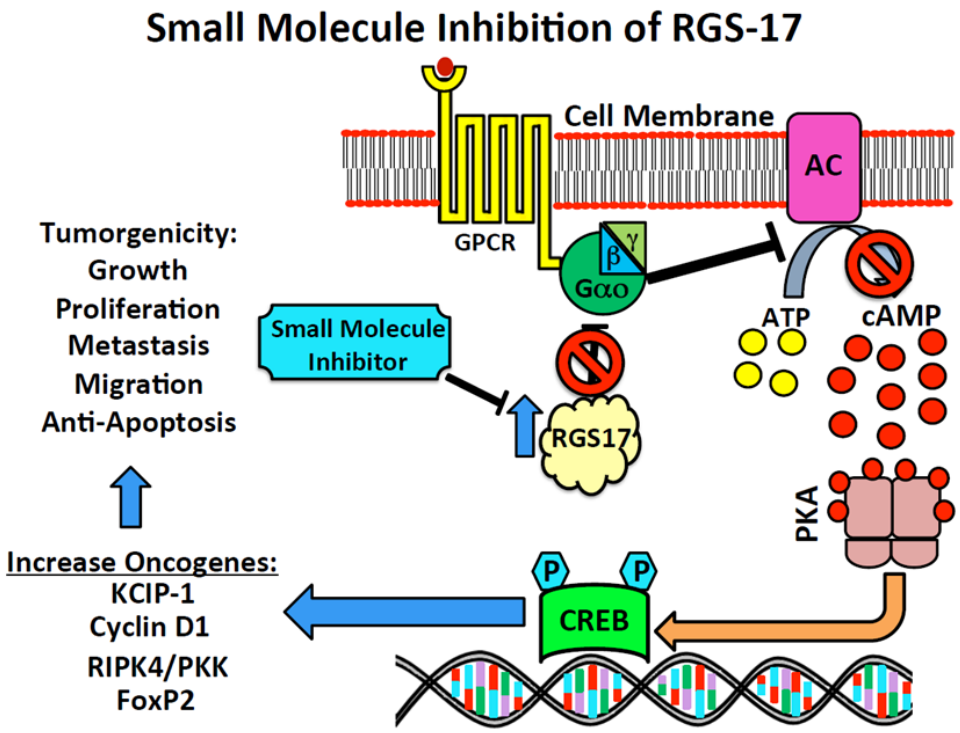

Figure 4. Pharmacological intervention with a RGS17 small molecule inhibitor. The inhibition of RGS17 alleviates the inhibition of the Gα subunit. This leads to the inhibition of adenylyl cyclase and a decrease in cAMP levels. The effects of the small molecule inhibitor will modulate the cAMP-PKA-CREB signaling cascade by returning the system to normal levels, allowing for the decrease in tumor proliferation and metastasis.

Scope of work

My hypothesis is that through the use of high-throughput screening, I will discover compounds that inhibit the activity of RGS17, which can be developed into molecular probes to understand RGS17 function and serve as pre-therapeutic leads for the treatment of lung and prostate carcinomas. Briefly, my goal is to test the hypothesis through the development and characterization of a novel high-throughput screening platform, AlphaScreen®, as well as the application of biophysical and biochemical methodologies to determine protein: ligand activity. Overall, my two specific aims for this research are:

1. To develop, characterize, and implement a novel high-throughput screening paradigm to investigate the protein: protein interaction between G_{α} proteins and the regulator of G protein signaling 17 (RGS17) protein.
2. To discover novel small molecule inhibitors as lead compounds for development as chemical probes and pretherapeutics.
    a) The development of molecule probes for the pharmacological investigation of RGS17's role in the initiation and progression of metastatic lung and prostate cancers would provide further validation of RGS17 as a druggable target.
    b) The discovery of pretherapeutic lead compounds and development into drug candidates would provide a new avenue for the treatment of prostate specific antigen (PSA) resistant prostate cancers often associated with relapse and increased high mortality rates.
3. To determine specific chemical moieties and elucidate novel pharmacophores centered on inhibition of RGS17's GTPase Accelerating Protein activity (GAP).

4. To investigate the mechanism of action through which these newly discovered RGS17 inhibitors elicit their inhibitory activity against RGS17.

To achieve the goals of this study, first a novel high-throughput screening paradigm was adapted and characterized that will allow for the rapid identification of lead compounds that inhibit the $G\alpha_o$: RGS17 ppi (Figure 5). Next, this screening platform was implemented to screen the NCI Diversity Set II, as the first pilot screen for inhibitors of the RGS17: $G\alpha_o$ protein: protein interaction. This screen achieved the discovery of the first biochemical RGS17 inhibitors reported to date.

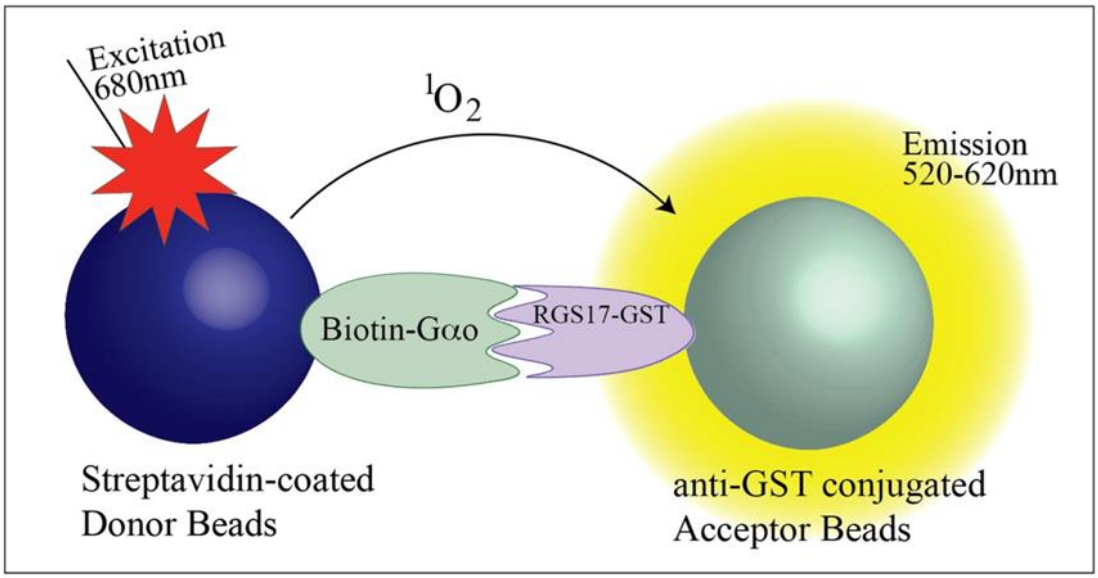

Figure 5. Graphical depiction of AlphaScreen HTS assay for protein: protein interactions. G protein alpha subunits are expressed and purified in E. coli, chemically biotinylated through maleimide chemistry and immobilized to donor beads. RGS17 is expressed in E. coli as a GST-fusion protein, and is immobilized onto an acceptor bead that is coated with anti-GST antibodies. When the G protein and RGS17 interact, the beads are brought into close proximity. Subsequent excitation of the donor bead results in a chemical reaction releasing a singlet oxygen species. This moiety can travel ~200 nm before decomposing, and will encounter an acceptor bead if the two proteins are interacting. Then a reagent contained the acceptor bead is excited by the oxygen and emits light at a 520-620 nm wavelength. The presence of inhibitors will block this protein: protein interaction and result in an attenuation of the signal.

Further work was then completed to increase the throughput as well as decrease cost through decreasing reagent use. This allowed for the rapid screening of two more compound sets, the MicroSource SPECTRUM and NDL3000 compound libraries, in a miniaturized format. Finally, this portion of the project allowed for the development of several powerful orthogonal assays to confirm the interaction with lead compounds and their target in biochemical, enzymatic, and cellular assays.

The overarching goal of this work was the development of novel biochemical and cell-based assays that will be used to identify inhibitors of Regulator of G protein signaling 17 (RGS17). RGS17 presented an unexplored target for pre-therapeutic development and a novel approach to the development of lead molecules in the fight against lung and prostate cancers. My work will lead to the discovery of RGS17 inhibitors that will provide a new avenue for both understanding the role of RGS17 in cancer progression as well as providing new small molecule leads for anticancer drug development. The outcome of this project is both the development of novel screening methodologies for RGS17 ligands and new probe molecules that will serve as molecular probes for studying RGS17 protein function and provide initial molecules for pre-therapeutic optimization.

CHAPTER III: DEVELOPMENT AND IMPLEMENTATION OF A NOVEL HIGH-THROUGHPUT SCREENING PARADIGM FOR THE DISCOVERY OF RGS17: Gα PROTEIN: PROTEIN INTERACTION INHIBITORS

The work presented in this chapter, in part, has been published in the Journal of Biomolecular Screening; Mackie, D. I.; Roman, D. L., Development of a novel high-throughput screen and identification of small-molecule inhibitors of the Galpha-RGS17 protein-protein interaction using AlphaScreen. *J Biomol Screen* **2011,** *16* (8), 869-77 [111].

Abstract

In this chapter, AlphaScreen® technology was utilized to develop a high-throughput screening method for interrogating small molecule libraries for inhibitors of RGS17. RGS17 is implicated in the growth, proliferation, metastasis and the migration of prostate and lung cancers. RGS17 is up-regulated in lung and prostate tumors up to a 13-fold increase over patient-matched normal tissues. Studies show RGS17 knockdown inhibits colony formation and decreases tumorigenesis in nude mice. Our screen utilizes a measurement of the Gα: RGS17 interaction, with an excellent Z-score that exceeded 0.73 and a signal to noise ratio >70. This allows for the screening of over 1,000 compounds per hour. The NCI Diversity Set II was screened and from this investigation 35 initial hits were discovered of which 16 were confirmed after screening against controls. The 16 compounds exhibited IC50 <10μM in dose-response experiments. Four exhibited IC50 values <6μM while inhibiting the Gα: RGS17 interaction >50% when compared to a biotinylated-GST control. This chapter describes the first high throughput screen for RGS17 inhibitors, as well as a novel paradigm adaptable to many other RGS proteins, which are emerging as attractive drug targets for modulating GPCR signaling.

Introduction

The largest known family of cell surface receptors is the G protein coupled receptors (GPCRs) [1]. These hepta-helical plasma membrane spanning receptors transduce signals initiated by extracellular stimuli such as hormones and light, by coupling to intracellular G proteins. As described in chapter 1, G proteins are heterotrimers consisting of α and $\beta\gamma$ subunits. α subunits are grouped into subfamilies comprised of $G\alpha_{o/i}$, $G\alpha s$, $G\alpha_{q}$, $G\alpha_{12/13}$, $G\alpha_{olf}$ and $G\alpha_{z}$. GPCRs have become the target of over 50% of current therapeutic agents on the market and are thus the subject of great research interest [2]. Mechanistically, GPCRs are activated upon agonist binding, and through conformational changes which cause an exchange of GDP for GTP in the $G\alpha$, which causes dissociation of the heterotrimer into α and $\beta\gamma$ subunits [27]. $G\alpha_{o}$ subunits exhibit slow intrinsic GTPase activity, which inactivates the G protein when GTP is hydrolyzed and returns the α subunit to its inactive GDP-bound form. Once inactive the α subunit re-associates with the $\beta\gamma$ subunit and reforms the heterotrimer, which can reassociate with the GPCRs. Modulation of inhibitory $G\alpha$ subunit signaling activity, such as that mediated by $G\alpha_{i/o}$, occurs by the Regulator of G Protein Signaling (RGS) proteins. RGS proteins are GTPase activating proteins (GAPs) and accelerate the slow intrinsic GTPase activity of $G\alpha$ subunits by binding to the active, GTP-bound form of $G\alpha$ and facilitating the more rapid hydrolysis of GTP to GDP. RGS proteins are not directly responsible for hydrolysis of GTP but instead cause structural changes in the active $G\alpha$-GTP complex, which results in a more favorable conformation of the complex for efficient hydrolysis of GTP [4, 112-113].

Structurally, RGS proteins are hallmarked by the RGS homology (RH) domain that defines them as GAPs [4]. The mammalian family of RGS proteins contains more than thirty members, all of which possess the canonical 120 amino acid RH domain [12, 113]. RGS proteins are divided into eight subfamilies according to the shared sequence identities found outside of the RH domain [4, 113]. Members of the A/RZ and B/R4

subfamilies are the smallest RGS proteins and consist of the RH domain flanked by small but variable N- and C-terminal regions [4, 12, 113]. Members of the other six families are multidomain proteins that vary in size and function within the cell.

1 in 4 deaths in the United States are due to cancers [110]. A growing number of studies have implicated the over expression of RGS proteins as playing a role in the progression of cancer. Some examples include the over expression of RGS1 in melanoma and ovarian cancer [13-14], RGS2 in breast cancer [81], RGS5 in melanoma, multiple myeloma, acute myeloid leukemia, ovarian and breast cancer [90], RGS19 in ovarian cancer [15], RGS20 in melanoma [76] and RGS17 in lung and prostate cancers [72-73]. These RGS proteins present a unique target for advances in cancer drug discovery leading to new avenues for anticancer therapies and treatment options for patients diagnosed with cancer.

My research involves the role of RGS proteins in lung and prostate cancer. In this chapter, I focus on RGS17. RGS17 is normally expressed in the human central nervous system with the highest levels of mRNA expressed in the cerebellum, nucleus accumbens and putamen [114]. RGS17 regulates $G\alpha_{i/o}$, $G\alpha_z$, and $G\alpha_q$ and accelerates the rate of GTPase activity by these alpha subunits [71]. The $G\alpha_{i/o}$ and $G\alpha_z$ subunits inhibit adenylate cyclase and down-regulate cAMP formation which attenuates the cAMP-PKA-CREB signaling cascade. PKA is a holoenzyme that is assembled as an inactive tetrameric complex consisting of two regulatory subunits (R-PKA) and two catalytic subunits (C-PKA) [115-117]. In response to the elevated cAMP levels in the cell the C-PKA subunits move into the nucleus where they phosphorylate the transcription factor, cyclic AMP response element (CRE)-binding protein (CREB) [118-120]. Once CREB is phosphorylated, transcription of more than 4,000 genes begins [118, 121]. Recently, it has been reported that CREB is involved in the development and tumorigenesis of endocrine tissues and lung adenocarcinoma [122-123]. Normal levels of RGS17 serve to modulate the cAMP-PKA-CREB signaling cascade but in lung cancers RGS17

transcripts are increased in 80% of tumors by an average of 8.3-fold over patient matched normal lung tissues [72].Transcript accumulation also occurs in prostate tumors by an average of 7.5-fold when compared to patient matched normal tissue samples [72]. The increase in RGS17 acts to attenuate $G\alpha_{i/o}$ and $G\alpha_z$ signaling which results in increased cAMP in tumor cells, which activates the cAMP-PKA-CREB pathway that induces tumor cell proliferation and tumorigenesis [72-73].

This chapter describes the development and implementation of a high-throughput screening assay to identify small molecules that inhibit the $G\alpha_o$: RGS17 ppi, using AlphaScreen® technology (Perkin Elmer). AlphaScreen® has been previously used to screen for numerous antagonists of protein: protein interactions including STAT-SH2 [124] and Hsp90-cochaperone [125]. This chapter describes the first use of AlphaScreen® for RGS protein interactions. Previous HTS efforts using different methods, such as the flow cytometry protein interaction assay (FCPIA), have been used to identify inhibitors for RGS4 [126-128]. This method was formatted in 96 well plates and involved screening approximately 160 compounds per/hour. The goal for developing a new HTS assay was to increase the amount of compounds screened to over 1,000 compounds/ hour while maintaining a robust Z factor with an excellent signal to noise ratio.

Using AlphaScreen®, a pilot screen was established in which 1,364 compounds from the NCI diversity set II (National Cancer Institute) were screened to identify inhibitors of the $G\alpha_o$: RGS17 ppi in preparation for screening large libraries as part of my research goals. This pilot screen resulted in four putative RGS17 inhibitors (Figure 6), all of which exhibited IC50 values less than 6 μM. This chapter reports the development and describes the evolution of bead-based high throughput screening for RGS protein interactions into a faster and more robust assay, as well as the first high throughput screening paradigm for RGS17 inhibitors focused on anticancer lead development.

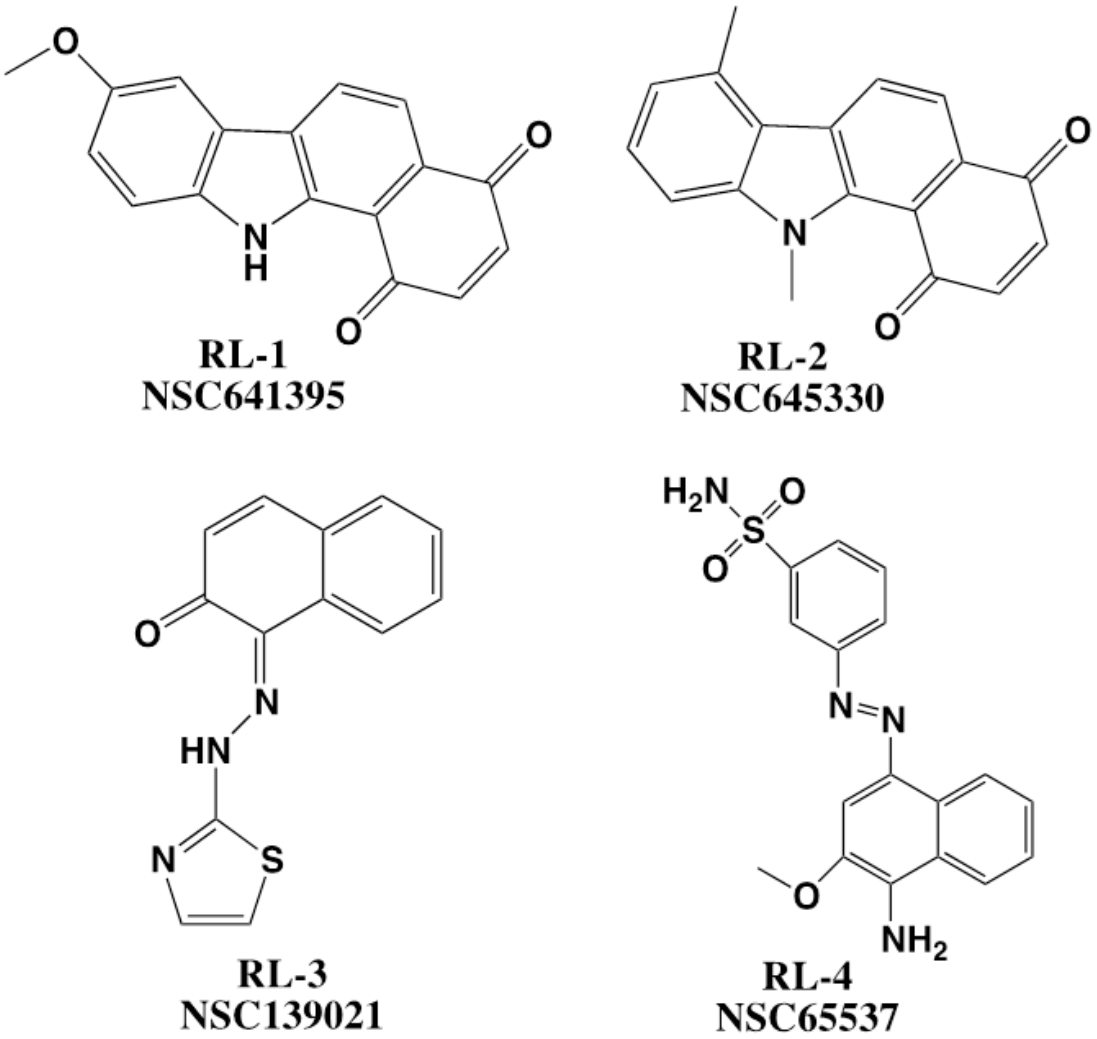

Figure 6. Four initial RGS17 inhibitors discovered from the pilot screening of the NCI diversity set II. RL-1, NSC641395 is known as 8-methoxy-11H-benzo[a]carbazole-1,4-dione, RL-2, NSC645330 is known as 7,11-dimethylbenzo[a]carbazole-1,4-dione. These two compound represent the most active compounds from the initial screen of the NCI library. They both contain the 1,4-dione moiety which have been implicated in toxicities from the generation superoxide from the oxidation-reduction cycling. RL-3, NSC139021 is 1-(2-Thiazolylazo)-2-naphthol, NSC65537 is 3-[(4-amino-3-methoxynaphthalen-1-yl)diazenyl]benzenesulfonamide. These two compounds showed a loss of activity when tested in orthagonl FCPIA testing.

Materials and methods

RGS protein expression and purification

Human RGS17 in the pcDNA3.1 (+) vector was purchased from the Missouri S&T cDNA resource center (Rolla, MO; www.cdna.org). The RGS17 open reading frame was amplified using the following primers:

5′- ggggacaagtttgtacaaaaaagcaggcttaatggagagtatccaggtc-3′ and

5′-ggggaccactttgtacaagaaagctgggtaagattcagaagaagagcc-3′.

This also created an attB-flanked PCR product compatible with gateway (Invitrogen, Irvine CA) cloning. The attB-flanked PCR product was combined with the donor vector pDONR221, using gateway technology with Clonase II (Invitrogen, Carlsbad, CA) according to manufacturer's protocols. The gateway technology uses the lambda recombination system to facilitate transfer of heterologous DNA sequences flanked by modified att sites between vectors. The resulting pDONR221/RGS17 vector was transformed into DH5-α bacteria, colonies were picked, and DNA was mini-prepped (Qiagen, Valencia, CA). The donor vector containing RGS17 was combined with the expression vector pDest565 (Addgene plasmid 11520, Dominic Esposito, Saic-Frederick) in LR recombination reaction (Invitrogen) according to the manufacturer's instructions. This produced RGS17 with an N-terminal Glutathione-S-Transferase (GST) and a C-terminal 6xHis tag. RGS17/pDest565 was transformed into BL-21 (De3) bacteria, and a single colony was picked and expanded into a 2-L culture of LB containing 100 μg/mL ampicillin and induced at OD600 = 0.6 with 500 μM isopropyl β-D-1-thiogalactopyranoside (IPTG) for 4 h at 37 °C. Bacteria were pelleted and resuspended in RGS17 buffer (50 mM Hepes [pH 7.4], 100 mM NaCl, 2 mM $MgCl_2$, 1 mM β-mercaptoethanol, 0.1% triton X-100) with added protease inhibitors (final concentrations: 1 μM e-64, 1 mM phenylmethanesulfonylfluoride [pmsf], 1 μM leupeptin, and 1 μM pepstatin a) and treated with 0.5 mg/ ml lysozyme for 15 min while stirring on ice. The

suspension was flash-frozen in liquid nitrogen and thawed. Following lysis, DNAse I was added while stirring on ice. The lysate was centrifuged for 45 min at 36,500 rpm (~100,000x g) in a Sorvall T-647.5 rotor. The supernatant was filtered (0.45 μm) and applied to a 5-mL nickel-NTA agarose column (Qiagen). The resin was washed with 15 mL RGS17 buffer containing 40 mM imidazole. Protein was eluted with RGS17 buffer containing 200 mM imidazole in 1.5-mL fractions. Following sodium dodecyl sulfate polyacrylamide gel electrophoresis (SDS-page) analysis, RGS17 fractions were pooled and diluted with RGS17 buffer to 50 mM imidazole concentration and incubated with 3 mL GST resin (Qiagen) for 3 h at 4 °C on an inversion mixer. RGS17 was eluted using a batch method with 10 mM reduced glutathione and taking 10 x 1-ml fractions. This procedure resulted in ~95% pure RGS17 (20 mg at 1.2 mg/mL).

$G\alpha_o$ protein expression and purification

6x-His-tagged $G\alpha_o$ was expressed and purified from transformed BL-21 (DE3) bacteria as described previously with the exception of 1 mM Tris(2-carboxyethyl)phosphine hydrochloride (TCEP) in the buffer in place of 1 mM dithiothreitol (DTT) as the reducing agent [129].

Chemical biotinylation of $G\alpha_o$ protein

$G\alpha_o$ proteins were biotinlyated with 1-biotinamido-4-[4′-(maleimidomethyl)cyclohexanecarboxamido] butane (533.68 g/ mol) using eZ-link Biotin-Bmcc (thermo scientific, Rockford, IL). Protein was labeled at a 5:1 biotin: protein ratio following manufacturer protocols. Excess biotin was removed by applying the sample to an 8-mL fast-flow desalting fast protein liquid chromatography (FPLC) column running at 1 mL/min on an AKTA (GE healthcare, Piscataway, NJ) purifier system. Fractions were pooled and concentrated to 1.66 mg/mL using an ultracel 10k centrifugal filter (Millipore, Billerica, MA) and snap-frozen in liquid nitrogen.

DMSO tolerance test

PerkinElmer provided AlphaScreen® beads in a suspension of 5 mg/mL. Four sets of 10 wells were used to determine the tolerance of the assay to an upper limit of 3.3% DMSO, which represents the maximum theoretical concentration of DMSO in planned follow-up dose–response experiments, and a concentration in excess of our screening concentration of <1.5%. Then, 24.4 μg (4.88 μL) of anti-GST acceptor beads was incubated with GST–RGS17 at a 30nm concentration in 200 μL of assay buffer (50 mM Hepes, 100 mM, 0.1% lubrol, 1% bovine serum albumin [BSA], pH 8.0) for 30 min at room temperature while streptavidin donor beads (PerkinElmer) were incubated with biotin–$G\alpha_o$ at a 30 nM concentration in 200 μL assay buffer. Following the coupling incubation, RGS17–anti-GST beads were brought to a final volume of 610 μL with assay buffer. $G\alpha_o$–biotin–streptavidin beads were split into two equal aliquots designated + or – AMF (50 mM NaF, 50 mM $MgCl_2$, 50 μM $AlCl_3$, and 5 μM GDP). +AMF beads were diluted with 200 μL of assay buffer that contained AMF and were incubated for 10 min at room temperature (RT) to form the stable $G\alpha_o$–GDP– $AlF4^-$ complex, which RGS binds with high affinity [127]. The beads designated –AMF received 200 μL assay buffer without AMF. Then, 15 μL of RGS17–anti-GST beads was added to 96 wells of a 384-well plate. Half of these wells received $G\alpha_o$–biotin– streptavidin beads with AMF, and half received $G\alpha_o$–biotin– streptavidin beads without AMF. Half of each set of assay wells received 1 μL DMSO, which allowed us to assess the conditions of +AMF, +DMSO; +AMF, –DMSO; –AMF, +DMSO; and –AMF, –DMSO. The plate was then incubated at 4 °C in the dark for 40 min and read on a synergy 2 plate reader (Biotek, Wisnooski, VT) with a sensitivity setting of 200, excitation at 680 nm, and emission read at 570 nm.

Z factor calculation

Experiments were performed in Corning (Corning, New York, NY) 384-well white flat-bottom plates, and samples were read on a Biotek Synergy 2 plate reader. All data were collected using Gen5 (Biotek) and analyzed with Graphpad prism 5.0 (Graphpad software, San Diego, CA).

The 384-well plates were used to determine the positive and negative control values for the protein interaction assay. In total, 192 wells of the plate were –AMF and represented no protein: protein interaction (background), and 192 wells contained +AMF, which supports the high-affinity protein–protein interaction (maximal signal). In total, 105 μg (21 μL) of anti-GST acceptor beads and 105 μg (21 μL) streptavidin donor beads were coupled to RGS17–anti-GST and $G\alpha_o$–biotin–streptavidin at a 30 nM concentration in 2.6 mL of assay buffer. The protein/bead mixtures were incubated in the dark at 4 °C for 30 min. Upon completion of coupling, the RGS17–anti-GST beads were resuspended in a total of 7.8 mL of assay buffer. The $G\alpha_o$–biotin–streptavidin bead mixture was split into two tubes of 1.3 mL each. One tube was combined with 2.6 mL of assay buffer without AMF or GDP for the no-binding control (-AMF). For the positive binding control, the second tube received assay buffer and a final concentration of 50 mM NaF, 50 mM $MgCl_2$, 50 μM $AlCl_3$, and 5 μM GDP (+AMF) and was incubated on ice for 10 min. Then, 15 μL of RGS17–anti-GST beads was added to each well of a 384-well plate. In total, 192 wells received 15 μL of $G\alpha_o$– biotin–streptavidin beads with AMF and 192 wells received 15 μL of $G\alpha_o$–biotin–streptavidin beads without AMF using a Labsystems Multidrop dispenser (Thermo scientific). Plates were incubated in the dark on ice for 30 min and read at RT using a Synergy 2 plate reader (Biotek) with a sensitivity setting of 200 using the AlphaScreen protocol with excitation at 680 nm and emission at 570 nm.

A Z-factor was calculated using the following equation: $Z\text{-factor} = (1- 3x (\sigma p+\sigma n))/(|\mu p-\mu n|))$, where σ represents the standard deviation of positive and negative (binding and nonbinding) (p, n) controls, and μ represents the mean of positive and

negative control values. Positive controls were determined using the 192 wells containing AMF and GDP, resulting in a $G\alpha_o$: RGS17 protein: protein interaction. The negative controls were determined from the 192 wells that lacked AMF and GDP, resulting in no protein: protein interaction.

Saturation binding

For saturation binding experiments, 10 nM of RGS17 was used to prepare RGS17–anti-GST beads, prepared as above using 40 μg (8 μL) of each bead to couple to each protein. Biotin–$G\alpha_o$ was serially diluted to yield a final concentration from 0.39 and 200 nm. $G\alpha_o$ protein was labeled in 33.3 μL of assay buffer containing 0.8 mL of beads and incubated for 30 min on ice. The mixture was split into equal tubes of 16.65 μL. Half of the sample received 33.35 μL of assay buffer without AMF (nonspecific binding), whereas the other half received assay buffer with 50 mM NaF, 50 mM $MgCl_2$, 50 μM $AlCl_3$, and 5 μM GDP (specific binding). The tubes were incubated in the dark on ice for 10 min. Then, 15 μL of the RGS17–anti-GST beads was added to each well. After 10 min, 15 μL of the +AMF and –AMF samples was added to their respective wells. The plate was incubated in the dark at 4 °C for 40 min and read on a Synergy 2 plate reader (Biotek) with a sensitivity setting of 150 using the AlphaScreen protocol with excitation at 680 nm and emission at 570 nm.

Competition binding

For competition binding, 10 nM of RGS17 was used to prepare RGS17–anti-GST as previously described using 10.8 μg (2.15 μL) of beads to couple the protein to the beads. $G\alpha_o$–biotin–streptavidin beads were prepared to yield a final concentration of 35 nM. A sample of 20 μL of $G\alpha_o$–biotin–streptavidin beads was removed and used as the negative control (-AMF). Half-log dilutions of free $G\alpha_o$ were plated to yield a final concentration from 1 μM to 3.16 pM. Then, 15 μL of RGS17–anti-GST beads was added to each well, to which 15 μL $G\alpha_o$–biotin– streptavidin beads were then added. Negative

controls were determined in the absence of free $G\alpha_o$ and AMF, which represents background. The positive control contained AMF without free $G\alpha_o$ to define maximal binding. Plates were incubated 45 min at 4 °C and read on a Synergy 2 plate reader (Biotek) with a sensitivity setting of 200 using the AlphaScreen protocol with excitation at 680 nm and emission at 570 nm.

AlphaScreen HTS

In total, 1364 compounds from the NCI Diversity set II were screened at a concentration of 33 μM. RGS17–anti-GST and $G\alpha_o$–biotin–streptavidin beads were prepared as previously described. In brief, 100 μg (20 μL) of beads were coupled to 20 ng (10 nM) of each binding partner ($G\alpha_o$ or RGS17) and incubated for 30 min on ice. The 384-well plates containing 352 compounds and 32 wells of DMSO controls were used. Then, 15 μL of RGS17–anti-GST beads were added using a Labsystems Multidrop (Thermo Scientific) and incubated for 10 min while the $G\alpha_o$–biotin–streptavidin beads were incubated with AMF. After incubation, 15 μL of $G\alpha_o$–biotin–streptavidin beads were added to compound containing wells and incubated on ice for 30 min and read on a Synergy 2 plate reader (Biotek) with a sensitivity setting of 200 using the AlphaScreen protocol with excitation at 680 nm and emission at 570 nm.

Dose–response experiments

Experiments were carried out similarly to the high-throughput AlphaScreen® assay except this was completed using Corning 384-well white flat bottom plates and the final total volume was 60 μL. First, 20 μL of RGS17–anti-GST beads at a final concentration of 10 nM were added to each well. Then, 20 μL of compounds in a half log dilution series to yield a final range from 1 nM to 100 μM was added to RGS17–anti-GST beads and incubated for 10 min in the dark. Finally, 20 μL of $G\alpha_o$–biotin–streptavidin beads were then added in the presence of AMF and GDP. Negative controls

were determined in the absence of AMF and compound. Maximum binding was determined in the absence of compounds but in the presence of AMF and GDP.

AlphaScreen TrueHits control

Compounds that inhibited the protein: protein interaction with an IC50 <10 μM were counter screened in a control assay containing biotinlyated GST. Biotin–GST binds both the anti-GST and streptavidin-coated beads, bringing the beads together artificially and forcing an interaction. Compounds were diluted to yield a range from 1 pM to 10 μM at a 3x concentration, and 20 μL was added to each well. In 5.28 mL of assay buffer, 211 ng (42.24 μL) of anti-GST beads was incubated with 300 ρM biotin–GST for 30 min at RT. Then, 211 ng (42.24 μL) of streptavidin beads was added and incubated for 30 min on ice. After conjugation was complete, 40 μL of the anti-GST–biotin–GST–streptavidin bead complex was added to each well of compounds, incubated for 10 min, and read at RT at a sensitivity setting of 200 on a Synergy 2 plate reader (Biotek) using the AlphaScreen protocol with excitation at 680 nm and emission at 570 nm.

Chemical labeling of G protein with Alexa488 for flow cytometry protein interaction assay (FCPIA)

$G\alpha_o$ proteins were labeled using Alexa488 Thiol-Reactive Probe protocol from Invitrogen (Life Technologies Grand Island, NY). In brief, a five molar excess was used to label the G protein. Dye was added to the protein reaction mixture drop wise and allowed to proceed at room temperature for 2 hours. The reaction was quenched with 3 μL β-mercaptoethanol at 14.3 M. Protein was purified using a fast desalting column and concentrated to 2.8 mg/mL.

Flow cytometry protein interaction assay

Flow cytometry protein interaction assay was carried out with Alexa488 labeled G protein and GST-RGS17RH (RGS Homology Domain) conjugated to SPHERO™

Glutathione Polystyrene Particles, 6.0-8.0 µm (Spherotech inc. Lake Forest, Illinois). To conjugate GST-RGS17RH to the beads 30 nM or 3x GST-RGS17RH was incubated with 14.5 µL of stock beads in 10 mL assay buffer (50 mM Hepes, 100 mM, 0.1% lubrol, 1% bovine serum albumin [BSA], pH 8.0). Conjugation proceeded for 30 mins.

Next, three concentrations of compound for RL1, RL2, RL3, and RL4 were prepared at 1 µM, 10 µM and 30 µM. Control samples of no compound and no AMF were prepared to represent the negative and positive controls, respectively. Compounds were mixed into solution containing 10 nM of each binding partner and incubated for 30 mins at room temperature. Experiments were carried out on a Becton Dickinson FACScan (Becton Diskinson Franklin Lakes, NJ) in the University of Iowa Flow Cytometry Core Facility. Gating was completed with mock or blank beads to determine the expected window of fluorescence.

Differential scanning fluorimetry

All Differential Scanning Fluorimetry experiments were carried out using white 384-well µltraAMP PCR plates (Sorenson BioSciences; Salt Lake City, Utah). All experiments were carried out as previously described by Phillips and Hernandez de la Pena [130]. In brief, a 1: 2000 dilution of Sypro Orange was made by adding 1 µL of Sypro Orange to 2 mL of PBS at pH 7.5. First, 1.2 mg/mL protein was incubated with 50 µM of each compound at room temperature for 15 min in a 10 µL volume. Upon completion of the incubation, 110 µL of the Sypro Orange-PBS solution was added to each compound/protein mixture. This yielded a final volume of 120 µL containing 0.1 mg/mL protein. Finally, 20 µL of the Sypro Orange/compound/protein mix for each compound and RGS17 or $G\alpha_o$ proteins was added to four wells of the 384-well plate. The experiment was run on the Roche LightCycler 480 (Roche, Switzerland) using a two-step method. Starting with a 25 °C baseline step and a second step with a target temperature of 95 °C with continuous acquisition and set acquisition rate of 3 per ^{o}C. All data was

collected using the Roche LightCycler data acquisition ability and analyzed with Graphpad Prism 6.0, using first and second derivatives of the fluorescent melting curves.

Results

DMSO tolerance

The stability of the assay was tested at 3.3% DMSO, my maximum conceived concentration for follow-up dose response experiments. The actual DMSO concentration for the HTS portion of this study was <1.5% (v/v). Under these conditions $G\alpha_o$: RGS17 screening was completed without DMSO interfering with the beads or functionality of the proteins (Figure 7).

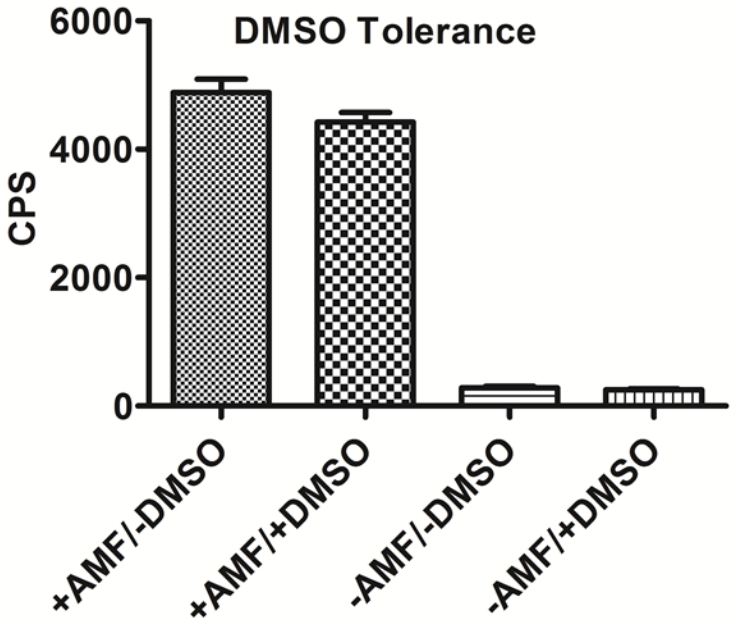

Figure 7. DMSO tolerance. The stability of the AlphaScreen® assay was tested to a maximum of 3.3% (v/v) DMSO. This DMSO concentration resulted in minimal loss of AlphaScreen® signal.

The +AMF, +DMSO resulted in a non-significant loss of signal when compared to the positive control of +AMF, -DMSO. As expected the –AMF with and without DMSO resulted in a negligible background signal.

Affinity of RGS17 for $G\alpha_o$

Next, the affinity of RGS17 for $G\alpha_o$ was determined using Alphascreen®. Non-specific binding was determined using $G\alpha_o$-Biotin-Streptavidin beads without AMF, which was subtracted from total binding data to yield specific binding. Non-specific binding was less than 2% of total binding. Figure 8 exhibits the saturation isotherm of specific binding of the RGS17 protein with $G\alpha_o$. RGS17 (10 nM) exhibited high affinity for $G\alpha_o$ (0 nM to 200 nM) with a K_d of 29.2±4.4 nM (n=5, in triplicate).

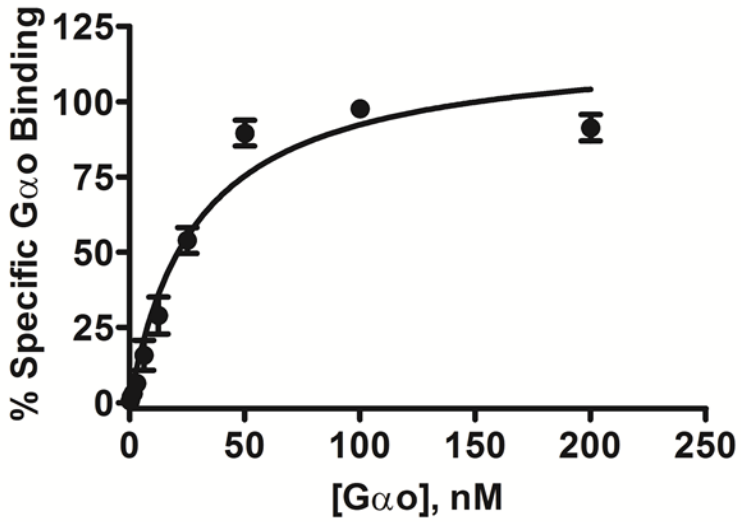

Figure 8. Specific binding for the RGS17: $G\alpha_o$ interaction. Increasing concentration of biotinylated $G\alpha_o$ was added to the RGS17 on beads (10 nM; final RGS concentration) in the presence of AMF to yield the percentage of specific $G\alpha_o$ bound to RGS17. The saturation assay exhibited robust specific binding with affinity binding of 29.2 ± 4.4 nM. Nonspecific binding, determined in the absence of AMF, is less than 2% of the total binding. n=5, performed in triplicate, with error bars indicating the standard error of the mean (SEM). [111]

The protein: protein interaction of RGS17 and $G\alpha_o$ on beads was shown to be reversible by using free $G\alpha_o$ as a competitor, yielding an IC50 of 46±1.1nM and a Hill slope of -1.3 (Figure 9, n=4, in triplicate).

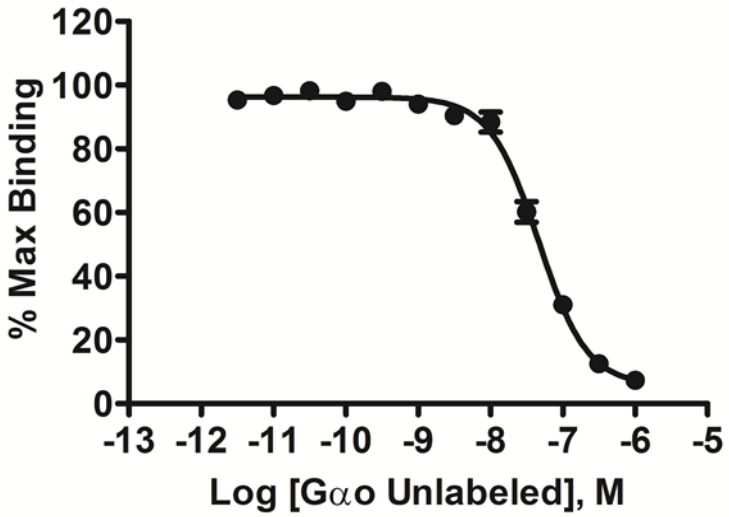

Figure 9. Competition binding assay for $G\alpha_o$: RGS17 interaction. Increasing concentrations of unbiotinlyated $G\alpha_o$ were added to fixed concentrations of RGS17 (10 nM) and biotinlyated $G\alpha_o$ (35 nM). Competition of the free $G\alpha_o$ with the tagged G-protein yielded an IC50 of 46 ± 1.1 nM. The graph is the average of 4 independent experiments (n = 4), preformed in triplicate, with error bars indicating the standard error of the mean (SEM). [111]

Z-factor determination

One hundred ninety two wells of a 384-well plate were used for positive controls in the presence of AMF, which affords the high-affinity $G\alpha_o$: RGS17 complex and 192 wells were used as negative controls without AMF (Figure 10). The Z-factor was determined to be 0.73 with a signal/noise ratio of 73. This Z-factor is well above the threshold 0.5 value indicating a screening paradigm suitable for HTS [131].

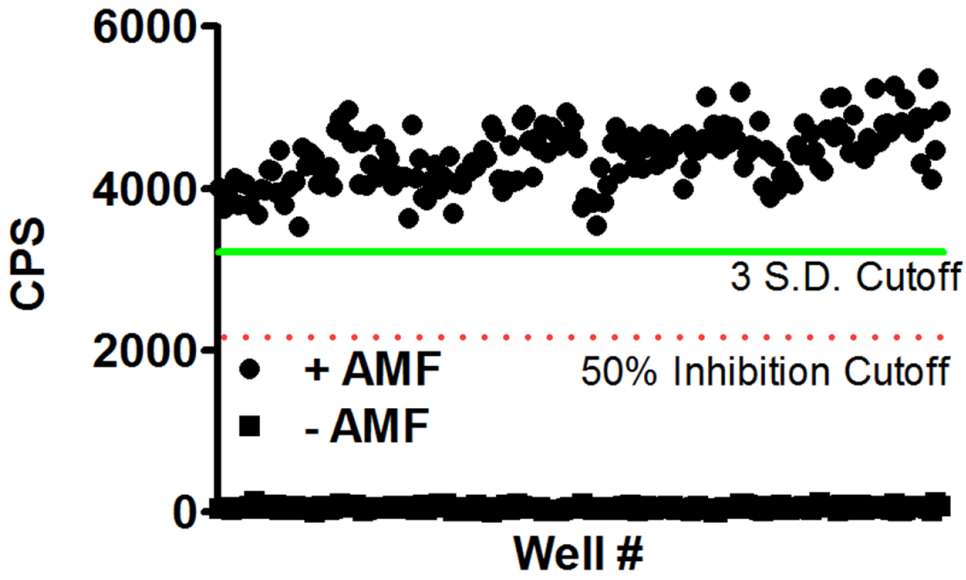

Figure 10. Determination of the Z factor. This factor assesses the suitability of the assay for high-throughput screening. In a 384-well plate, 192 wells were used as a positive control (+AMF) and 192 wells were deprived of guanosine diphosphate (GDP) and AMF and represented negative controls. The high signal-to-noise ratio (73), coupled with the Z factor of 0.73, allows for a large screening window for compounds that inhibit the protein: protein interaction greater than 50%. A mild interplate effect was observed during the screen based on the time for reading one plate of 20 min and the proteins coming to equilibrium of the protein: protein interaction during the incubation. CPS, counts per second. [111]

Discovery of the first RGS17 inhibitors

This high-throughput screen focused on identifying compounds that function as inhibitors of the $G\alpha_o$: RGS17 ppi in the presence of 50 mM NaF, 50 mM $MgCl_2$, 50 µM $AlCl_3$ with 5 µM GDP. The NCI Diversity set II was interrogated, which consisted of 1,364 compounds. RGS17 and activated $G\alpha_o$, coupled to their respective beads and in the presence of compounds at 33 µM, were read on the Synergy 2 plate reader at a sensitivity setting of 200. I used a cutoff of 50% inhibition or greater to consider an initial hit. I observed a 2.5% initial hit frequency (35 compounds) with 16 of those compounds confirmed with dose-response curves to exhibit an IC50<10 µM (Table 3), yielding a confirmed hit rate of 1.17%.

Table 3. High-Throughput Screening Results

Initial NCI Library	1364
Primary Hit (> 50% inhibition)	35 (2.5%)
Confirmed Hits (DRC w/ RGS17)	16 (1.17%)
Inhibitions of > 50% versus biotin-GST Control (TrueHits)	4 (0.29%)
IC50 < 6 μM	4 (0.29%)
Confirmed by FCPIA	2 (0.14%)

[a]Results of the high-throughput screening assay of the NCI Diversity Set II.

[b]From the 1364 compounds screened, 35 were initial hits (>50% inhibition).

[c]Primary hits were reconfirmed with a dose–response assay, and 16 compounds resulted in IC50 values <10 μM. GST, glutathione-S-transferase. [111]

These 16 compounds were then subjected to a counter screen against the biotinylated-GST control to eliminate compounds that interfere with the AlphaScreen® assay itself. Table 4 shows the effect of the compounds on the $G\alpha_o$: RGS17 ppi as compared to their effect on the AlphaScreen® assay reagents itself using biotin-GST. Twelve of the sixteen compounds showed minimal activity in the counter screen.

Table 4. Summary of Dose Response Curves from Initial Hits

Compounds	% inhibition of Biotin-GST (TrueHits) Control at 10 µM	% inhibition of RGS17: $G\alpha_o$ ppi at 10 µM	IC_{50} for Biotin-GST Control	IC_{50} for RGS17: $G\alpha_o$ ppi
RL-1	14.3	80.7	1.40 µM	1.40 µM
RL-2	15.9	74.5	10.00 µM	2.40 µM
RL-3	41.45	89.75	727 M	0.620 µM
RL-4	21.2	74.2	12.00 µM	5.40 µM
RL-5	50.11	75	0.004 M	8.40 µM
RL-6	30.8	75	31.00 µM	23.60 µM
RL-7	45.2	75	0.003 M	4.10 µM
RL-8	35	63.4	1.90 M	5.00 µM
RL-9	64.3	91.8	22.00 µM	0.800 µM
RL-10	59.8	67	0.021 M	15.00 µM
RL-11	53.3	64.4	0.052 M	3.00 µM
RL-12	51.95	75.7	0.120 M	3.40 µM
RL-13	73	80.7	1.40 µM	2.70 µM
RL-14	57.3	80.5	2.38 M	0.17 µM
RL-15	32	63.5	3.20 M	2.80 µM
RL-16	66.9	63.1	0.86 µM	2.20 µM

[a]Compounds screened against the biotin–GST control resulted in four compounds exhibiting ≥50% inhibition of the $G\alpha_o$: RGS17 interaction at a compound concentration of 10 µM when compared to the screen against the biotin–GST control at 10 µM.

[b]Compounds RL1-RL4 exhibited IC50 values <6 µM against the RGS17: $G\alpha_o$ interaction

[c]The activity against the $G\alpha_o$: RGS17 dose response curves was held to a standard of ≥50% inhibition against the control.

[d]The four compounds RL-1, RL-2, RL-3, and RL-4 were found to have activity in the biotin–GST control as shown by favorable IC50s but were chosen for their activity of inhibition at 10 µM concentrations. [111]

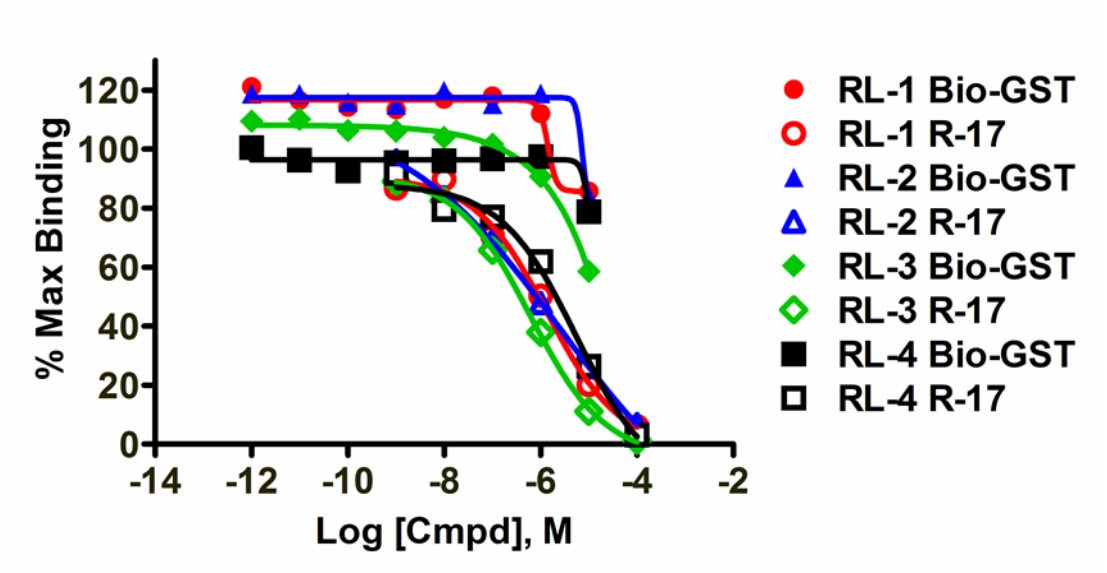

Figure 11. Dose–response curves for the four compounds using AlphaScreen®. RGS17–GST fusion protein (10 nM) and biotinylated $G\alpha_o$ (10 nM) were coupled to their respective beads. RGS17 beads were preincubated with increasing concentrations of compound before addition of 5 nM AMF-activated $G\alpha_o$ beads. All four exhibited $G\alpha_o$: RGS17 protein: protein interaction with IC50 values of 1.4 µM (RL-1), 2.4 µM (RL-2), 0.62 µM (RL-3), and 5.4 µM (RL-4). Error bars indicate the standard error of the mean (SEM). [111]

Four compounds were found to inhibit the $G\alpha_o$: RGS17 ppi greater than 50% at 10 µM (Figure 11). The >50% inhibition was determined by comparison of the dose-response and counter screen and resulted in a confirmed hit rate of 0.29%, and four new compounds identified as inhibitors of the $G\alpha_o$: RGS17 ppi. These four compounds were subjected to a counter-screen for activity using the flow-cytometry protein interaction assay (FCPIA) that yielded two confirmed lead compounds RL-1 and RL-2 (Figure 12).

The RL series of compounds were further examined for RGS17 binding specificity through the usage of DSF (Figure 13). This measure of protein thermal stability change upon ligand binding was used to determine if the activity of the RL series of compounds to disrupt the $G\alpha_o$: RGS17 ppi was because of binding to RGS17 or G protein. My results were found a weak interaction between the RL compounds (RL-1 and

RL-2) and RGS17, while there was no detectable interference with the thermal stability of the binding partner, the G protein (Figure 13). From these results, the compounds RL-1 and RL-2 are specific for RGS17 while possessing micromolar IC50s.

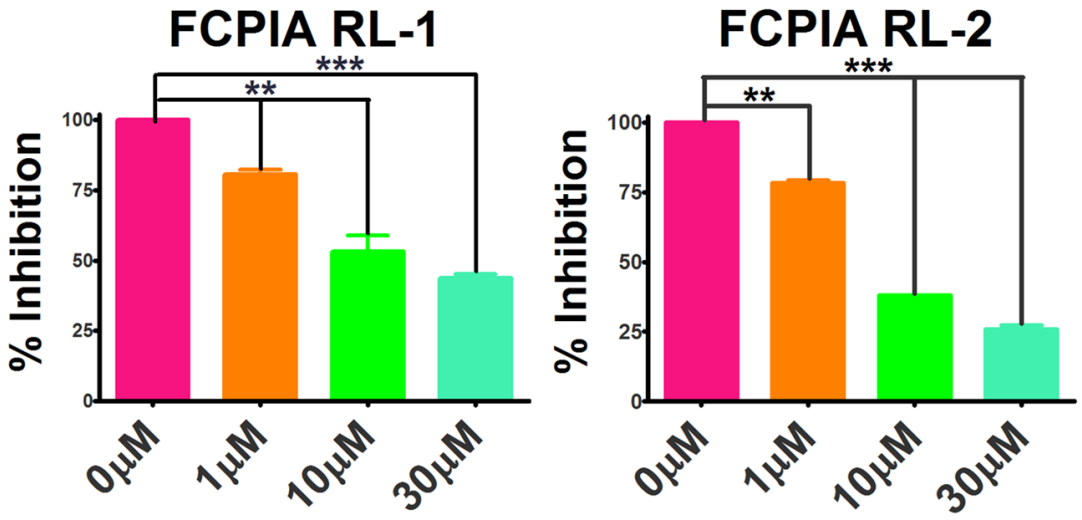

Figure 12. Orthogonal verification of RGS17 inhibition through Flow Cytometry Protein Interaction Assay. Compounds RL-1 and RL-2 showed the ability to disrupt the protein: protein interaction down to 1 μM. Nanomolar concentration of Alexa488 labeled G protein and GST-RGS17box conjugated to SPHERO™ glutathione polystyrene particles were preincubated with varying concentrations of compound before the addition of 5 nM AMF-activated $G\alpha_o$. Compounds RL-3 and RL-4 failed to disrupt the RGS17: $G\alpha_o$ interaction up to the highest concentration tested (30 μM).

Discussion

RGS proteins continue to emerge as attractive targets to exploit to modulate GPCR signaling [4, 7, 132-134]. Recent years have seen the establishment and advancement of high-throughput screening for inhibitors of RGS proteins. Early work that utilized yeast-based screening for inhibitors of RGS4 were fully automated and performed in 384- well format [135]. The first structure of a small molecule RGS

inhibitor was described for RGS4 by Roman et al [127]. These studies provided the proof of principle that small molecules could modulate the action of RGS proteins.

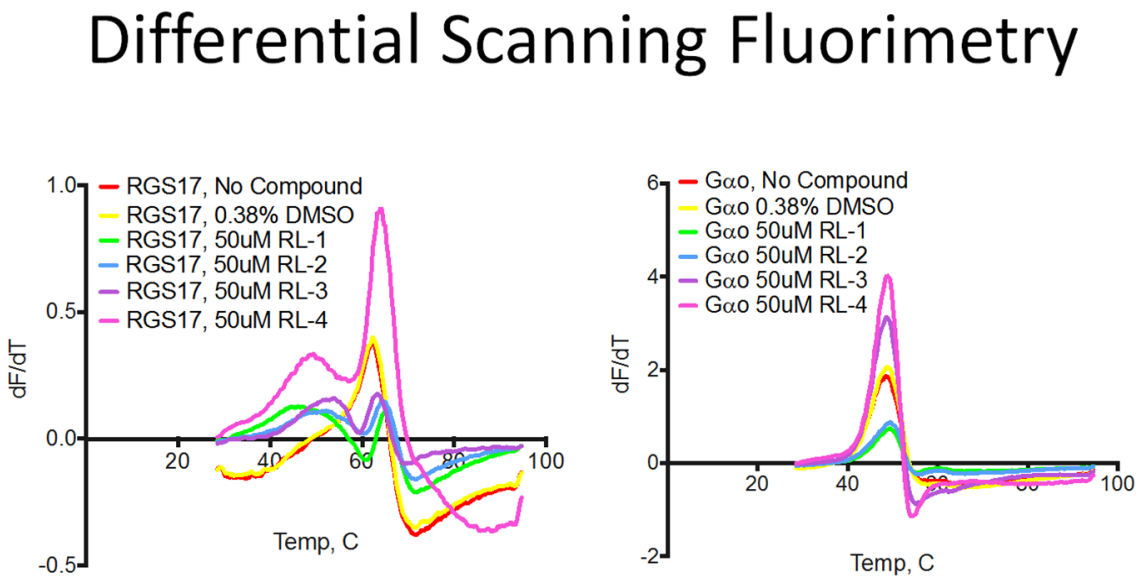

Figure 13. Measuring protein stability upon ligand binding through Differential Scanning Fluorimetry (DSF). The RL compound series (RL-1 to RL-4) were tested for specific binding to the RGS17 versus the $G\alpha_o$ subunit when compared to DMSO controls. All four compounds were found to weakly stabilize RGS17 against thermal denaturing. RL-1 and RL-2 were found to affect the melting temperature greatest when compared to DMSO controls.

This chapter focused on the inhibition of the $G\alpha_o$: RGS17 protein interaction with the aim of simplifying the assay and increasing the throughput by which I could interrogate small molecule libraries while maintaining a robust Z-factor and excellent signal to noise ratio. With this novel screening assay I was able to achieve both of these goals while reducing the amount of expensive protein and reagents.

In order to establish the most suitable screening parameters for this AlphaScreen® assay, I first fully characterized the binding characteristics of purified $G\alpha_o$ subunit and RGS17, with the $G\alpha_o$ subunit in its high affinity state induced by GDP and AMF [127],

which binds stably to RGS proteins. Sternweis et. al. showed that activation of the Gα subunit by the introduction of AMF into the buffer produced an affinity state which mimicked the physiological affinity of the protein: protein interaction [136]. RGS17 was purified from E. coli as an N-terminal-GST fusion protein and bound to anti-GST coated acceptor beads. $G\alpha_o$ purified from E. coli as previously described [126, 129, 137] was chemically biotinylated using maleimide chemistry and subsequently bound to streptavidin coated donor beads. A protein: protein interaction is detected between the binding partners via the donor: acceptor beads when they are brought within 200 nm of each other. Mechanistically, singlet oxygen, O_2, is released from the donor bead upon excitement at 680 nm. In its short lifetime (<3μs) the singlet oxygen species can travel up to 200 nm to reach an acceptor bead and induce a chemiluminescent reaction within the acceptor bead that results in photon emission that can be detected at 570 nm.

In this chapter, I demonstrated that the $G\alpha_o$: RGS17 ppi could accurately be detected and quantitated (Figures 7-10). The saturation study also allowed for the determination of the relative K_d value for the $G\alpha_o$: RGS17 interaction to be 29±4.4 nM. The determined K_d value for RGS17 compared very favorably to the K_d determined by FCPIA screens for other RGS proteins in both multiplex and singlet for RGS4 (115±6 and 91±9 nM), RGS8 (23±2 and 24±2 nM), RGS16 (54±7 and 37±6 nM), RGS6 (478±27 and 340±52 nM) and RGS7 (63±2 and 72±5 nM) [126]. Next, the competition binding experiment results demonstrated that I could displace the biotin-$G\alpha_o$ with untagged $G\alpha_o$ with an IC_{50} value of 46±1.1 nM. This was important as it demonstrates the reversibility of the $G\alpha_o$: RGS17 interaction even in the high affinity binding state afforded by AMF and GDP. These experiments guided me in choosing a screening concentration of 10 nM for $G\alpha_o$ that was within the linear portion of the saturation curve, and would provide sensitive detection of inhibitors.

In this screen 35 compounds were identified as primary hits for an initial hit rate of 2.5% and upon further filtering those hits by dose-response curves, sixteen compounds

with IC_{50} values less than 10 μM were determined, for a confirmation rate of 1.17%. Then these sixteen compounds were screened against a biotinlyated-GST (TrueHits) control that artificially brings donor and acceptor beads together. Any inhibition of the signal by a compound would indicate a non-specific action of that compound on the AlphaScreen® assay. This powerful and convenient control screen was done to eliminate compounds that could possibility inhibit the AlphaScreen® signal. Potential reasons for inhibition could be from O_2 quenchers, absorbance at the excitation wave length for the donor beads (680 nM), interference with the anti-GST antibody used to conjugate the RGS17-GST fusion protein to the donor bead or interference with the chemiluminescent reaction within the bead. The possibility of compound aggregates as a potential reason for signal inhibition was eliminated by the addition of detergent in the assay buffer which has been shown to suppress the nonspecific effects of aggregates in high-throughput screening [138]. Following controls, I identified 4 novel compounds that acted to specifically inhibit the $G\alpha_o$: RGS17 interaction. These four compounds that were confirmed to inhibit the RGS17: $G\alpha_o$ ppi greater than 50% over the biotinylated-GST control were counter-screened for activity using the FCPIA [126-127]. Compounds RL-1 and RL-2 exhibited strong concentration dependence that correlated with AlphaScreen® results (IC_{50} ca. 10 μM) whereas compounds RL-3 and RL-4 did not inhibit the RGS17: $G\alpha_o$ ppi. These compounds were further tested for binding activity by DSF. While RL-1 and RL-2 exhibited binding specifically to RGS17, the effects on thermal stability were weak. It was encouraging that both compounds left the binding partner, the G protein, unaffected leading to the hypothesis that RGS17 can be specifically targeted with the interrogation of larger chemical space.

One of the major advancements in this chapter is the discovery of the first small-molecule inhibitors for the $G\alpha_o$: RGS17 ppi. These lead molecules exhibit potencies that are less than 6 μM. Each of these newly discovered compounds represent three different classes of molecular scaffolds with varying chemical liabilities as lead molecules. First,

the compounds RL-1 and RL-2 are conjugated ring systems with the 1,4-dione or *p*-quinone moiety. The *p*-quinone moiety has been extensively studied and is known to alkylate proteins and DNA as well as redox cycling which generates adducts and reactive oxygen species, respectively [139]. Next, compound RL-3 contains the 2-naphthol which has been investigated for possible DNA intercalation [140]. These studies found that 2-naphthol exhibited weak DNA intercalation properties but it is worth noting the possible interaction between the planer conjugated ring system and DNA during the initial structural evaluation. Finally, the last compound in the RL series, RL-4 contains the benzenesulfonamide moiety which has been implicated in adverse reactions that may be due to hypersensitivity or direct toxic effects [141]. Possible hypersensitivity reactions include urticaria, angioedema, anaphylaxis, skin rashes, drug fever, polyarthritis, hemolytic anemia, hepatocellular damage, immune cell cytotoxicity and agranulocytosis. Optimization of the structure of these RL compounds to avoid these chemical liabilities is necessary to develop a molecule with increased potency and avoiding possible idiosyncratic or adverse drug reactions. Nevertheless, these findings added to the growing literature of small molecule RGS inhibitors, and represent a novel HTS assay, in 384-well format that can be adapted for use with other RGS proteins and their binding partners.

The second advancement of in the chapter is the increase in the amount of compounds that can be screened without a decrease in robustness of the assay. One of the current methods used in screening for small molecule inhibitors is the FCPIA approach. This is done using 96-well plates and methods described in Roman et. al. [126-127]. Another method that has been applied to high-throughput screening is time-resolved fluorescence resonance energy transfer (TR-FRET), which has been used to identify the first small-molecule inhibitors of an RGS protein that exhibited activity in cells and was completed in 384-well format [137]. The AlphaScreen® resulted in an initial hit rate of 2.5% of 1,300 compounds in the primary screen, with a DRC confirmation rate of 1.17% and filtered results for an overall hit rate 0.29%. This compares favorably with the

polyplexed FCPIA screen for inhibitors of multiple RGS protein interactions [126] (initial hit rate 1.5%-3.9%, filtered results 0.3%-1.4% and overall hit rate of 0.375%). The AlphaScreen® exhibited a high initial hit rate when compared to the TR-FRET screens but was well within the overall expect hit rate [137]. The new approach represents a screening paradigm that increases throughput while maintaining a very robust Z-factor and signal to noise ratio. Furthermore, the screen allowed me to screen three 384-well plates per hour, resulting in 1,056 compounds screened in one hour. One limitation of the throughput in this study is the speed of the plate reader – other readers, such as the EnVision from Perkin Elmer can read 384-well plates in less than 2 minutes and a 1536-well plate in 11 minutes, which would allow this assay's throughput to be increased manifold. This AlphaScreen® assay format should prove powerful, as it could be readily adapted to many RGS protein interactions.

This chapter focused on RGS17 as a novel target for discovery of potential novel anticancer agents. Recent fine mapping studies of chromosome 6q23-25 has revealed the RGS17 gene as a likely candidate gene in cases of familial lung cancer [73]. Effective RNAi knockdown studies have shown that tumor burden and proliferation can be significantly reduced in cell culture and nude mice models injected with H1299-cells (Non-small cell lung carcinoma cell line) that have been subjected to RGS17 knockdown by RNAi [72-73]. Therefore the development of a small molecule inhibitor that could act on RGS17 in a similar way as the RNAi knockdown experiments presents another therapeutic approach for cancer treatment for this novel application of the AlphaScreen® technology for usage in high-throughput screening.

In conclusion, this chapter demonstrates that the AlphaScreen® technology could be adapted to allow for the interrogation of small molecule chemical libraries yielding the first inhibitors of specific protein: protein interactions involving RGS17 and $G\alpha_o$. In addition, this method, using GST-fusion proteins for purification and bead-coupling greatly simplifies the preparation of material for the screen. This method is also powerful

in that it can be adapted for many RGS proteins and their cognate G-protein alpha subunits. This study presents a method that can increase the amount of compounds screened and provides another target for utilizing AlphaScreen® as a method of high-throughput screening for inhibitors of protein: protein interactions.

CHAPTER IV: DISCOVERY AND CHARACTERIZATION OF THE FIRST BIOCHEMILCAL RGS17 GAP INHIBITORS

The work presented in this chapter, in part, has been published in the Public Library of Science (PLOS) ONE139. Monroy, C. A.; Mackie, D. I.; Roman, D. L., A high throughput screen for RGS proteins using steady state monitoring of free phosphate formation. PLoS One 2013, 8 (4), e62247. [142]

Abstract

Regulator of G-Protein Signaling (RGS) proteins modulate the complex signaling pathways elicited by G protein coupled receptor activation. Recent studies have implicated RGS proteins in the development and progression of multiple cancers. Interest in developing small molecule inhibitors of RGS proteins has led to the discovery of several compounds through an array of high throughput screens; however, the majority of these compounds function as covalent modifiers. In this chapter, the discovery of inhibitors of RGS17 that function as reversible, non-covalent inhibitors is presented.

RGS17 is of great interest due to previously discussed studies that implicated its overexpression as playing a role in proliferation and metastatic potential of prostate and lung cancers. In chapter 3, a novel high-throughput screening platform was developed. In this chapter we adapted this paradigm to a miniaturized platform from a 384 to 1536-well format. With this new format, a pilot screen of the MicroSource (Discovery Systems, Inc. Gaylordsville, CT) and TimTec NDL-3,000, Natural Products Derivatives libraries (TimTec LLC, Newark, DE) was completed that focused on identification of small molecules that disrupt the $G\alpha_o$: RGS17 ppi. These campaigns yielded four compounds (UI5, UI1590, UI1907, and UI1956) that inhibited the $G\alpha_o$: RGS17 interaction in multiple biochemical assays and exhibit low μM to nM dissociation constants as determined by isothermal titration calorimetry (ITC). These compounds represent unique molecular scaffolds and provide first-in-class RGS17 inhibitors that will serve as probes

for the development of therapeutics that may hold promise as novel treatments for lung and prostate cancers.

Introduction

Many cellular processes are governed by signaling through membrane-spanning G protein coupled receptors (GPCRs). This occurs through the extracellular activation of the GPCR, which is a guanine nucleotide exchange factor (GEF) for the intracellular G protein alpha (Gα) subunit and leads to the exchange of guanosine diphosphate (GDP) for guanosine triphosphate (GTP) [27, 143]. Upon the exchange of GDP to GTP, the Gα and βγ subunits dissociate from the activated receptor, as well as each other, and lead to multiple signaling cascades [5]. The G protein signaling cascade is terminated by hydrolysis of the γ-phosphate of the bound GTP and the re-association of the heterotrimeric Gα and βγ subunits. A family of proteins called Regulators of G Protein Signaling (RGS) temporally modulate this signaling [112]. RGS proteins interact with GTP bound Gα proteins and effect the termination of the signaling cascade by accelerating the hydrolysis of the γ-phosphate of the bound GTP, returning the alpha subunit to the GDP-bound, inactive form. This GTPase accelerating protein (GAP) activity allows for RGS proteins to "fine tune" the G protein signaling cascade. Normal expression levels of RGS proteins provide critical control of cell signaling events, however; alterations in RGS protein expression can often lead to deleterious outcomes, including malignant neoplasias. The link between abnormal expression of RGS proteins and prostate [72], lung [73], ovarian [15], melanoma [14], and breast [81] cancers are just a few examples. As scientific knowledge continues to link aberrant RGS protein expression and disease states, we hypothesize that RGS proteins will provide promising opportunities for development of novel pharmacological interventions [2].

Chapter 3 focused on the development of a novel high throughput screen to discover inhibitors of the $G\alpha_o$: RGS17 ppi. As discussed in previous chapters, RGS17 is a

member of the A/RZ family of RGS proteins that can induce tumor cell proliferation through the cyclic AMP-PKA-CREB signaling pathway [72]. James et al. discovered that RGS17 expression is induced in 80% of lung tumors by an average of 8.3-fold and is also increased in prostate tumors when compared to patient matched normal tissues. RGS17's ability to control the growth properties of tumor cells was evaluated through the construction of lentiviral shRNAs that were utilized to stably knock-down RGS17 transcript levels. In human H1299 non-small cell lung cancer cells, RGS17 levels were decreased resulting in a decrease in the proliferation rate when measured by 3-(4,5-Dimethylthiazol-2-yl)-2,5-diphenyltetrazolium bromide (MTT) cell proliferation assay over 10 days [73]. The *in vivo* significance of RGS17's effects was demonstracted by using athymic nude mice with H1299 human lung cancer cells exhibiting reduced tumor load and growth (average tumor weights reduced from 148 to 23 mg and average tumor volume reduced from 385 to 47 mm^3. Subsequently, RGS17 was identified as a candidate gene for lung cancer and as a susceptibility marker for prostate cancer [144]. Interestingly, the association of the RGS17 gene with prostate cancer susceptibility was determined to be 4.34×10^{-18} (p-value), which represented one of the most significant p values reported in this Genome-wide association study (GWAS) [144]. Considering the high association of RGS17 with lung and prostate cancer and that, in 2014, lung and prostate cancers will account for an estimated 38% of cancer related deaths in males, and lung cancer will account for 26% of all cancer related deaths in females [110], we continue to pursue RGS17 as a novel target for pharmacological intervention.

Chapter 4 presents the investigation and discovery efforts to identify small molecule inhibitors of the $G\alpha_o$: RGS17 ppi. In this study, an AlphaScreen® based high throughput screen in 1536-well format was implemented. The results of this screening campaign led to the identification of four unique chemical entities that represent the first compounds known to inhibit the GTPase acceleration activity of RGS17 (Figure 14).

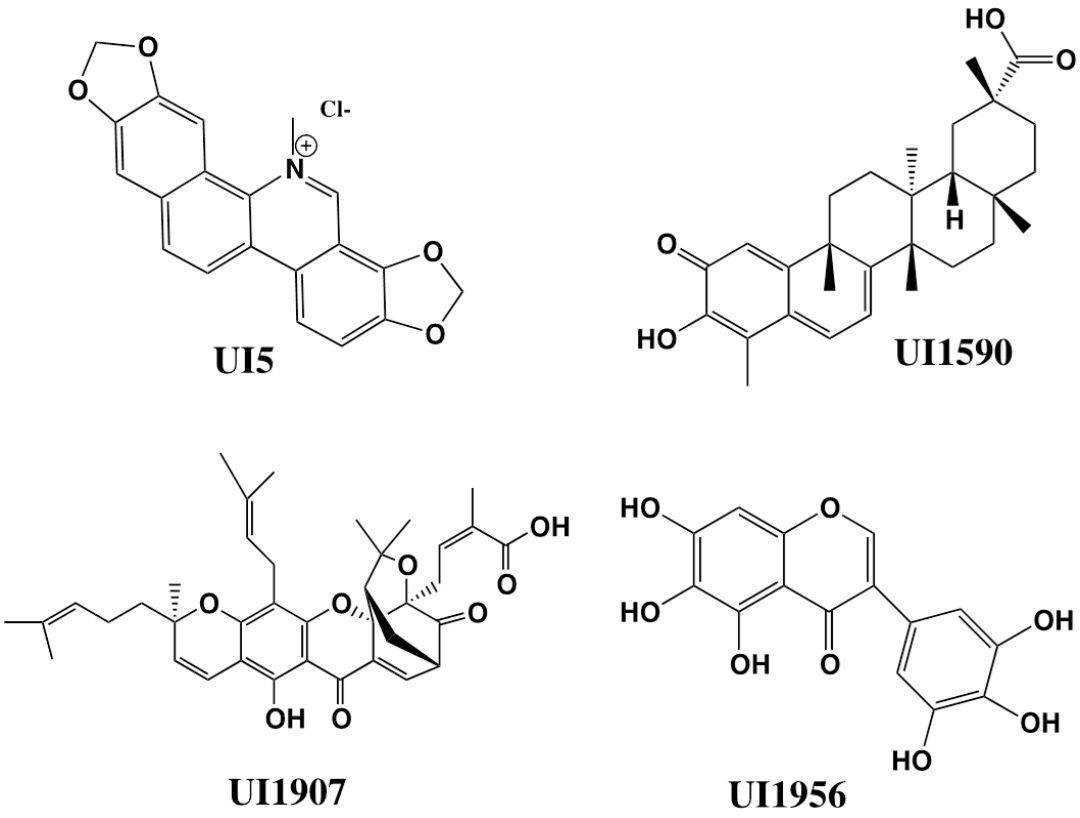

Figure 14. Chemical structures of the newly discovered RGS17 inhibitors. These four unique chemical structures represent the first in class RGS17 inhibitors with biochemical activity and a unique mechanism of action. UI1956 exhibited selectivity for RGS17 over RGS8 and RGS4. UI1590 and UI5 also exhibited selectivity but were found to also have activity against RGS4.

Furthermore, it is recognized that substructures in these compounds may provide opportunity for chemical reactivity (such as Michael Acceptors), and previous work on other RGS protein inhibitors widely identified covalent modifying compounds. These previously published compounds, while profoundly useful, are less desirable for drug development because of their mechanism of action [4, 126, 134, 137]. Interestingly, three compounds UI5, UI1590, and UI1907 were also identified in a separate HTS campaign as having activity against RGS4 [142]. Compared to the previously published data from Monroy et al., UI5 was 10-fold more selective for RGS17, UI1907 was similarly active

against both RGS4 and RGS17 and UI1590 was found to be more selective for RGS4 by ~8-fold [142]. This chapter presents the discovery and characterization of the first RGS17 GAP inhibitors.

Materials and methods

Protein expression and purification

$G\alpha_o$ was purified as described previously [111]. In brief, 6x-his-tagged $G\alpha_o$ was expressed and purified from transformed BL-21 (DE3) bacteria as described with the exception of 1 mM tris(2 carboxyethyl) phosphine hydrochloride (TCEP) in the buffer in place of 1 mM dithiothreitol (DTT) as the reducing agent. Protein purity was >95%, and the concentration of active G protein was determined by GTP$\gamma[S]^{35}$ binding as described previously [5]. RGS17 was purified as previously described [111]. This procedure resulted in ~95% pure RGS17 (20 mg at 1.2 mg/mL). Purity was determined by coomassie stain and densitometry.

Chemical biotinylation of $G\alpha_o$

$G\alpha_o$ proteins were biotinlyated as previously described using EZ-link Biotin-BMCC (Thermo scientific, Rockford, IL) [111]. Protein was labeled at a 5:1 biotin/protein ratio following manufacturer protocols. Fractions were pooled and concentrated to 1.66 mg/mL using an ultracel 10k centrifugal filter (Millipore, Billerica, MA) and protein purity was >95%. The concentration of active G protein was determined by using GTP$\gamma[S]^{35}$ binding as described previously [5].

Z factor calculation in 1536 well format

Experiments were performed in Nunc (Thermo scientific, Rockford, IL) 1536-well white flat-bottom plates, and samples were read on a Perkin Elmer EnVision Alpha Multimode plate reader. All data were collected using EnVision software and analyzed with Graphpad Prism 6.0 (Graphpad software, San Diego, CA).

The 1536-well plates were used to determine the positive and negative control values for the protein interaction assay. In total, 768 wells of the plate were –AMF and represented no protein: protein interaction (background), and 768 wells contained +AMF, which supports the high-affinity protein: protein interaction (ppi) (maximal signal). In total, 144 µL of anti-GST acceptor beads and 240 µL streptavidin donor beads were coupled to RGS17–anti-GST and $G\alpha_o$-biotin–streptavidin at a 30 nM concentration. This was completed in either 6 mL or 10 mL of assay buffer (AlphaScreen Buffer: ASB) (50 mM HEPES, 100mM NaCl, 0.1% Lubrol, 1% bovine serum albumin [BSA], pH 8.0). The RGS17-anti-GST coupling was completed in 6 mL while the $G\alpha_o$-biotin–streptavidin was completed in 10 mL due to the need to split this sample into two sets for +AMF and –AMF conditions. The protein/bead mixtures were incubated in the dark on ice for 30 min. Upon completion of coupling, the RGS17–anti-GST bead mixture was resuspended in a total of 12 mL of assay buffer. The $G\alpha_o$–biotin–streptavidin bead mixture was split into two tubes of 5 mL each. One tube was combined with 10 mL of assay buffer without AMF or GDP for the no-binding control (-AMF). For the positive binding control, the second tube received 10 mL of assay buffer that also contained a final concentration of 50 µM NaF, 50 µM $MgCl_2$, 50 nM $AlCl_3$, and 5 µM GDP (+AMF) and was incubated on ice for 10 min. Then, 4.5 µL of the RGS17–anti-GST mixture was added to each well of a total of 1536 wells in a 1536-well plate. In total, 768 wells received 4.5 µL of $G\alpha_o$–biotin–Streptavidin beads with AMF and 768 wells received 4.5 µL of $G\alpha_o$–biotin–Streptavidin beads without AMF using a FlexDrop IV (PerkinElmer). The plate was incubated in the dark for 1.5 hr and read at room temperature using the EnVision plate reader.

A Z-factor was calculated using the following equation: $Z\text{-factor} = (1-3x(\sigma p+\sigma n))/(|\mu p-\mu n|)$, where σ represents the standard deviation of positive and negative (binding and nonbinding) (p, n) controls, and µ represents the mean of positive and negative control values. Positive controls were determined using the 768 wells containing

AMF and GDP, resulting in a $G\alpha_o$: RGS17 ppi. The negative controls were determined from the 768 wells that lacked AMF and GDP, resulting in no protein: protein interaction.

Initial AlphaScreen HTS in miniaturized format

In total, 5360 compounds from the SPECTRUM and NDL-3000 chemical libraries were screened at a concentration of 40 µM. White Nunc 1536-well plates (Thermo Fisher Scientific, Waltham, MA) containing 1,280 compounds and 128 wells of DMSO controls were used. RGS17–anti-GST and $G\alpha_o$–biotin–streptavidin beads were prepared as previously described. In brief, 100 µg (20 µL) of beads were coupled to 20 ng (10 nM) of each binding partner ($G\alpha_o$: RGS17) and incubated for 30 min on ice. Then, 4.5 µL of RGS17–anti-GST beads were added using a FlexDrop IV (PerkinElmer, Waltham, MA) and incubated for 10 min with compound while the $G\alpha_o$–biotin–streptavidin beads were incubated with AMF. After incubation, 4.5 µL of the $G\alpha_o$–biotin–streptavidin bead/protein mixture was added to compound-containing wells and incubated for 1.25 hours and read at room temperature using the EnVision plate reader with monochromators.

Dose-response experiments

Experiments were carried out similarly to the high-throughput AlphaScreen® assay except this was completed using Corning 384-well white flat bottom plates and the final total volume was 60 µL. First, 20 µL of RGS17–anti-GST beads at a final concentration of 10 nM were added to each well. Then, 20 µL of compounds in a half log dilution series to yield a final range from 1 nM to 100 µM was added to RGS17–anti-GST beads and incubated for 10 min in the dark. Finally, 20 µL of $G\alpha_o$–biotin–streptavidin beads were then added in the presence of AMF and GDP. Negative controls were determined in the absence of AMF and compound. Maximum binding was determined in the absence of compounds but in the presence of AMF and GDP.

AlphaScreen TrueHits counter screen

Compounds that inhibited the protein: protein interaction with an IC50 <20 µM were counter screened in the TrueHits control assay containing biotinlyated GST. This was completed using Corning 384-well white flat bottom plates (Corning, New York). Biotin–GST binds both the anti-GST and streptavidin-coated beads, bringing the beads together artificially and forcing an interaction. Compounds were diluted to yield a range from 1 nM to 100 µM, and 20 µL was added to each well. In 5.28 mL of ASB, 211 ng (42.24 µM) of anti-GST beads was incubated with 300 pM biotin–GST for 30 mins at room temperature. Then, 211 ng (42.24 µL) of streptavidin beads was added and incubated for 30 min on ice. After conjugation was complete, 40 µL of the anti-GST–biotin–GST–streptavidin bead complex was added to each well of compounds (final volume of 60 µL), incubated for 10 min, and read at room temperature on the EnVision plate reader.

Malachite green steady-state GTPase assay

First, stock solutions of each of the 3 components of the developing solution were prepared according to Monroy et al [142]. The RGS17 malachite green assay was conducted using a 5-component mixture, with a 1 min spin at 500xg between each addition. The first component was 10 µL of compound diluted into Malachite Green Assay Buffer (MGB; 50 mM HEPES at pH 7.5, 100 mM NaCl, 5 mM EDTA, 10 mM $MgCl_2$, 0.01% lubrol) into a clear 384-well plate. Compounds were seeded using a half-log dilution with the highest final concentration of compound at 100 µM down to 1 nM. The second component dispensed was 10 µL of a 4x stock of RGS17 with the target final concentration of 1 µM, diluted in MGB. After 30 min incubation, 10 µL of the third component, a 4x stock of $G\alpha_{i1}$ diluted in MGB, was dispensed at a concentration of 4 µM into each well with a final target concentration of 1 µM. This was incubated for a minimum of 5 min. Then, 10 µL of the fourth component, 4x GTP at 1.2 mM diluted in

MGB, was added to the wells, with a final concentration of 300 µM. To terminate the reaction, 10 µL of a Developing Solution (DS) (50:12.5:1 malachite: molybdate: Tween-20) was added to each well using a Microlab Star liquid handling robot (Hamilton Robotics; Reno, NV), this achieved a final ratio 4:1 (sample: developing solution) absorbance was read at 642 nm.

Differential scanning fluorimetry

All Differential Scanning Fluorimetry experiments were carried out using white 384-well µltraAMP PCR plates (Sorenson BioSciences; Salt Lake City, Utah). All experiments were carried out as previously described by Phillips and Hernandez de la Pena [130]. In brief, a 1: 2000 dilution of Sypro Orange was made by adding 1 µL of Sypro Orange to 2 mL of PBS at pH 7.5. First, 1.2 mg/mL protein was incubated with 50 µM of each compound at room temperature for 15 min in a 10 µL volume. Upon completion of the incubation, 110 µL of the Sypro Orange-PBS solution was added to each compound/protein mixture. This yielded a final volume of 120 µL containing 0.1 mg/mL protein. Finally, 20 µL of the Sypro Orange/compound/protein mix for each compound and RGS17 or $G\alpha_o$ proteins was added to four wells of the 384-well plate. The experiment was run on the Roche LightCycler 480 (Roche, Switzerland) using a two-step method. Starting with a 25 °C baseline step and a second step with a target temperature of 95 °C with continuous acquisition and set acquisition rate of 3 readings per ^oC. All data was collected using the Roche LightCycler data acquisition ability and analyzed with Graphpad Prism 6.0, using first and second derivatives of the fluorescent melting curves.

Isothermal titration calorimetry

RGS17 was concentrated in ITC sample buffer (50 mM HEPES pH 7.5, 100 mM NaCl and 1 mM beta-mercaptoethanol) at 50 µM. Compounds UI1956 and UI5 were diluted into ITC sample buffer to reach a final concentration of 500 µM. DMSO concentration in both compounds and RGS17 sample was 1% to account for any DMSO

effects. Total injections for UI1956 were set to 5 μL with a duration time of 10 secs and spacing of 240 secs and for UI5 were set to 12 μL with a duration time of 24 secs and spacing of 240 secs. The total amount of injections for UI1956 and UI5 were 32 and 23 injections, respectively. All experiments were conducted on a GE MicroCal VP-ITC System (General Electric, Piscataway, NJ). at 25 ^{o}C. Heats of dilution were determined by averaging the heat evolved by the last five injections and subtracted from the raw data. The values for affinity, stoichiometry and change in enthalpy were then determined using the ORIGIN software provided by the manufacturer.

Investigation of compound reversibility

First, stock solutions of all four compounds were made at a 3x concentration or 300 μM for a final concentration of 100 μM. The final DMSO concentration in the assay was 1% (v/v). Next, RGS17 and $G\alpha_o$ were diluted into 300 μL of assay buffer (AlphaScreen Buffer: ASB) (50 mM HEPES, 100mM NaCl, 0.1% Lubrol, 1% bovine serum albumin [BSA], pH 8.0) at a 3x concentration of 30 nM. Next, 7.2 μL of AlphaScreen beads were added to each separate protein. The protein and bead solution was incubated on ice for 30 mins in the dark. Upon completion of protein: bead conjugation, 600 μL of ASB was added to RGS17. To the $G\alpha_o$ sample, 279 μL of AMF (final concentration of 10 μM NaF, 10 μM $MgCl_2$, 10 nM $AlCl_3$, and 5 μM GDP) and 321 μL of ASB were added. The RGS17 sample was split into 90 μL tubes and 90 μL of each compound or DMSO vehicle was added to the RGS17: bead mixture and incubated for 15 mins. Upon completion of compound incubation, the RGS17: bead mixture was washed 3 times with 1.8 mL of ASB. The RGS17 protein: bead samples were pelleted after each wash through centrifugation at 15, 000 x g for 10 mins. After the final wash step, the RGS17 protein: bead pellet was resuspended in 180 μL of ASB. Next, to a 384 white plate, 30 μL of the RGS17 protein: bead: compound samples, either washed or unwashed, were added to each well in triplicate. Finally, 15 μL of the $G\alpha_o$ protein: bead sample was

added to each well. The plate was incubated at room temperature in the dark for 1.25 hours and read on a Synergy2 plate reader (Biotek, Wisnooski, VT) with a sensitivity setting of 200, excitation at 680 nm, and emission read at 570 nm. All data were analyzed with Graphpad Prism 6.0. All data were compared to DMSO controls and corrected for possible bead loss due to washing steps.

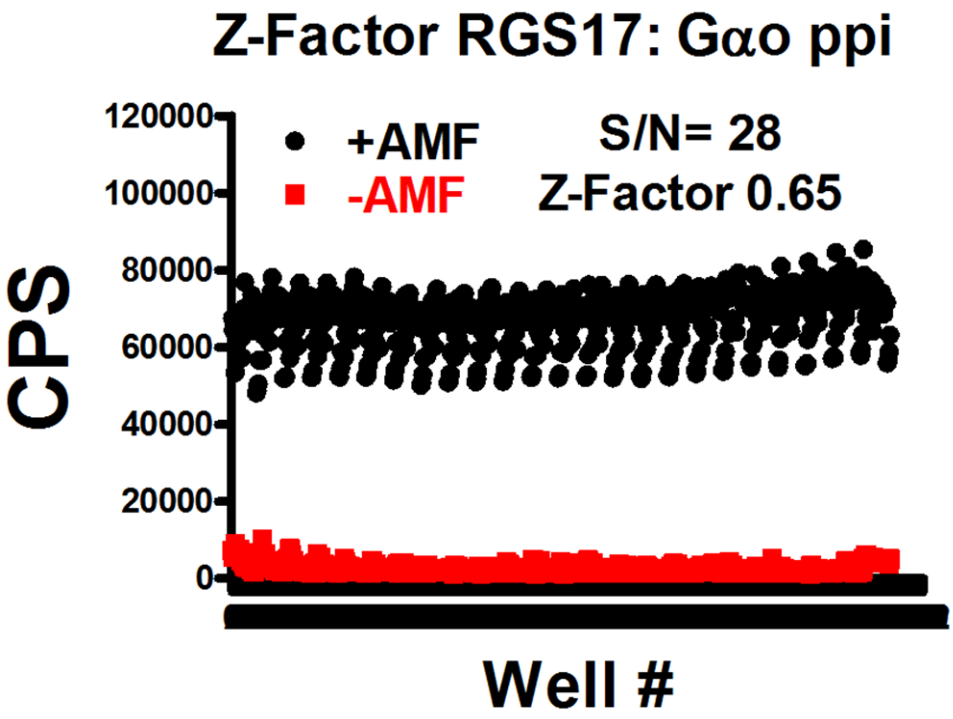

Figure 15. Determination of the Z Factor and screening window in 1536-well format. In a 1536-well plate, 768 wells were used as a positive control (+AMF) and 768 wells were deprived of guanosine diphosphate (GDP) and AMF, representing the negative control. The signal-to-noise ratio of 28, coupled with the Z factor of 0.65, allows for a large screening window to discover compounds that inhibit the RGS: $G\alpha_o$ protein: protein interaction greater than 50%. CPS, counts per second.

Results

Miniaturization and assay validation

768 wells of a 1536-well plate were used for positive controls in the presence of AMF, which affords the high-affinity $G\alpha_o$: RGS17 complex, while the remaining 768 wells were used as negative controls without AMF in which the formation of $G\alpha_o$: RGS17 complex is not observed (Figure 15). The calculated Z factor was determined to be 0.65 with a signal-to-noise ratio of 28. This Z factor is well above the commonly held threshold value of 0.5, indicating a screening paradigm suitable for high-throughput screening (HTS) [131].

AlphaScreen HTS

The primary biochemical screen was designed to identify compounds that function as inhibitors of the $G\alpha_o$: RGS17 ppi. This was accomplished by miniaturizing our previously published HTS paradigm from a 384-well plate-based format to a 1536-well format. This allowed an increase in throughput from 1,000 compounds/ hour to over 7,500 compounds/ hour. We interrogated the MicroSource SPECTRUM Diversity and NDL-3000 libraries (Figure 16). We used a cutoff of 50% inhibition or greater to consider a compound as an initial hit. We observed a 4.26% initial hit frequency (99 compounds) with 41 of those compounds confirmed using a single point biotinlyated GST counter screen control assay (PE Truehits paradigm) (Table 5). Of these 41 initial hits, seven compounds exhibited an IC50 <20 μM, yielding a confirmed hit rate of 0.3%. These seven compounds were then analyzed by dose-response control experiments using the non-target TrueHits control assay. Four compounds were found to have no activity in the TrueHits assay when compared to the $G\alpha_o$: RGS17 ppi (Figure 17). These four compounds (Figure 14) were then chosen for follow-up studies.

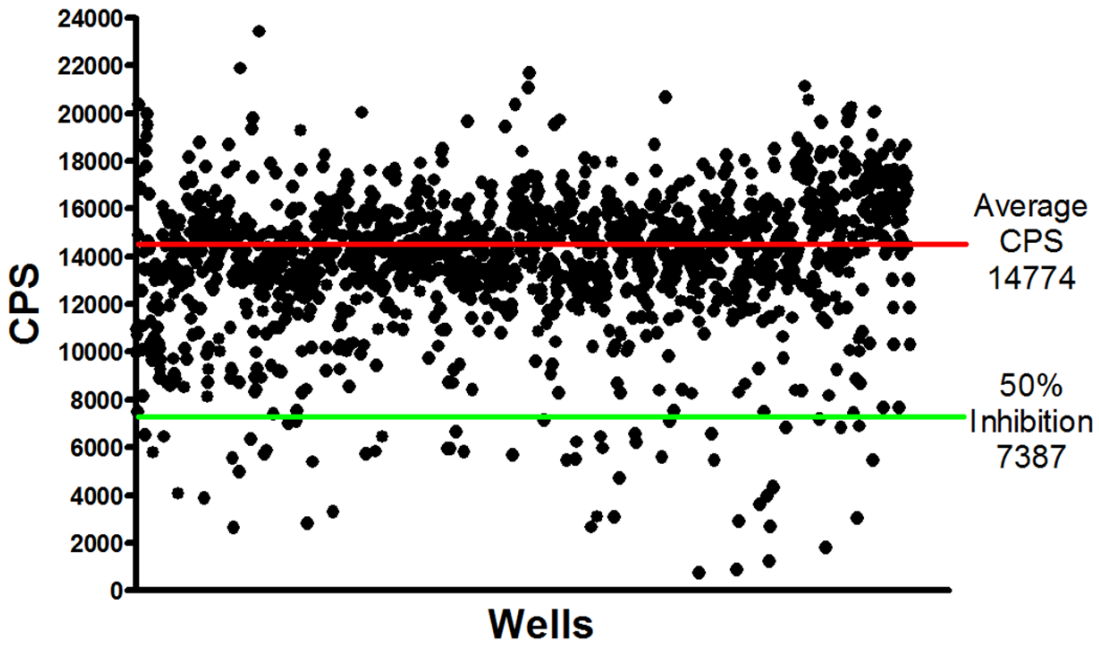

Figure 16. High-Throughput screening of the MicroSource SPECTRUM and NDL3000 libraries. A representative plate of the initial screen of the over 5,000 compounds was conducted in the 1536 well format.

Analysis of ligand binding using differential scanning fluorimetry (DSF)

Further evaluation of the compounds designated UI5, UI1590, UI1907 and UI1956 was conducted using Differential Scanning Fluorimetry (DSF). This method allows for the rapid measurement of protein stability based on the melting transition (T_m) of the target protein that is bound by ligand. A shift of T_m indicates a change in protein stability to melting due to stabilization added by the small molecule binding to the target protein. The four lead compounds were incubated at 50 μM with RGS17 or $G\alpha_o$ in the presence of Sypro Orange. In aqueous solution, the fluorescence emission from the dye is very weak. However, when the dye binds to hydrophobic regions of a protein a significant increase in florescence intensity is observed [145]. The hydrophobic regions of a native, fully folded protein in solution are generally buried within the protein and therefore not

accessible to the dye resulting in little fluorescence emission. When the protein unfolds the dye molecules can bind to the exposed hydrophobic regions resulting in fluorescence. Three of the compounds were found to affect the T_m of RGS17, while UI1907 was found to alter the thermal stability both RGS17 and $G\alpha_o$.

Table 5. High-Throughput Screening Results

Spectrum and NDL3000 Libraries	5,360 Compounds	Hit Rate
Initial AlphaScreen Hits	**134 Compounds**	**2.5%**
Non-Hit Single Point TrueHits Counter Screen	**41 Compounds**	**0.76%**
Compounds with Favorable IC50s (<20μM) and Structures	**7 Compounds**	**0.13%**
Compounds Dose-Response Curves, IC50s RGS17 vs TrueHits	**4 Compounds**	**0.07%**
RGS17 Specific Differential Scanning Fluorimetry Compounds	**3 Compounds**	**0.056%**
"True Hits" Post Filtered Compounds	**3 Compounds**	**0.056%**

[a]5,360 compounds were screened and 99 were initial hits (>50% inhibition).

[b]Primary hits were reconfirmed by dose-response curves and in the malachite green GTPase assay.

[c]Seven compounds resulted in IC50 values <20 μM.

[d]Of these 7 compounds, 3 were specific for RGS17 versus $G\alpha_o$ by differential scanning fluorimetry assay.

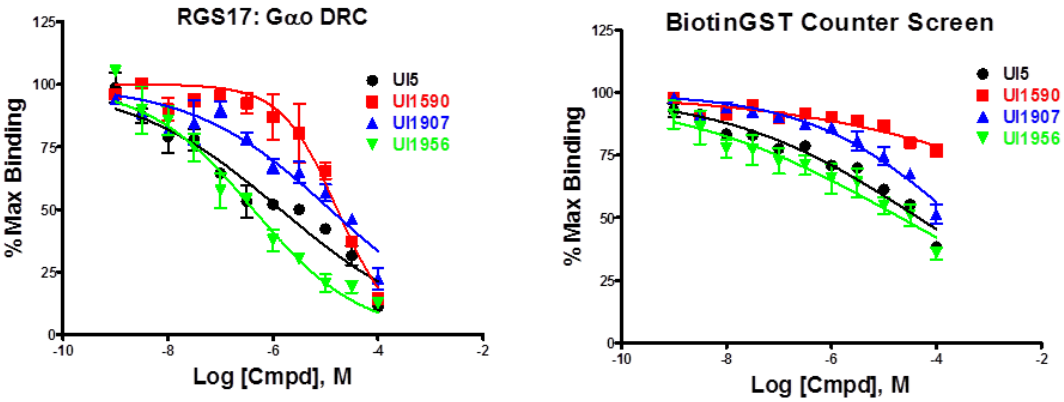

	UI5	UI1590	UI1907	UI1956
HillSlope	-0.3070	-0.8225	-0.3292	-0.4284
IC50	1.386e-006	1.681e-005	1.226e-005	4.232e-007

	UI5	UI-1590	UI-1907	UI1956
HillSlope	-0.2349	-0.1631	-0.3068	-0.2030
IC50	4.589e-005	0.3096	0.0002294	2.099e-005

Figure 17. Determination of the RGS17: $G\alpha_o$ protein: protein interaction by AlphaScreen®. Four compounds (UI5, UI1590, UI1907 and UI1956) were determined to inhibit the interaction of RGS17 with $G\alpha_o$ in a dose dependent manner.

UI1907 can be considered a non-specific RGS17: $G\alpha_o$ protein: protein interaction inhibitor as it affects both binding partners, decreasing the thermal stability of the $G\alpha_o$ subunit, as well as affecting the stability of RGS17. UI5, UI1590 and UI1956 shifted RGS17s T_m by 2.08 ^oC, 1.377 ^oC and 1.03 ^oC, respectively (Figure 18).

Inhibition of RGS17 accelerated $G\alpha_{i1}$ GTPase activity

Next, we examined the ability of our lead compounds to inhibit the "GAP" activity of RGS17. The lead compounds were tested using a previously described malachite green assay [142], which allows for the detection of free phosphate liberated during the enzymatic cleavage of GTP to GDP by Gα subunits (Figure 19). In this assay UI5, UI1590, UI1907, and UI1956 were determined to inhibit RGS17's activity with IC50s of 12 µM, 6 µM, 10 µM and 35 µM, respectively (Figure 20).

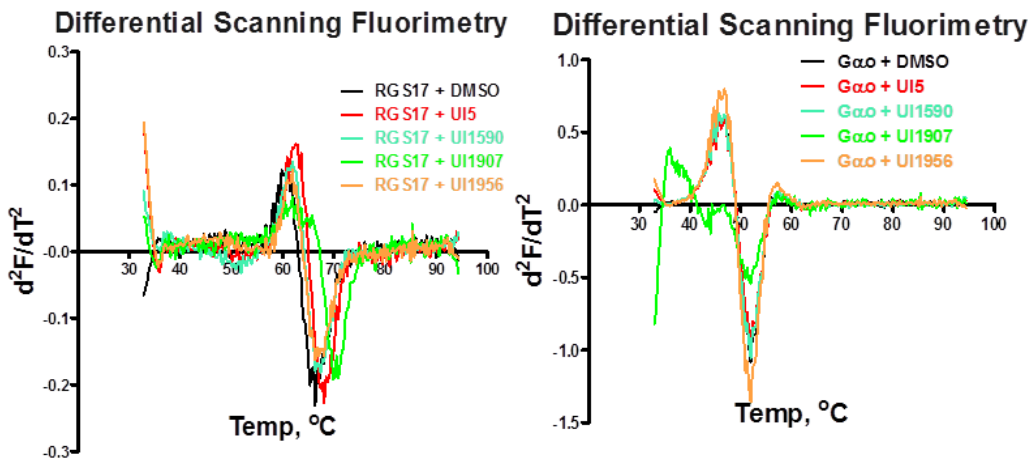

Figure 18. Measure of protein stability upon ligand binding through Differential Scanning Fluorimetry (DSF). All four compounds were tested for specific binding to the RGS protein versus the $G\alpha_o$ subunit when compared to DMSO controls. UI5, UI1590 and UI1956 were found to stabilize RGS17 against thermal denaturing. UI1907 was found to bind both the RGS and G protein subunit in a non-specific manner.

Characterization of the ligand binding properties through isothermal titration calorimetry (ITC)

ITC was used to determine the binding properties of the lead compounds in solution. ITC allowed for the determination the dissociation constant (Kd) and stoichiometry (n) of the interaction between RGS17 and the inhibitor compounds. Two compounds, UI5 and UI1956, were amenable to ITC and exhibited high affinity for RGS17 with Kd's of 1.02 µM and 714 nM, respectively (Figure 21). UI5 exhibited a stoichiometry of 0.82, while compound UI1956 was determined to bind with a stoichiometry of 0.33. The corresponding Gibbs free energies of the bindings were -8168 cal/mol for UI5 and -8389 cal/mol for UI1956. Decomposing the binding thermodynamics revealed that these two compounds have favorable binding enthalpies. While UI5 exhibited the lower enthalpy (ΔH=-148 cal/mol), the larger entropic ($T\Delta S$=8020.235 cal/mol) component of this compound fully compensated for this significantly lower enthalpy. UI1956 was

determined to have a significantly higher enthalpy component (ΔH=-2158 cal/mol), as well as a lower entropic component (TΔS=6231.335 cal/mol). Interestingly, ITC experiments showed that UI1956 had the most favorable binding enthalpy and the highest binding affinity of the two compounds. One compound, UI1590 was not soluble at the high concentration of ligand required in our buffer system. The results from the four different biochemical techniques led us to further evaluate the mechanism by which these compounds might be eliciting their effects on RGS17.

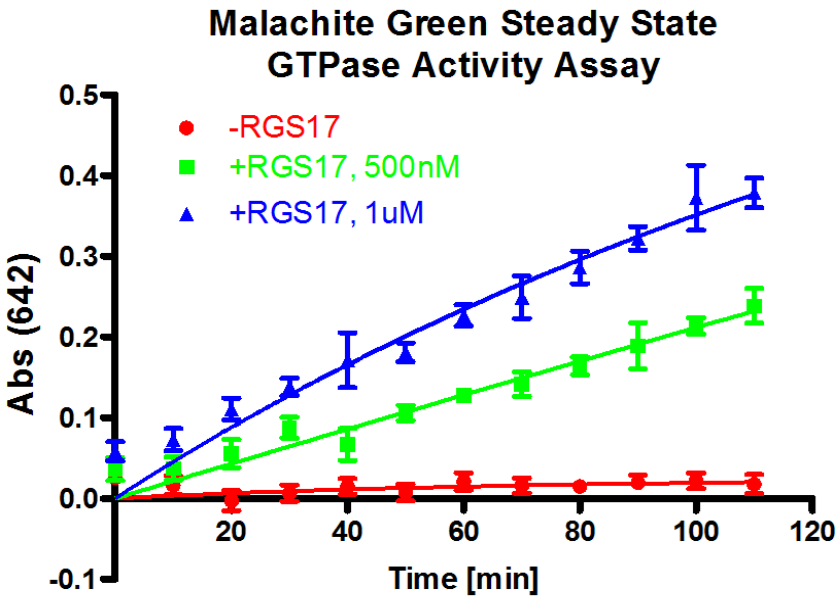

	-RGS17	+RGS17, 500nM	+RGS17, 1μM
Best-fit values			
Vmax	0.03717	~ 9.227	1.391
Km	90.78	~ 4257	295.9

Figure 19. Characterization of the Malachite Green Steady State GTPase Assay. Using a $G\alpha_i$ double mutant protein with an accelerated K_{off} for GDP exchange and decrease K_{cat} for GTPase activity we can monitor the effect of RGS17 on the intrinsic GTPase activity of the $G\alpha_i$ subunit. (Figure adapted from Monroy CA, Mackie DI, Roman DL. PLoS One. 2013 April) [142]

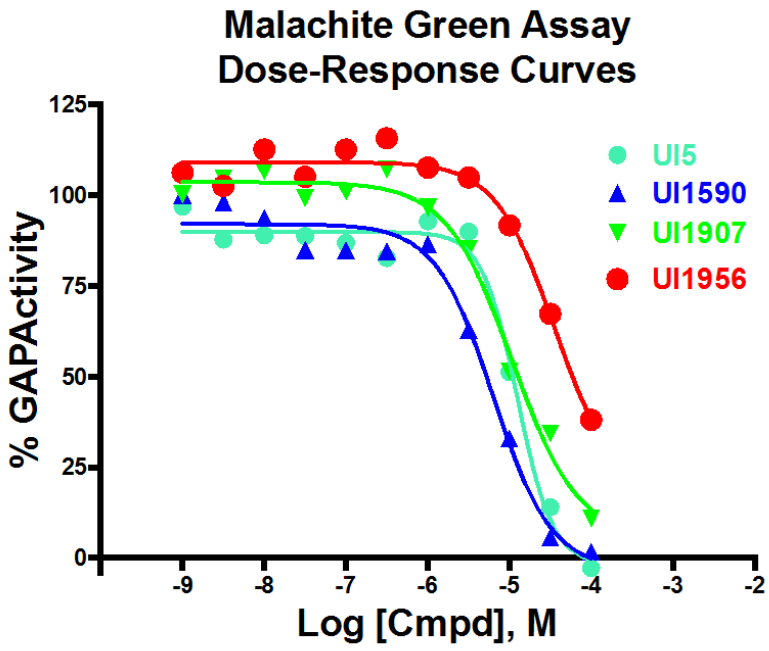

	UI5	UI1590	UI1907	UI1956
HillSlope	-2.006	-1.227	-1.081	-1.205
IC50	1.252e-005	6.359e-006	1.079e-005	3.551e-005

Figure 20. Inhibition of RGS17's GAP activity with $G\alpha_o$ by malachite Green assay. All four compounds were tested for inhibition of the GTPase acceleration activity of RGS17 in the malachite green steady-state GTPase activity assay. UI1590 exhibited the most potent activity with an IC50 of 6.4 µM. Data represents n=3, normalized in triplicate.

Investigation of compound reversibility

To determine the reversibility of inhibition of the RGS17: $G\alpha_o$ protein: protein interaction, RGS17 was treated with 100 µM compound. This concentration was determined through the earlier dose-response experiments to inhibit the AlphaScreen assay >75% for each of the compounds (UI5, UI1590, UI1907 and UI1956). Upon completion of incubation with compounds, each sample was washed three times with ASB buffer.

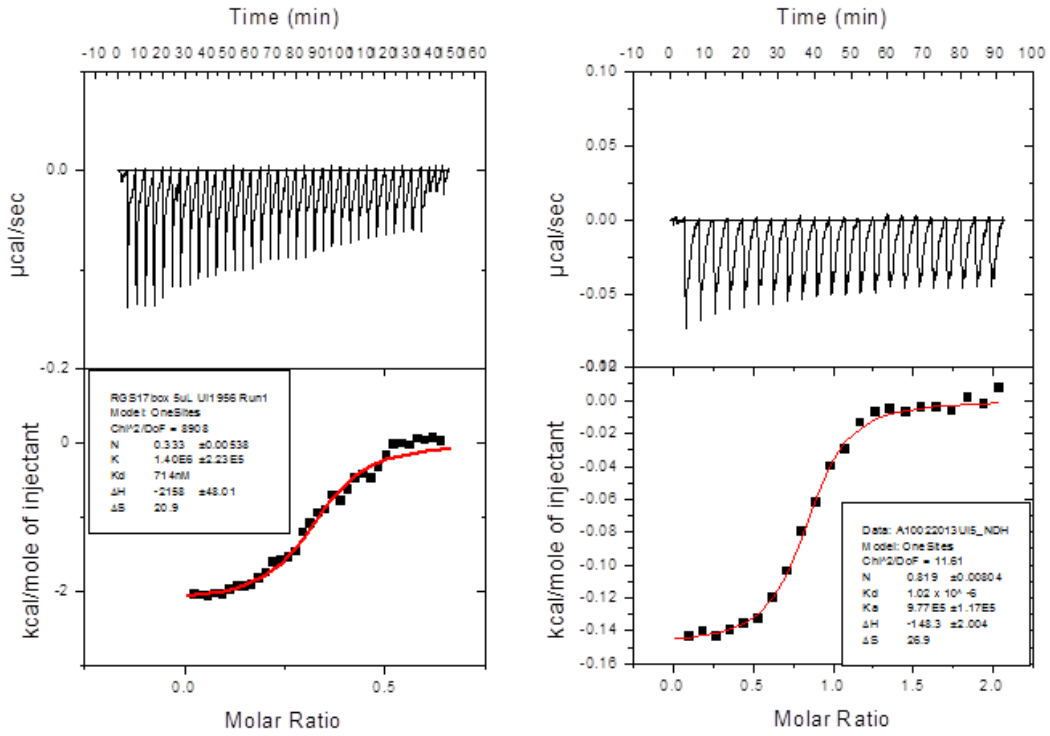

Figure 21. Determination of dissociation constants through Isothermal Titration Calorimetry (ITC). UI5 and UI1956 were further characterized through ITC and their dissociation constants were calculated to be 1.02 µM and 0.714 µM, respectively. UI1590 and UI1907 were not amendable to ITC due to solubility issues at the increase ligand concentration. UI5 exhibited a stoichiometry (n) of 0.819 and UI1956 was determined to have a stoichiometry (n) of 0.333.

This method reverses the equilibrium of any compounds that are non-covalent, while not affecting any covalent modifiers. In this experiment, all four compounds were found to fully inhibit the maximum binding of RGS17 to the G alpha subunit (Figure 22). The corresponding washed samples were found to restore binding when compared to vehicle (DMSO) treated and washed samples. This restoration of binding confirms the reversible nature of the UI series of compounds, but further validation of non-covalent modification will be pursued in future studies.

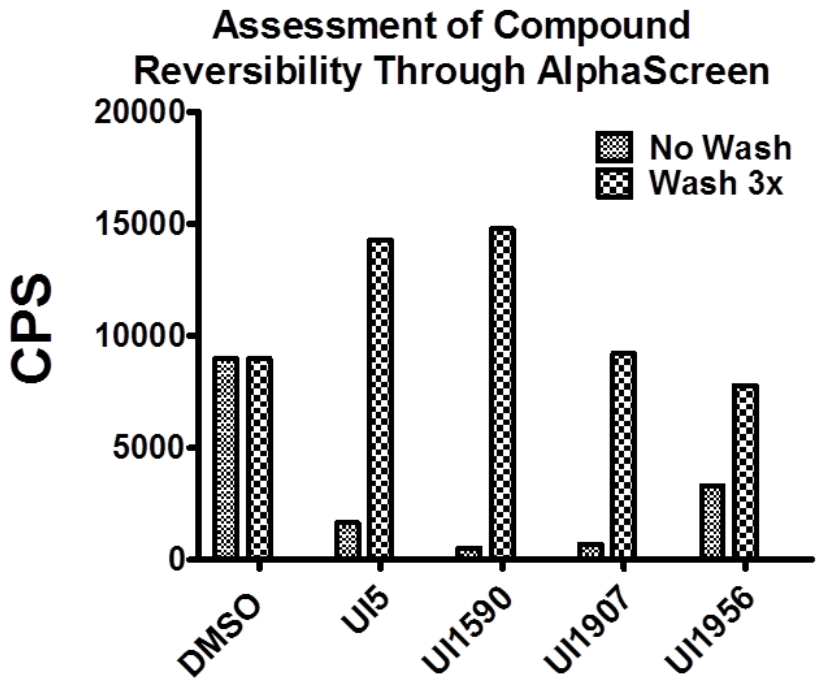

Figure 22. Exploring the mechanism of action of the UI Series of RGS17 inhibitors. RGS17 was incubated with a 100 mM concentration of inhibitors (UI5, UI1590, UI1907 and UI195). Upon completion of the incubation, samples were split into two separate conditions (washed and unwashed) and assayed using AlphaScreen® technology. Inhibition by all four compounds was found to be reversible by the restoration of the AlphaScreen® signal when compared to vehicle controls (DMSO). Unwashed samples retained the signal suppression by the UI series of small molecule protein: protein interaction inhibitors.

Discussion

Small molecule inhibitors of RGS proteins can act to disrupt the RGS: Gα interaction. The inhibition of this interaction leads to prolonged G protein activation. These signaling cascades can be temporally and aberrantly blunted by the overexpression of RGS proteins in different disease states [2, 55]. These examples have led to an increased interest in the pharmacological targeting of RGS proteins for therapeutic intervention [7, 133, 137, 146-148]. Investigation of RGS17 has shown that it is localized to the central nervous system, exhibiting prominent neuronal expression in healthy

individuals [70, 114, 149]. RGS17's expression pattern changes during pathological states, including being upregulated in both lung and prostate cancers [72-73]. In these oncogenic states, RGS17 acts to suppress the normal $G\alpha_{i/o}$ mediated inhibition of adenylyl cyclase. This leads to unregulated adenylyl cyclase activity (i.e. overproduction of cAMP) and increased activation of the PKA-CREB signaling pathway. The up-regulation of CREB is linked to the differential expression of several strong candidate CREB responsive gene products such as oncogenes *FoxP2*, *CyclinD1*, and *KCIP1*, as well as tumor suppressors *FoxO4* and *Hnt*. Microarray studies determined that the increase in RGS17 increased the expression of a member of the forkhead box P (FoxP1-4) family, FoxP2. The FoxP family members have been implicated in several different oncogenic states as FOXP1 is a tumor suppressor in breast cancer [150] and has been suggested to play a role in prostate cancer [151]. FOXP4 expression is down-regulated in kidney cancer [152] and inactivated by translocation in several breast cancer cell lines. In a recent study, FOXP2 has also been implicated with cancer as Campbell *et al* found FOXP2 overexpression as a strong discriminator between normal lymphocytes and multiple myeloma [153]. Further investigation of FoxP2 found that its expression is significantly linked to tumor aggressiveness; especially in non-fusion type prostate cancer [154].

Next, Cyclin D1 is a key regulator of the G1 phase progression of the cell cycle [155]. Recent studies looking at Cyclin D1 as a potential therapeutic target for the treatment of cancer found its overexpression to be associated with non-small-cell lung cancer [156-158], as well as metastatic prostate cancer to bone [155]. Perhaps more important is the link between *in vitro* and *in vivo* data that indicates a role of sustained overexpression of Cyclin D1 in androgen-independent sub-cultured prostate cancer cell lines [159]. Another gene affected is KCIP1, Kinase C Inhibitor Protein 1, also known as 14-3-3ε. In lung adenocarcinoma, KCIP1 was identified as a putative oncogene by a comprehensive functional genomic approach [160].

Dysregulation of RGS17 expression also effects the expression of two important tumor suppressor genes, *FoxO4* and *Hnt* [72]. FoxO4 encodes the forkhead box protein O4. The FoxO family of transcription factors plays critical roles in a number of physiological and pathological processes including cancer [161]. A recent investigation into the role that FoxO4 plays in prostate cancer identified metastasis-suppressor activity through counteracting the PI3K/AKT signaling pathway [162]. Also of interest is the newly discovered low expression of the FoxO4 gene in non-small cell lung cancer [163], the other cancer type where RGS17 over expression has been implicated in tumor development. Further investigation into the role of FoxO4 in non-small cell lung cancer found the loss of FoxO4 correlated with an increase in epithelial-mesenchymal transition [163].

Since all of these significant genes are differentially regulated by the loss or gain of RGS17 expression through the PKA-CREB signaling pathway, it can be hypothesized that repression of these tumor suppressors, or a combination of the repression with the activation of CREB-responsive genes may lead to or may be necessary for the proliferation of tumor cells. An RGS17 inhibitor could act to mitigate the effects of RGS17 up-regulation and return the cAMP-PKA-CREB signaling cascade to normal physiological levels by prolonging the activation of the $G\alpha_{i/o}$ subunit [118, 122]. To this end, we hypothesize that the development of RGS17 specific small molecule inhibitors may be therapeutically beneficial for the treatment of these oncogenic states.

Chapter 3 reported the first RGS17 inhibitors, RL1 and RL2 [111]. These compounds were found to be selective for RGS17, but while proving useful as proof-of-concept compounds, they contained unattractive chemical moieties such as the paraquinone. These quinones are well-known Michael acceptors, and cellular damage can occur through alkylation of crucial cellular proteins and/or DNA [139]. Additionally, quinones are highly redox active molecules which can redox cycle with their semiquinone radicals, leading to formation of reactive oxygen species (ROS), including

superoxide, hydrogen peroxide, and ultimately the hydroxyl radical. Thus, this chapter describes a larger-scale investigation of chemical space by screening the SPECTRUM MicroSource and NDL3000 libraries in search of more attractive molecular scaffolds. During the campaign described here, four unique RGS17 inhibitors were discovered.

Of these four compounds, three were specific for RGS17. UI5 is commonly known as sanguinarium chloride. It consists of a planar conjugated polyaromatic ring system that contains a charged nitrogen atom. UI1590 is the known pre-therapeutic anticancer compound celastrol [164], a pentacyclic triterpenoid that contains a quinone methide. Celastrol is a natural product isolate from T. regelii. This plant known as 'Thunder God Vine' and has been historically used in traditional Chinese medicine [165]. It exhibits anticancer activity against the HSP90 and MAPKK pathways [164, 166-168]. Interestingly, crosstalk between PKA and MAP kinase pathways has been previously identified as being important in cell survival and anti-apoptosis in fibrotic lung diseases and lung cancer, as well as playing a role in estrogen signaling in breast cancer cells [169]. UI1956, is known as irigenol, a polyphenolic flavonoid. These three compounds inhibit the *in vitro* protein interaction between RGS17 and $G\alpha_o$ as determined by AlphaScreen® with IC50s of 1.386 µM, 16.81 µM and 0.4232 µM, respectively. Notably, UI1956 exhibited the most potent RGS17 inhibition reported to date.

An issue with previously discovered RGS inhibitors is potentially undesirable mechanisms of action through a covalent cysteine modification. While this does not automatically discount a lead compound from consideration, it does raise concerns about the therapeutic potential as these reactivities can often have deleterious side effects [146]. In the course of these studies, we investigated the sensitivity of RGS17 to thiol modification using N-ethylmaleimide (NEM) (Figure 23). NEM is a small organic compound derived from maleic acid that is reactive toward thiols and is commonly used to modify cysteine residues in proteins and peptides. This Michael acceptor did not inhibit the RGS17: Gα protein: protein interaction (Figure 23), which led us to postulate

that RGS17 is perhaps more resistant to inhibition by cysteine modification than other RGS proteins, a promising development in attempting to target RGS17.

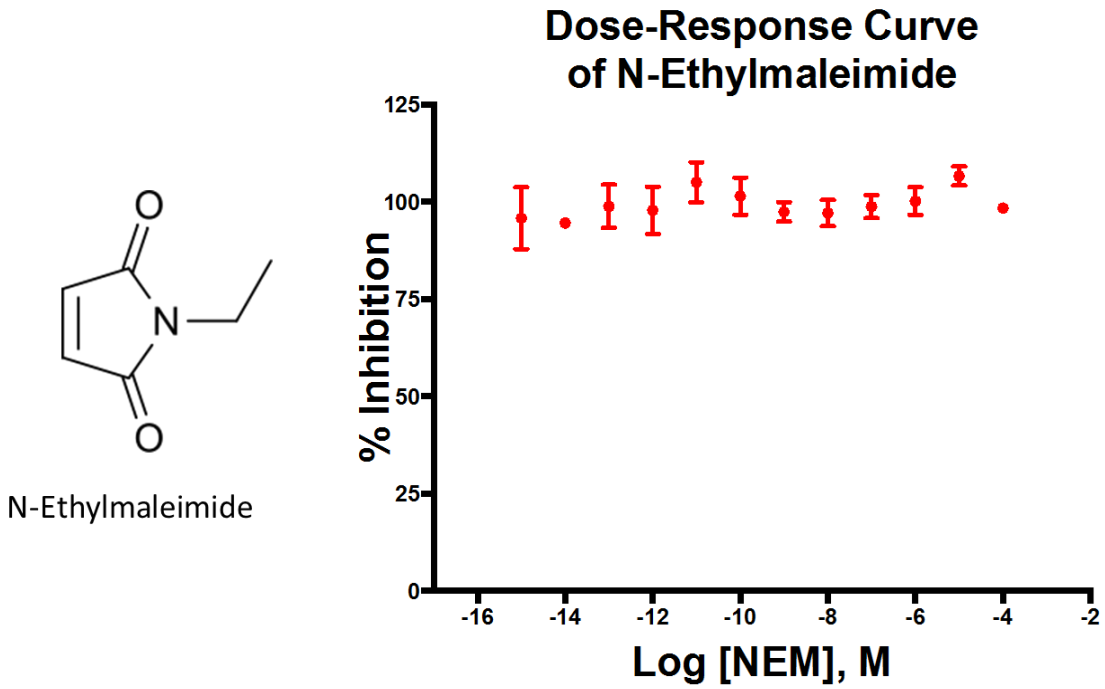

Figure 23. N-Ethylmaleimide is an organic compound that is derived from maleic acid. It contains the imide functional group, but more importantly it is an alkene that is reactive toward thiols and is commonly used to modify cysteine residues in proteins and peptides. RGS17 showed no dose-dependent inhibition when tested against NEM.

These data suggests that the UI series of compounds or related analogues should be useful pharmacological tools for investigating the physiological role of RGS17, as well as provide structural scaffolds as potential pre-therapeutic leads.

In this chapter, the first-in-class inhibitors of RGS17 were characterized and reported. This series of compounds avoids the significant liabilities of many previously discovered RGS inhibitors. This increases their potential as scaffolds for the treatment of lung and prostate cancers, as well as valuable experimental tool compounds for

investigating the pharmacologic modulation of RGS17. Furthermore, all three compounds must be examined for the possibility of inhibiting the RGS17: $G\alpha_o$ protein: protein interaction in living cells. Future directions will focus on characterizing the structure-activity relationship of each of these three unique lead compounds and adapting these studies to determine compound activity in physiological models of RGS17 activity. Also, the activity and selectivity of these compounds in several cancer cellular models in apoptosis and growth arrest and migration, two hallmarks of oncogenesis, must be investigated. This report represents a significant advance in the development of RGS inhibitors as drugs for the treatment of lung and prostate cancer.

CHAPTER V: RESEARCH SUMMARY

Although progress has been made to aid in the prevention, detection and treatment of several cancer types since cancer death rates rose for most of the 20th century until 1991, peaking at 215.1 deaths from cancer per 100,000 [110]. This increase was largely driven by rapid increases in lung cancer deaths among men as a consequence of the tobacco epidemic. Over the past 2 decades, however, there has been a steady decline in the cancer death rates to 171.8 per 100,000 in 2010 [110].

This decline can be attributed to several factors such as advances in prevention, early detection, and treatment. As a result of this decline, it is estimated that 1,340,400 cancer deaths, 952,700 in men and 387,700 in women, have been averted [110].Yet, even with these significant reductions in cancer mortality, 2010, the most recent year with available statics for cancer related deaths, saw a record total of over 500,000 total related deaths in the United States [110]. With over 23% of the total deaths attributed to cancer, cancer became the second leading cause of death following only heart disease. It is evident that even with these advances there is still room for development of safe, effective treatments for the most frequent types of cancer such as lung (in men and women) and prostate (in men) cancers. The goal of this thesis was to address the development and implementation of a novel screening platform for the rapid identification of lead compounds for the inhibition of the RGS17: $G\alpha_o$ protein: protein interaction.

RGS proteins interact with GTP bound Gα proteins and effect the termination of the signaling cascade by accelerating the intrinsic GTPase activity of the G protein. This returns the alpha subunit to the GDP-bound, inactive form, effectively terminating the signaling cascade. Previous studies implicated the upregulation of RGS17 in lung and prostate cancers and showed that through the inhibition of RGS17 the oncogenic phenotype can be reversed [72-73]. These results led to the hypothesis that the

pharmacological inhibition of RGS17 will lead to a marked reduction in growth and proliferation of metastatic non-small cell lung and prostate cancers. Due to the specific tissue distribution of RGS proteins, the successful targeting will allow for tissue and cell type specific drug treatments.

The first step, addressed in Chapter 3, was to develop and characterize a screening platform for the rapid and sensitive identification of RGS specific inhibitors. The technology that was chosen to achieve this goal was AlphaScreen®. This technology was adapted to allow for the detection of the RGS17: $G\alpha_o$ protein: protein interaction. This was originally characterized in a 384-well format that allowed for the screening of over 1,000 compounds in a 1 hour time frame. This throughput compared favorably with other screening platforms, such as Förster resonance energy transfer (FRET) [137] and Polyplexed FCPIA (Flow Cytometry Protein Interaction Assay) [126]. Upon the completion of fully characterizing the AlphaScreen® technology for RGS proteins, the first pilot screen for RGS17 was conducted. This initial screen of the NCI diversity set II led to the identification of the first biochemical inhibitors of RGS17 [111]. The RL series of compounds was the first major step toward the discovery of chemical probes and pre-therapeutic lead compounds.

The next step, which was addressed in chapter 4, was both to increase the throughput and to help reduce the cost associated with conducting the newly implemented high-throughput screening paradigm. This was accomplished by miniaturization of the screening platform from 384- to 1536-well plates. The resulting decrease in size allowed for an increase in screening capacity from 1,000 compounds to over 7,500 compounds per hour and the reduction of reagents by one-third. With the newly optimized platform well-characterized, two chemical libraries were interrogated for chemical entities that inhibited the RGS17: $G\alpha_o$ interaction. From the screening of the SPECTRUM and NDL3000 chemical libraries, four unique chemical compounds were discovered. This chapter also addressed the assay development and full biophysical

characterization used for the validation of the newly discovered RGS17 inhibitors. Three main techniques (differential scanning fluorimetry, isothermal titration calorimetry, malachite green steady state GTPase assay) were adapted and developed to confirm the discovery of RGS inhibitors that can be applied to characterize inhibitors for all RGS proteins.

After establishing that RGS17 inhibitors can be rapidly identified and properly filtered through several different biophysical techniques, one can envision the development of orthogonal cell based assays. This is partially pursued by observing the cellular localization of RGS proteins though live cell imaging. This has been achieved for RGS4 [146] and has been applied to RGS17 by current members of the Roman laboratory. Further advancement in cellular techniques is discussed in the next chapter.

The purpose of this thesis was to develop and implement the first pilot screens for the discovery and characterization of RGS17 inhibitors. This work was based on the observed ability of shRNA knockdown to reduce the tumor burden in nude mice [72-73]. With interrogation of three chemical libraries, a total of six novel “tool” compounds were discovered. These compounds were further filtered down to three compounds that avoided previous barriers toward pre-therapeutic development, in that no adducts were observed. The findings presented also demonstrate the utility of high-throughput screening in the discovery of RGS inhibitors.

Although G protein coupled receptors have been well-known drug targets for the treatment of multiple disease states, the field of drug discovery has only recently begun to acknowledge the possibilities of targeting the intracellular regulators of these drug targets, RGS proteins. RGS proteins provide a wide array of possible drug targets to selectively modulate GPCR signaling. RGS17, the newest member of the now over 30 proteins that are part of the RGS family, represents one such example of a unique drug target specific for lung and prostate cancers. Although the successful targeting of RGS proteins is still in its infancy, it is possible to envision that every RGS protein could

represent a unique target for each disease state in which they are implicated. The work present in this thesis represents one of the first attempts in which an RGS protein can successfully be targeted. Further research directed towards large scale screening and development of reliable and reproducible cellular based assays are still needed to advance RGS proteins into main stream drug discovery efforts. Even with these needed advancements, RGS proteins have and will continue to garner more attention as viable drug targets.

CHAPTER VI: CURRENT AND FUTURE DIRECTIONS

The application of label-free technology to determine the effects of RGS inhibitors on cellular signaling

Introduction

Understanding nature in its most basic manifestations of life, as in the form of the prokaryotic and eukaryotic cells, has been one of humankind's longest lasting quests [170]. The major driving force behind this endeavor is the desire to understand life, because understanding life at its most basic level creates the ability to create a healthier and longer lasting life. From this desire the field of medicine, *the art of healing*, emerged and medicinally driven technologies and procedures have also grown. Early drug discovery was achieved mainly through two strategies, target-based and phenotypic approaches [171-172]. The target-based screening approach utilizes high-throughput and label-dependent molecular assays to measure the effect of compounds on a specific target protein. In the phenotypic screening approach, an unbiased phenotypic assay is used to examine the effect of test molecules on a specific phenotype of cells, tissues or animals. In recent years, the phenotypic screening methodology has gained more interest as the technologies and advanced computer processing have grown to allow for the collection and analysis of larger data sets through complex high-content screening methodologies. Most cell-based assays measure a specific cellular event including second-messengers, the translocation of a particular fluorescently labeled target, the expression of a reporter gene or the alteration of a phenotype [173-175]. These methods require some manipulation to the cells or the system. Such manipulations pose significant issues investigating the cellular physiology and the role of the target of interest. The ability to examine living cells as close to their native and physiologically relevant context is crucial to understanding the biological functions of cellular targets and to the success of drug discovery and development [173].

Continued success in drug discovery and development requires an evolution in assay technologies and methodologies. This section will address one such technological evolution, the cell-based label-free assay. The label-free assay is one of the cutting-edge biosensor technologies that have attracted considerable attention in the area of drug discovery. Compared to traditional phenotypic approaches, label-free cell phenotypic profiling techniques afforded by optical or electric biosensors offer clear advantages in rich information content, real-time kinetics, highly flexible assay formats, and high-throughput in addition to the wide pathway coverage and ability in multi-target profiling and screening that are common to all phenotypic assays [176-178]. In the past decade there has been a dramatic increase in the number of available biosensors based on different optical and electrical phenomena. Figure 24 depicts three types of commercially available optical biosensors: surface plasmon resonance (SPR), resonant waveguide grating (RWG) and interferometric biosensors.

First, SPR utilizes a prism to direct a wedge of polarized light, covering a range of incident angles, into a planar glass substrate having a thin gold film to excite surface plasmons [179-180]. The plasmon is a charge density oscillation or wave that exists at the interface between two media with dielectric constants of opposite signs. The resonant angle at which a minimal intensity of reflected light occurs is a function of the local refractive index at or near the gold surface, and it is the function of the local refractive index at or near the gold surface [181-182]. Next, the RWG biosensor relies on the resonant coupling of light into a waveguide by a diffraction grating. A polarized light, covering a range of incident wavelengths is used to illuminate the waveguide. This results in light at specific wavelengths to be coupled and propagated along the waveguide [179, 183]. RWG instruments can be subdivided into two different systems based on angle-shift or wavelength shift measurements [173]. Finally, interferometry biosensors use a spectrometer to capture interference patterns in the reflected light from the biosensor

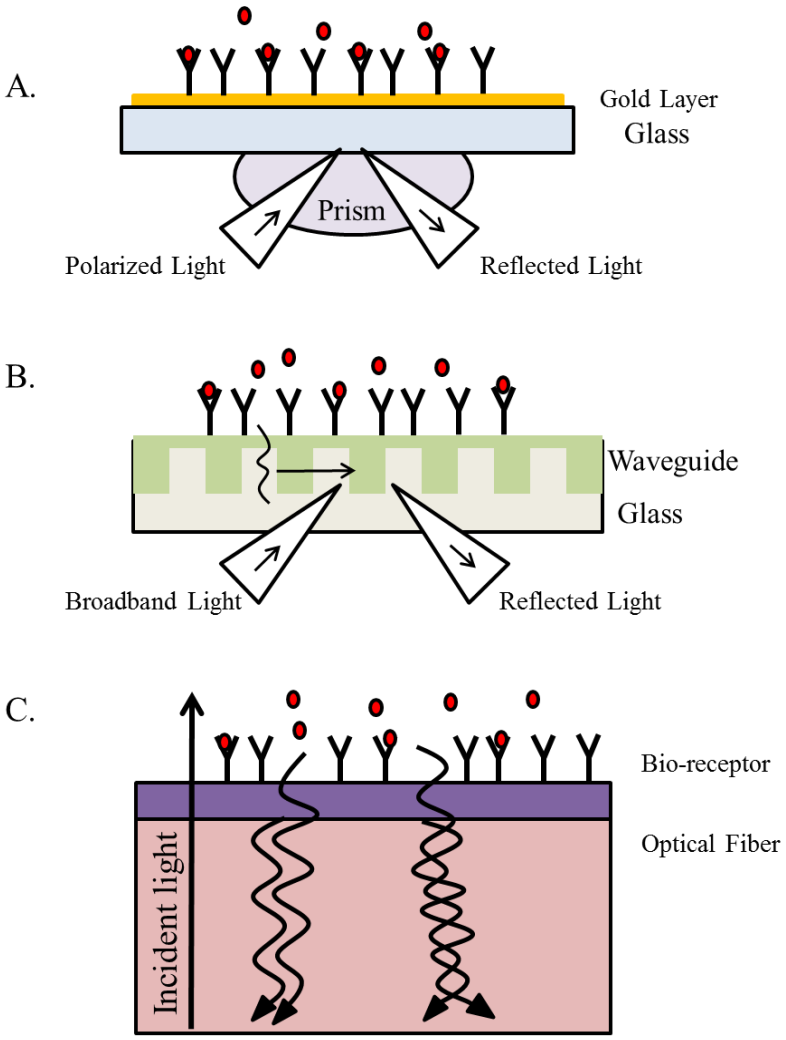

Figure 24. Principles of the three types of optical biosensors for biomolecular interaction analysis. A. SPR. The receptor (Y) is covalently coupled to the derivatized surface of a thin layer of gold, which is deposited onto a glass substrate. The light incident on the gold layer is directed by a prism. The reflectance of the gold surface is a function of incident angle. The resonance angle shifts when target molecules in solution bind to the immobilized receptors. B. RWG biosensor. The coupling of incident light into the waveguide is achieved by the diffraction grating. The intensity of reflected light is a function of the resonant wavelength. The binding of target molecules in a sample to the immobilized receptors results in a shift in the resonant wavelength. C. Interferometric biosensor. A broadband light resource is directly incident at the solution-surface interface. Two types of reflected light waves originated from the two reflecting surfaces, the interface with the optical layer and the surface of bio-receptors, interact each other, leading to interference patterns. The binding of biomolecules to the bio-receptors alters the inference pattern. (Figure adapted from Fang Y. Non-Invasive Optical Biosensor for Probing Cell Signaling. Sensors 2007 October)

interface. This interference is detected as a pattern of intensity variations by wavelengths with a characteristic profile of peaks and troughs.

While each of these technologies affords benefits, the rest of this section will focus on the use of the optical biosensor utilizing resonant waveguide grating (RWG) and the methods being employed to measure drug-induced dynamic mass redistribution (DMR) in label-free whole cell assays. Resonate waveguide grating optical biosensors are sensitive to cell numbers, cell signaling and morphological changes. Figure 25 depicts the great number of cellular phenotypes these biosensors permit when screening and profiling compounds by label-free methods. These phenotypes range from cell adhesion to cell life-cycles (cell cycle progression, division and growth), receptor signaling, cell death, viral infection, cell migration and invasion, and cell-cell communication [178]. Two successful applications of the label-free optical biosensors utilizing resonant waveguide grating are the determination of ligand-directed functional selectivity on β2 adrenoceptor in A431 cells [184] and the characterization of DMR of epidermal growth factor receptor signaling in living cells [185]. Further research has reported many more receptor classes and/or protein/enzyme activation or modulation through characteristic biosensor responses in living cells (Figure 26) [178].

Label-free technology has been successful in drug discovery for the modulation of cellular receptors and has had varied success at examining intra-cellular events. The goal of this section is to apply RWG and DMR to monitor not only the G protein signaling cascade, but also the intra-cellular proteins that govern the duration and intensity of the signaling cascade, the regulators of G protein signaling family of proteins. To date, the investigation of the effects of RGS proteins on GPCR signaling by label-free technology has never been attempted. This section presents the first characterization of RGS proteins activity through label-free techniques as well as insights into the first attempts to monitor pharmacological modulation of RGS proteins GTPase acceleration activity in living cells.

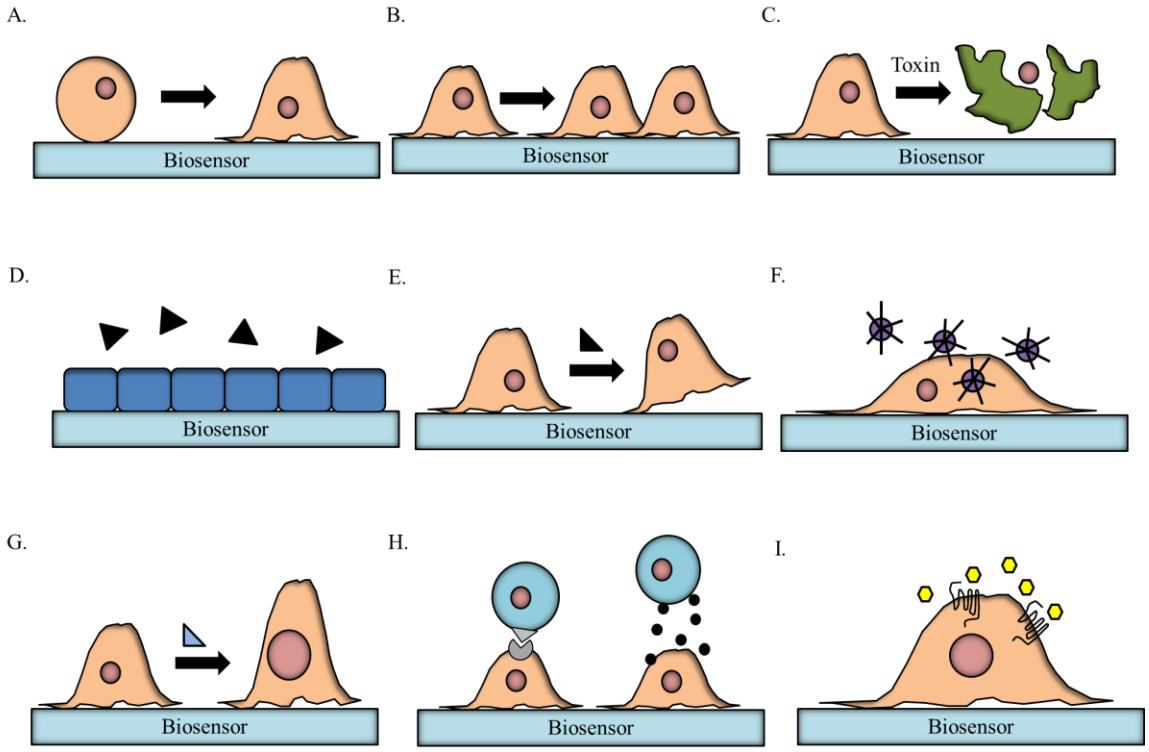

Figure 25. Representative label-free cellular phenotypes examined with label-free techniques. Label-free biosensors can be used to monitor in real-time a great number of cellular process ranging from cell adhesion (A), to cell proliferation (B), cell death (C), cell barrier function (D), cell migration (E), viral infection (F), cell morphology (G), cell–cell communication (H), and cell signaling (I). To monitor different cellular phenotypes, different assay conditions may be applied. (Figure Adapted from Fang Y. Label-free drug discovery. Front Pharmacol. 2014 March)

The ability to monitor not only the GPCR signaling cascade but the intra-cellular regulators of the GPCR signature and pharmacological perturbation of these regulators of the signaling cascade would vastly accelerate the discovery of active lead compounds and represent the first real time cellular measurement of RGS activity in the context of the cellular environment.

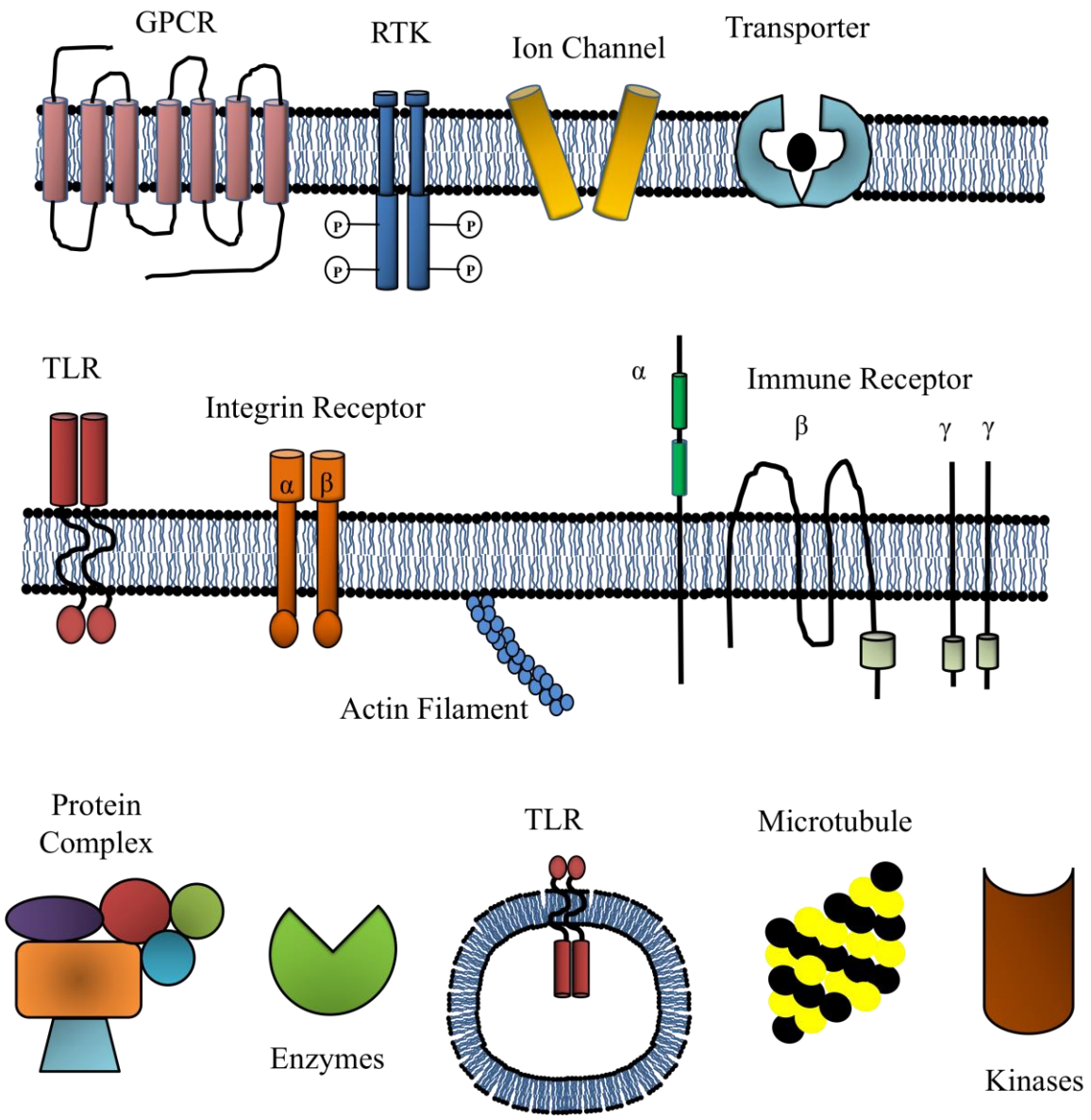

Figure 26. Representative target receptor classes, enzymes, and proteins whose activation or modulation has been shown to trigger characteristic biosensor responses in living cells. Label-free receptor signaling profiling has wide coverage in targets and pathways. GPCR, G protein-coupled receptor; RTK, receptor tyrosine kinase; TLR, Toll-like receptor. (Figure Adapted from Fang Y. Label-free drug discovery. Front Pharmacol. 2014 March)

Preliminary data: results and discussion

Monitoring the integration of cell signaling in real time, if realized, would provide a new dimension for understanding cell biology and physiology [179]. Optical biosensors, including RWG biosensors, allow for the detection of physiologically relevant and integrated cellular responses related to dynamic mass redistribution of cellular components. This provides a non-invasive method for the study of cellular signaling in the context of the cellular environment. Figure 27 represents the theoretical cell-based principles of using DMR to measure the effects of GPCR activation and subsequent RGS effects.

To begin the investigation of the effects of the RGS proteins on the G protein signaling pathway, the proper cell type, receptor, G protein and RGS protein must be determined. To this end, the dopamine subtype 2 long (D2L) and mu (μ) opioid (MuOP3) receptors were chosen as the primary GPCRs to investigate. These two receptors both couple to the intracellular $G\alpha_{i/o}$ G proteins and regulate the production of cAMP through inhibition of the membrane bound enzyme adenylate cyclase. Further reasoning behind these choices in receptors and G proteins relies on the RGS proteins which are currently under investigation. The RGS4, RGS8, and RGS17 proteins are of increased interest for their roles in heart disease [186-188] and lung and prostate cancers [72-73], respectively. It has been shown that RGS4, RGS8, and RGS17 all regulate the $G\alpha_{i1}$ G protein subunit [189]. Upon investigation it has been determined that the G protein is not the only determinate for the RGS: Gα protein: protein interactions. The cellular context and the receptor are also factors that play a significant role in the signaling pathway. The RGS4 and RGS8 proteins are known to regulate the D2L receptor [189-190] while RGS17 has been shown to highly regulate the MuOP3 receptor [149, 191-192].

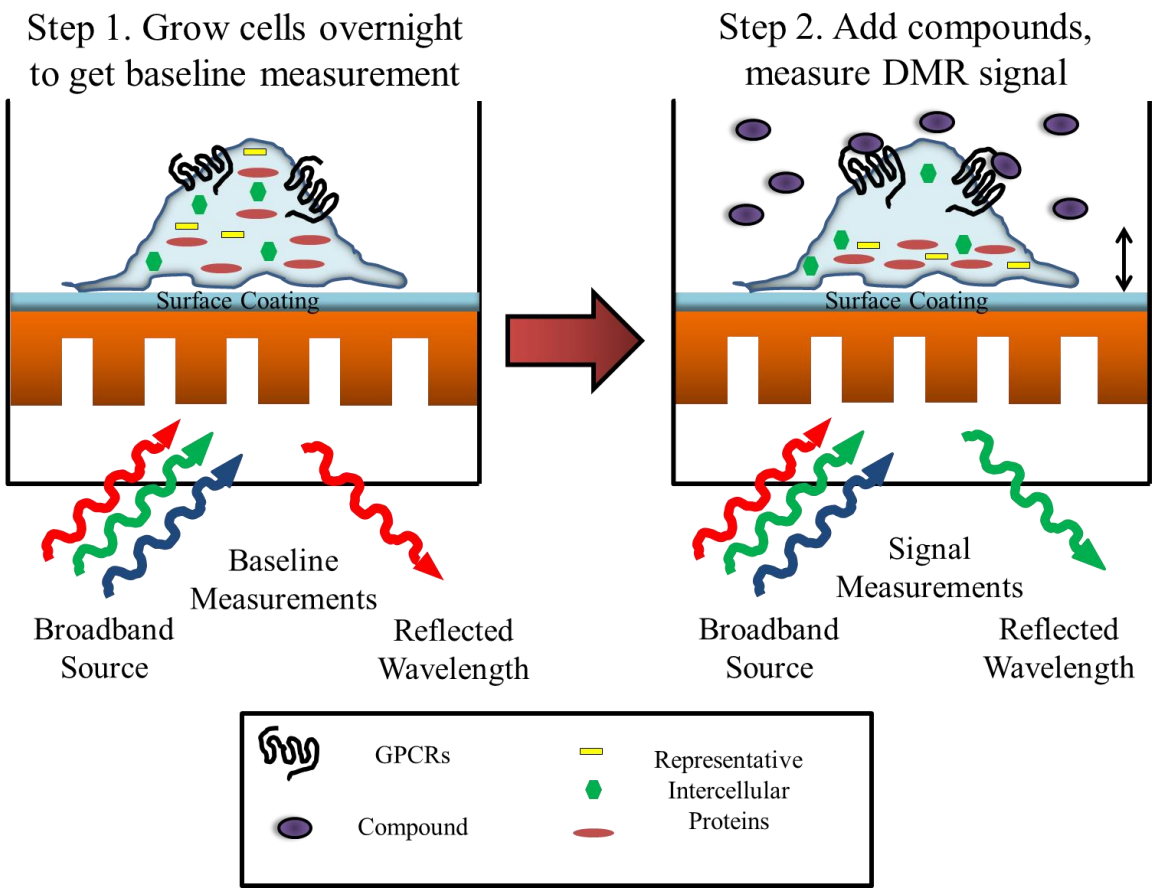

Figure 27. Diagram of the dynamic mass redistribution signaling upon activation of the G protein coupled receptors in a label-free assay using RWG. Cells are directly cultured onto the surface of surface coating above the biosensor. The biosensor consists of a glass substrate and a waveguide thin film within which a grating structure is embedded. Upon activation of the GPCR, the movements of cellular components are measured as shifts in the reflected wavelength. Only the mass redistribution within the bottom portion of cells is directly measured. (Figure adapted from Cloutier, T. et al. Combining labeled and label-free tools. Genetic Engineering & Biotechnology News, 2013 April)

Because of these factors, the two model systems that were most-suited for this initial label-free investigation included a human embryonic kidney 293 (HEK293) cell line stably expressing the D2L receptor and either RGS4 or RGS8 and a Chinese hamster ovary (CHO) cell line stably expressing the MuOP3 receptor along with transiently expressed RGS17ΔN or full length RGS17 (FLRGS17). Figure 28 shows the western blot

verification of the stable RGS4 and RGS8 D2L HEK293 cells, as well as the transiently transfected RGS17ΔN or FLRGS17 CHO cells.

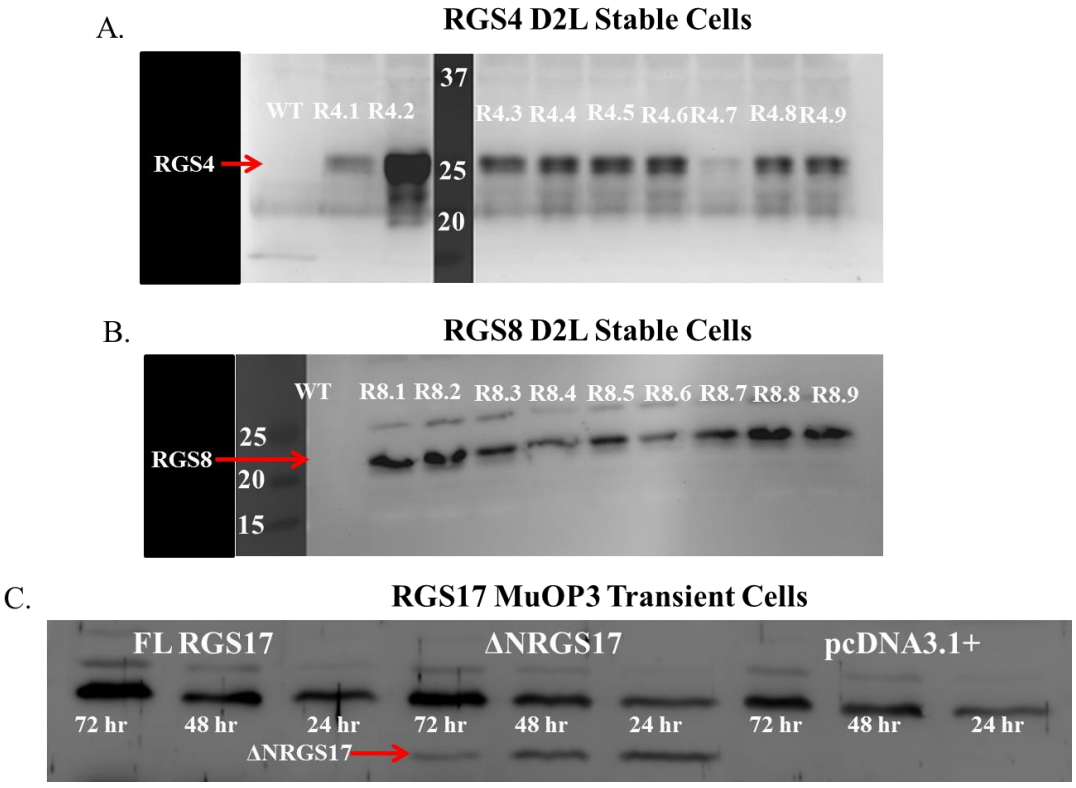

Figure 28. Western blot analysis of D2L HEK293 and CHO MuOP3 cell lines. A. Stably transfected HEK293 cells expressing the D2L receptor were western blotted for expression of RGS4. Expression was confirmed in all nine samples by the band at the predicted MW of 25 kDa with varying expression levels. Clones R4.1, R4.2, R4.3, R4.4 and R4.7 were chosen for cryogenic preservation and stored in liquid nitrogen. B. Stably transfected HEK293 cells expressing the D2L receptor were western blotted for expression of RGS8. Expression was confirmed in all nine samples by the band at the predicted MW of 21 kDa with varying expression levels. Clones R8.2, R8.3, R8.4, R8.5 and R8.6 were chosen for cryogenic preservation and stored in liquid nitrogen. C. Transient expression of two different forms of RGS17 was tested. The two constructs coded for either a ΔNRGS17 or FLRGS17 protein. The full length RGS17 protein was undected under each of the three time points post transfection. Expression of the ΔNRGS17 protein was confirmed by the presences of the predicted band at 24 kDa. Expression peaks between 24 and 48 hours but is still present after 72 hours of growth.

Once stable expression of RGS4 and RGS8 was verified, the effects of the RGS proteins were examined through the usage of the PerkinElmer EnSpire label-free system. The EnSpire uses RWG to measure the DMR of intracellular proteins. Upon activation of the D2L receptor in WT D2L HEK and RGS4/8 D2L HEK cells by the agonist quinpirole hydrochloride at varied concentration, a distinct DMR signature was discovered (Figure 29).

To analyze these signatures, two different parameters were chosen, "Peak in well" and "Area under the curve" (AUC). The peak in well parameter is a measure of the maximum DMR signal received after activation of the cognate receptors. In these initial experiments, there was a distinct dose-dependence of the maximum signal (peak in well) that correlated to the increasing amounts of agonist (Figure 30). Upon introduction of the RGS4 and RGS8 proteins into the D2L model system, there was a decrease in the DMR signature of the D2L-Gα-AC signaling cascade as determined by the decreased maximal response (Figure 30).

The introduction of the RGS proteins in the cellular model did not affect the EC_{50}. The RGS proteins did however decrease the amount of mass redistribution which can be interpreted in several ways. It can be envisioned that the introduction of the RGS proteins allows for less mass that can be detected since it terminates the signaling and decreases the mass movement into the detection zone above the RWG sensor. The decreased maximum signal may also be the result of the RGS protein's function as a GAP protein as it interacts with the activated Gα subunit to truncate the $G\alpha_i$ inhibition of the membrane bound adenylate cyclase, which in turn leads to less G protein movement within the cellular environment.

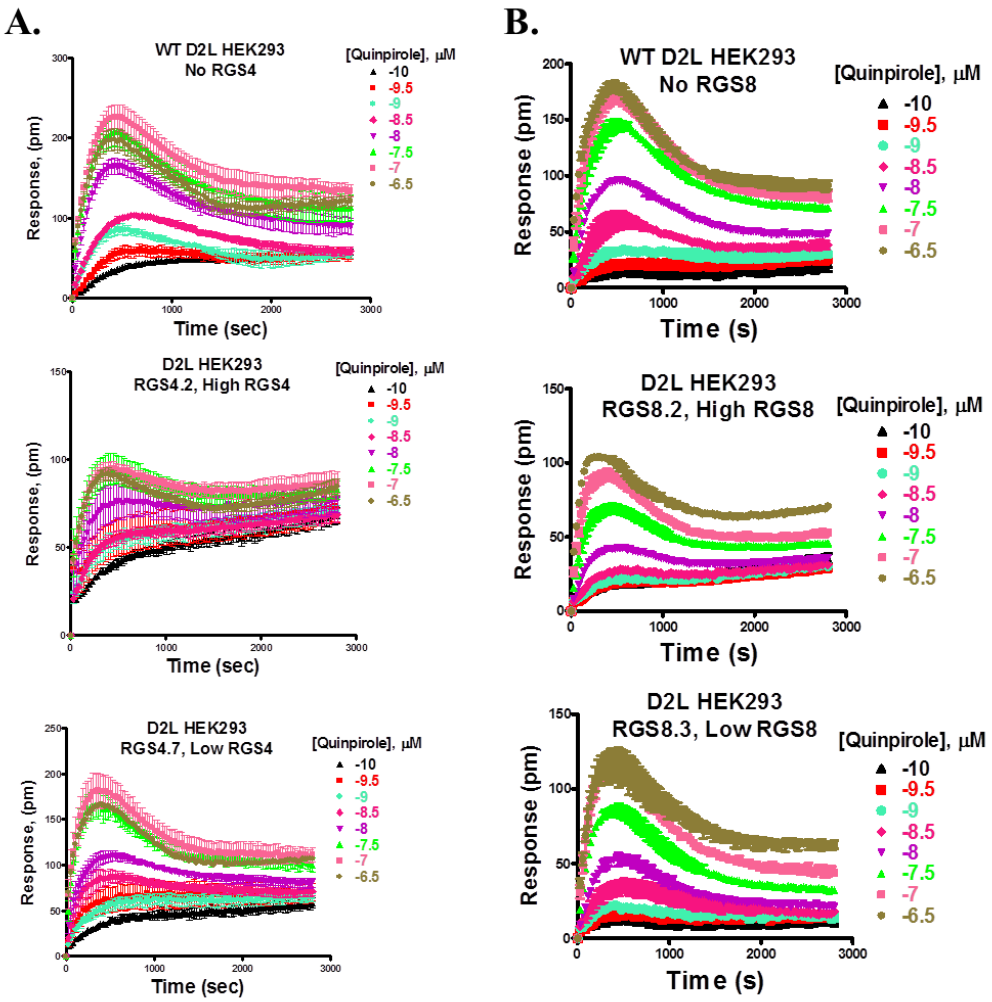

Figure 29. Cell specific DMR signal in response to quinpirole stimulation. The DMR signature of D2L HEK293 cells under different conditions. Cells were treated with increasing concentrations of quinpirole, a D2L agonist. A. Three different signatures were recorded from WT, High RGS4 and Low RGS4 expressing HEK293 cells. Upon stimulation with the agonist WT cells recorded a significant increase in the maximum mass redistribution as well as total area under the curve (AUC) when compared to the different RGS4 clones. B. Three different clones of D2L HEK293 cells were also tested in the label-free assay. These different signatures for both RGS4 and RGS8 exhibit a dependence on the expression levels that correlates with changes in maximum signal as well as total AUC.

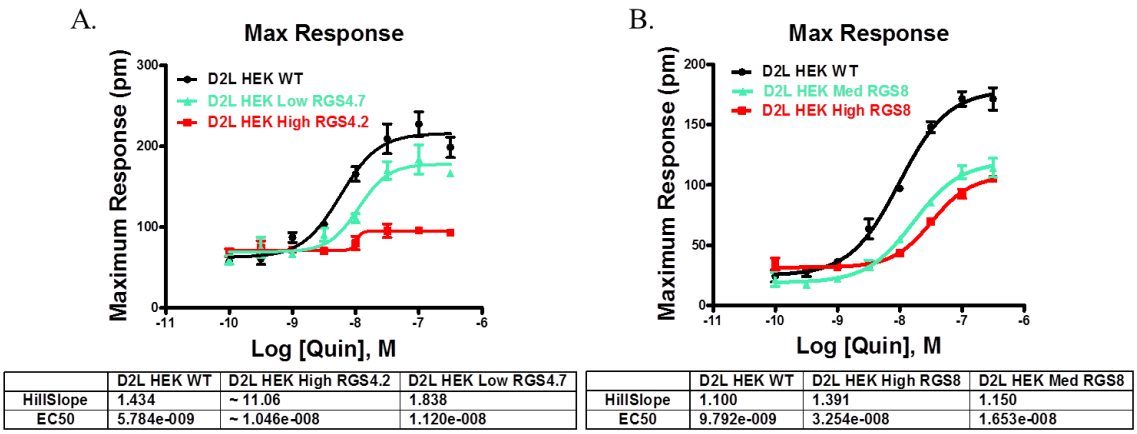

	D2L HEK WT	D2L HEK High RGS4.2	D2L HEK Low RGS4.7
HillSlope	1.434	~ 11.06	1.838
EC50	5.784e-009	~ 1.046e-008	1.120e-008

	D2L HEK WT	D2L HEK High RGS8	D2L HEK Med RGS8
HillSlope	1.100	1.391	1.150
EC50	9.792e-009	3.254e-008	1.653e-008

Figure 30. Effects of RGS expression on the dose-response curves as determined by maximum response. D2L HEK293 cells were treated with varying concentrations of the agonist quinpirole. The maximum response of each condition was recorded and fit using the log [quinpirole] versus maximum response with a variable slope. These results indicate a reduction in the maximum response as concentrations of RGS proteins increase. It can be envisioned that due to high amounts of membrane associated RGS proteins truncating the signaling of the G alpha and beta/gamma subunits, there is a resulting decrease in dynamic mass redistribution or DMR into the sensor range.

The second parameter applied to deconvolute the DMR signature is the "Area under the Curve" or AUC. When applying this method of analysis to the DMR signature a similar dose-dependence is observed (Figure 31).

The introduction of RGS4 and RGS8 into the cellular model leads to a decrease in the observed AUC. Again, the RGS proteins do not affect the EC_{50} of the agonist but their introduction does yield a unique DMR signal. It can be hypothesized that through modulation of the D2L $G\alpha_{i/o}$ RGS HEK293 signature in this model system, the effects of pharmacological intervention could be determined for RGS4 or RGS8 inhibitors.

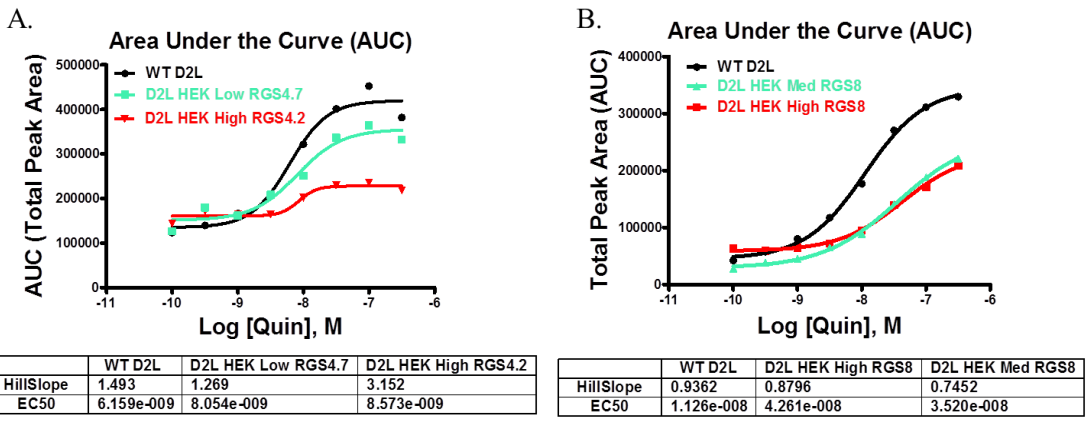

	WT D2L	D2L HEK Low RGS4.7	D2L HEK High RGS4.2
HillSlope	1.493	1.269	3.152
EC50	6.159e-009	8.054e-009	8.573e-009

	WT D2L	D2L HEK High RGS8	D2L HEK Med RGS8
HillSlope	0.9362	0.8796	0.7452
EC50	1.126e-008	4.261e-008	3.520e-008

Figure 31. Effects of RGS expression on the dose-response curves as determined by area under the curve. D2L HEK293 cells were treated with varying concentrations of the agonist quinpirole. The total AUC of each condition was recorded and the summation of the total area under each curve was calculated. This data was fit using the log [quinpirole] versus total AUC with a variable slope. These results indicate a decrease in the DMR signature that correlates with the increasing RGS protein expression.

Further investigation of the utility of the optical label-free system was determined in the second model system using a CHO cell line stably expressing the MuOP3 receptor along with transiently expressed ΔNRGS17 or full length RGS17 (FLRGS17). This model system was analyzed by the same two parameters, peak in well and AUC, as the D2L RGS4/-8 HEK293 model system. Interestingly, the peak in well and AUC parameters both resulted in an increase in either the maximum response or the total AUC, respectively (Figure 32 and Figure 33). This difference in the ΔNRGS17 samples is the opposite result seen in the RGS4 and RGS8 D2L HEK293 cell experiments. One can envision the difference being attributed to the free movement of the unanchored RGS17 protein which is missing the poly-Cys string on the N-terminus that allows the ΔNRGS17 protein to freely move about the intracellular compartment and increase the DMR signal.

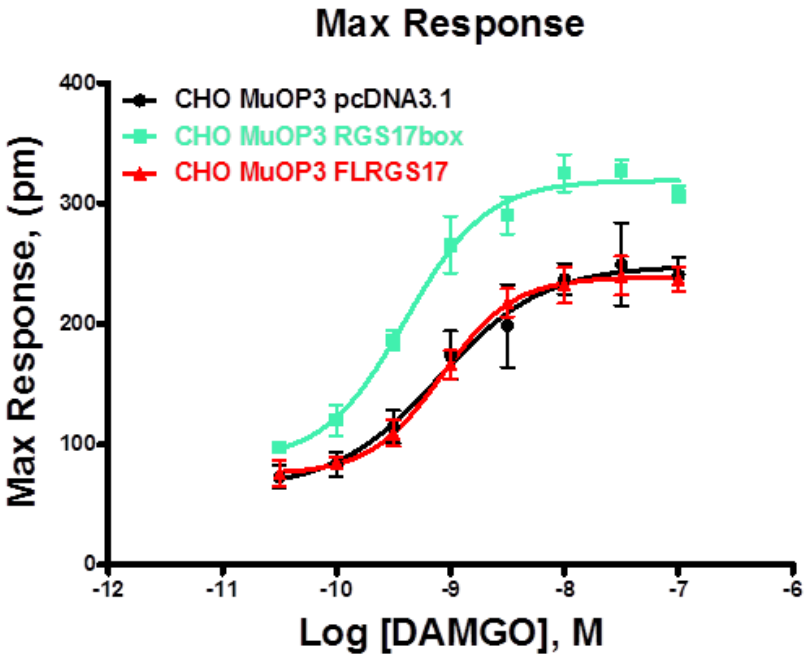

	CHO MuOP3 pcDNA3.1	CHO MuOP3 RGS17box	CHO MuOP3 FLRGS17
HillSlope	0.9515	1.219	1.378
EC50	7.939e-010	4.009e-010	8.368e-010

Figure 32. Effects of RGS expression on the dose-response curves as determined by maximum response. MuOP3 CHO cells were transiently transfected with ΔNRGS17 (RGS17RH), Full Length RGS17 (FLRGS17) or empty vector (pcDNA3.1+). Expression was verified through western blot analysis. WT and FLRGS17 MuOP3 cells were determined to lack expression RGS17 protein. The ΔNRGS17 cells were confirmed for RGS17 expression. Cells were treated with DAMGO ([D-Ala2, N-MePhe4, Gly-ol]-enkephalin), a synthetic opioid peptide with high μ-opioid receptor specificity and measured by label-free techniques in an EnSpire microplate reader. A significant increase in the maximum response was observed upon agonist stimulation. Due to the lack of the N-terminus, the protein representing the RGS17box is free to move about the cellular compartment and contribute to the increased DMR signature.

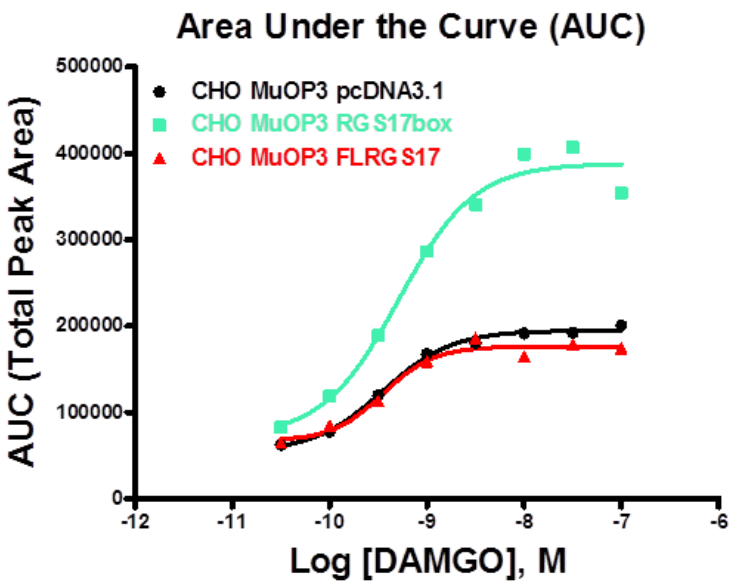

	CHO MuOP3 pcDNA3.1	CHO MuOP3 RGS17box	CHO MuOP3 FLRGS17
HillSlope	1.222	1.120	1.656
EC50	3.508e-010	5.124e-010	3.542e-010

Figure 33. Effects of RGS expression on the dose-response curves as determined by area under the curve. Again, MuOP3 CHO cells were transiently transfected with ΔNRGS17 (RGS17box), Full Length RGS17 (FLRGS17) or empty vector (pcDNA3.1+). In this experiment, a significant increase in the total area under the curve was observed upon agonist stimulation. The increase in DMR signaling as measure by AUC indicates a significant increase in the positive dynamic mass redistribution measurement.

Finally, to verify that the changes observed in these two different model systems are due to the regulation of the GPCR-Gα-AC signaling cascade by the introduction of different RGS proteins, further characterization is needed. To accomplish this, a set of $G\alpha_{i1}$ mutants have been cloned. First, the WT $G\alpha_{i1}$ DNA sequence was cloned into a mammalian expression vector. Next, a RGS insensitive $G\alpha_{i1}$ (RGSi $G\alpha_{i1}$) point mutant was cloned. This point mutant can be transiently expressed in the RGS stable cell lines, which should allow for the DMR signature to be unaffected by the RGS protein present in the system. Further characterization of the label-free system will require two more mutants, a pertussis toxin insensitive $G\alpha_{i1}$ (PTi $G\alpha_{i1}$) and an RGSi/PTi $G\alpha_{i1}$ dual mutant.

Transiently expressing the PTi $G\alpha_{i1}$ mutant, followed by subsequent treatment with pertussis toxin will validate that the only Gα being detected in the label-free system is the $G\alpha_{i1}$ transiently expressed. This control will verify the $G\alpha_{i1}$ signature as well as its regulation by RGS proteins. The RGSi/PTi $G\alpha_{i1}$ dual mutant control will provide two valuable DMR signatures. The first DMR signature is the PTi signal, which allows the researcher to inhibit WT $G\alpha_{i1}$ signaling by treatment with pertussis toxin. This will confirm the transfection and activation of the signaling cascade. Secondly this will provide the representative DMR signature for the basis of the inhibition of the Gα: RGS protein: protein interaction. The four different $G\alpha_{i1}$ expression vectors (WT $G\alpha_{i1}$, RGSi $G\alpha_{i1}$, PT $G\alpha_{i1}$ and RGSi/PTi $G\alpha_{i1}$) have been successfully cloned into expression vectors as verified by the University of Iowa DNA sequencing core facility and are stored in the Roman laboratory for future use.

Conclusion

Selection of lead molecules to progress through a drug discovery program is a major challenge faced by the pharmaceutical industry [176]. Early identification and elimination of false positives, as well as compounds with diminished activity *in vitro* or *in vivo*, will aid in decreased costs associated with late stage failures of drug molecules. In recent years there has been an increased interest in the development of more sensitive phenotypic methods to help identify possible lead compounds for drug development. Label-free receptor assays are emerging as a powerful assay platform to study receptor signaling and elucidate critical nodes of receptor signaling networks [183]. The initial studies presented in this chapter's section provide a further expansion of label-free technology beyond only investigating GPCR activation. This work provides the ground work to not only measure the regulation of GPCRs but the added dimension of investigating the various intra-cellular components involved in the signaling cascade in real-time.

Cell-based assays have become an integral part of the pre-clinical drug discovery process because they allow for the interrogation of protein targets and biochemical pathways in the context of the cellular environment [177]. The optically based label-free assay provides a non-invasive method to investigate and characterize drug-like molecules. This emerging technology taken together with smarter assay design and the development of novel methodologies for label-free assay data analysis will provide new perspectives into cellular biology and pharmacology.

Investigation of larger chemical space: screening of the ChemBridge 50k compound library and beyond

Introduction

Driven by chemistry but increasingly guided by pharmacology and the clinical sciences, drug research has contributed more to the progress of medicine during the past century than any other scientific factor [193]. The accelerated pace at which medicine has advanced along with the technology and tools for new drug discovery allows researchers to explore previously unfathomable diverse chemical space and biological processes. Over the past two decades, the field of high-throughput screening (HTS) has become a powerful tool for the identification of active compounds and pharmacophores against specific biological targets [194-195]. Through the application of HTS, tens of thousands to millions of samples are tested in a single screening campaign. In this section, the expansion of the RGS17 screening platform to include a larger chemical space and recent preliminary data from a larger screening campaign will be presented.

In the early years of HTS campaigns, the available compound libraries available for screening were limited and the diversity found to be restricted. In the past decade, commercial libraries have advanced to provide libraries that survey a much larger chemical space while containing a higher degree of molecular complexity. These advances have led to the typical HTS groups having access to more than 1 million

compounds [196]. In the previous chapters, three pilot screens were presented representing the screening of a relatively few compounds that yielded tremendous results by discovering unique RGS17 inhibitors. It is promising that out of this relatively small amount of compounds the first biochemical inhibitors of RGS17 were discovered. While the discovery of the first "tool" compounds represents a major advancement, it must be realized that they are far from ideal lead compounds from a chemical standpoint. The diversity of the molecular scaffolds and the potential that these compounds represent unique binding sites on RGS17 are very encouraging. Because of these results, it can be hypothesized that through an exploration of a larger chemical space, represented by the ChemBridge 50,000 compound library and even larger libraries such as the Scripps 640,000 compound library, the identification of unique chemical entities leading to the development of a pharmacophore representing a more chemically tractable lead for pre-therapeutic development will be discovered. To this end, the following section will present the preliminary data for the screening of the ChemBridge library of compounds.

Preliminary data: results and discussion

The application of the novel RGS17 AlphaScreen® HTS assay in 1536 well format was presented in the previous chapters. In this section, that miniaturized screening platform was applied to the first investigation of a much larger chemical space, as represented by the ChemBridge library. Figure 34 is a representative plate read-out of the initial investigation of this library.

The 50,000 compound library was screened in a total of forty 1536 well plates over four days of screening. This method of screening by batches was chosen to help decrease inter-plate variability and to maintain stability of the AlphaScreen® signal at room temperature.

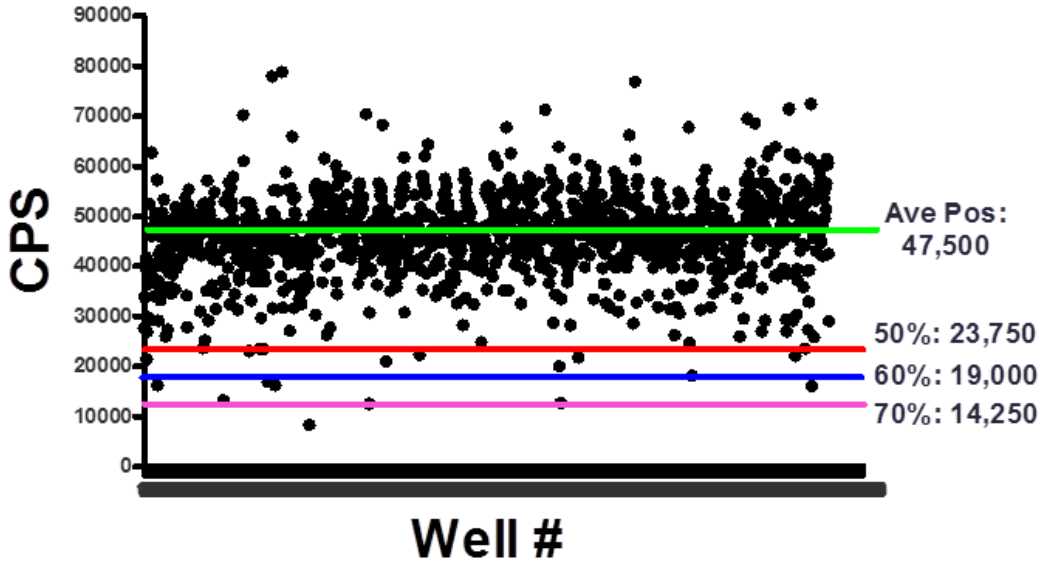

Figure 34. High-Throughput screening of the ChemBridge library. Initial screening of the 50,000 compounds was conducted using the 1536 well platform. This screen yielded three thresholds, >50%, >60%, and >70%. Further characterization will yield unique molecular scaffolds and lead compounds to add to the growing literature of RGS17 inhibitors.

From this screen three different cut offs were chosen. The thresholds of 50%, 60% and 75% inhibition of the AlphaScreen® signal were chosen to filter the initial hits for the ongoing follow-up studies currently being conducted. The 50% inhibition mark yielded 575 compounds, an initial hit rate of 1.15% where the 60% and 75% yielded a much more manageable and cost effective initial hit rates (>60%=277 compounds, initial hit rate 0.55% & >75%=77 compounds, 0.15%) (Table 6). The future of this larger investigation will rely on the battery of assays developed for the characterization of each chemical entity.

Table 6. Results of the high-throughput screening campaign against the Chembridge 50,000 compound library.

Chembridge Library	50,000 compounds
Initial Hits >50% Inhibition	575 compounds (1.15% Hit Rate)
Initial Hits >60% Inhibition	277 compounds (0.55% Hit Rate)
Initial Hits >75% Inhibition	77 compounds (0.15% Hit Rate)

Furthermore, expansion of the chemical space surveyed would be benefitted though the investigation of a much larger chemical library. A possible collaborative effort with the Scripps Institute would allow for the first larger-scale attempt to target an RGS protein's GAP activity as an anticancer target. These two large scale primary screens represent a very promising future for the development of an RGS17 inhibitor for a pre-therapeutic lead molecule.

Conclusion

Lead discovery by HTS has evolved as a discipline since its beginning about 20 years ago. Due to increases in automation and the availability of chemical libraries, the ability to discover unique compounds for the targeting of druggable proteins, enzymes, and receptors has expanded. In this section, the expansion of chemical space surveyed for RGS17 was discussed. The preliminary results from the ChemBridge compound library were presented. These initial hits are currently under investigation for confirmation of activity. The undertaking of a large screening campaign against over 500,000 compounds at the Scripps Institute will advance the RGS17 project far beyond the pilot screens presented here. These future studies have the possibility to advance the treatment options for lung and prostate cancers through the pharmacological targeting of RGS17.

REFERENCES

1. Pierce, K. L.; Premont, R. T.; Lefkowitz, R. J., Seven-transmembrane receptors. *Nat Rev Mol Cell Biol* **2002,** *3* (9), 639-50.

2. Dorsam, R. T.; Gutkind, J. S., G-protein-coupled receptors and cancer. *Nat Rev Cancer* **2007,** *7* (2), 79-94.

3. Rasmussen, S. G.; DeVree, B. T.; Zou, Y.; Kruse, A. C.; Chung, K. Y.; Kobilka, T. S.; Thian, F. S.; Chae, P. S.; Pardon, E.; Calinski, D.; Mathiesen, J. M.; Shah, S. T.; Lyons, J. A.; Caffrey, M.; Gellman, S. H.; Steyaert, J.; Skiniotis, G.; Weis, W. I.; Sunahara, R. K.; Kobilka, B. K., Crystal structure of the beta2 adrenergic receptor-Gs protein complex. *Nature* **2011,** *477* (7366), 549-55.

4. Roman, D. L., Chapter 11 Identification of Ligands Targeting RGS Proteins High-Throughput Screening and Therapeutic Potential. *Prog Mol Biol Transl Sci* **2009,** *86*, 335-56.

5. Sternweis, P. C.; Robishaw, J. D., Isolation of two proteins with high affinity for guanine nucleotides from membranes of bovine brain. *J Biol Chem* **1984,** *259* (22), 13806-13.

6. Roman, D. L.; Traynor, J. R., Regulators of G protein signaling (RGS) proteins as drug targets: modulating G-protein-coupled receptor (GPCR) signal transduction. *J Med Chem* **2011,** *54* (21), 7433-40.

7. Zhong, H.; Neubig, R. R., Regulator of G protein signaling proteins: novel multifunctional drug targets. *J Pharmacol Exp Ther* **2001,** *297* (3), 837-45.

8. Dohlman, H. G.; Thorner, J. W., Regulation of G protein-initiated signal transduction in yeast: paradigms and principles. *Annu Rev Biochem* **2001,** *70*, 703-54.

9. Druey, K. M.; Blumer, K. J.; Kang, V. H.; Kehrl, J. H., Inhibition of G-protein-mediated MAP kinase activation by a new mammalian gene family. *Nature* **1996,** *379* (6567), 742-6.

10. Koelle, M. R.; Horvitz, H. R., EGL-10 regulates G protein signaling in the C. elegans nervous system and shares a conserved domain with many mammalian proteins. *Cell* **1996,** *84* (1), 115-25.

11. Siderovski, D. P.; Hessel, A.; Chung, S.; Mak, T. W.; Tyers, M., A new family of regulators of G-protein-coupled receptors? *Curr Biol* **1996,** *6* (2), 211-2.

12. Cho, H.; Kehrl, J. H., Chapter 9 Regulation of Immune Function by G Protein-Coupled Receptors, Trimeric G Proteins, and RGS Proteins. *Prog Mol Biol Transl Sci* **2009,** *86*, 249-98.

13. Grunebach, F.; Erndt, S.; Hantschel, M.; Heine, A.; Brossart, P., Generation of antigen-specific CTL responses using RGS1 mRNA transfected dendritic cells. *Cancer Immunol Immunother* **2008,** *57* (10), 1483-91.

14. Rangel, J.; Nosrati, M.; Leong, S. P.; Haqq, C.; Miller, J. R., 3rd; Sagebiel, R. W.; Kashani-Sabet, M., Novel role for RGS1 in melanoma progression. *Am J Surg Pathol* **2008,** *32* (8), 1207-12.

15. Hurst, J. H.; Mendpara, N.; Hooks, S. B., Regulator of G-protein signalling expression and function in ovarian cancer cell lines. *Cell Mol Biol Lett* **2009,** *14* (1), 153-74.

16. Wieland, T.; Lutz, S.; Chidiac, P., Regulators of G protein signalling: a spotlight on emerging functions in the cardiovascular system. *Curr Opin Pharmacol* **2007,** *7* (2), 201-7.

17. Terzi, D.; Stergiou, E.; King, S. L.; Zachariou, V., Regulators of G protein signaling in neuropsychiatric disorders. *Prog Mol Biol Transl Sci* **2009,** *86*, 299-333.

18. Traynor, J., Regulator of G protein-signaling proteins and addictive drugs. *Ann N Y Acad Sci* **2010,** *1187*, 341-52.

19. Seeds, N. W.; Gilman, A. G., Norepinephrine stinulated increase of cyclic AMP levels in developing mouse brain cell cultures. *Science* **1971,** *174* (4006), 292.

20. Northup, J. K.; Sternweis, P. C.; Smigel, M. D.; Schleifer, L. S.; Ross, E. M.; Gilman, A. G., Purification of the regulatory component of adenylate cyclase. *Proc Natl Acad Sci U S A* **1980,** *77* (11), 6516-20.

21. Schleifer, L. S.; Garrison, J. C.; Sternweis, P. C.; Northup, J. K.; Gilman, A. G., The regulatory component of adenylate cyclase from uncoupled S49 lymphoma cells differs in charge from the wild type protein. *J Biol Chem* **1980,** *255* (7), 2641-4.

22. Kurjan, J.; Dietzel, C., Analysis of the role of SCG1, a G alpha homolog, and SST2 in pheromone response and desensitization in yeast. *Cold Spring Harbor symposia on quantitative biology* **1988,** *53 Pt 2*, 577-84.

23. Dietzel, C.; Kurjan, J., Pheromonal regulation and sequence of the Saccharomyces cerevisiae SST2 gene: a model for desensitization to pheromone. *Mol Cell Biol* **1987,** *7* (12), 4169-77.

24. De Vries, L.; Mousli, M.; Wurmser, A.; Farquhar, M. G., GAIP, a protein that specifically interacts with the trimeric G protein G alpha i3, is a member of a protein family with a highly conserved core domain. *Proc Natl Acad Sci U S A* **1995,** *92* (25), 11916-20.

25. Militello, R.; Colombo, M. I., Small GTPases as regulators of cell division. *Communicative & integrative biology* **2013,** *6* (5), e25460.

26. Rojas, A. M.; Fuentes, G.; Rausell, A.; Valencia, A., The Ras protein superfamily: evolutionary tree and role of conserved amino acids. *J Cell Biol* **2012,** *196* (2), 189-201.

27. Gilman, A. G., G proteins: transducers of receptor-generated signals. *Annu Rev Biochem* **1987,** *56*, 615-49.

28. Rodriguez, C. I.; Setaluri, V., Cyclic AMP (cAMP) signaling in melanocytes and melanoma. *Arch Biochem Biophys* **2014**.

29. Lefkimmiatis, K.; Zaccolo, M., cAMP signaling in subcellular compartments. *Pharmacol Ther* **2014**.

30. Gold, M. G.; Gonen, T.; Scott, J. D., Local cAMP signaling in disease at a glance. *Journal of cell science* **2013,** *126* (Pt 20), 4537-43.

31. Saunier, B.; Dib, K.; Delemer, B.; Jacquemin, C.; Correze, C., Cyclic AMP regulation of Gs protein. Thyrotropin and forskolin increase the quantity of stimulatory guanine nucleotide-binding proteins in cultured thyroid follicles. *J Biol Chem* **1990,** *265* (32), 19942-6.

32. Allgeier, A.; Offermanns, S.; Van Sande, J.; Spicher, K.; Schultz, G.; Dumont, J. E., The human thyrotropin receptor activates G-proteins Gs and Gq/11. *J Biol Chem* **1994,** *269* (19), 13733-5.

33. Jena, B. P.; Abramowitz, J., Catecholamine-induced heterologous desensitization of rabbit luteal adenylyl cyclase: loss of luteinizing hormone responsiveness is associated with impaired G-protein function. *Endocrinology* **1989,** *124* (4), 1942-8.

34. Jena, B. P.; Abramowitz, J., Human chorionic gonadotropin-induced heterologous desensitization of rabbit luteal adenylyl cyclase is associated with altered receptor and G-protein function. *Endocrinology* **1989,** *124* (4), 1932-41.

35. McCann, S. M.; Marubayashi, U.; Sun, H. Q.; Yu, W. H., Control of follicle-stimulating hormone and luteinizing hormone release by hypothalamic peptides. *Ann N Y Acad Sci* **1993,** *687*, 55-9.

36. Brown, D. A.; Sihra, T. S., Presynaptic signaling by heterotrimeric G-proteins. *Handbook of experimental pharmacology* **2008,** (184), 207-60.

37. Limbird, L. E., Beta-adrenergic stimulation of adenylate cyclase and alpha-adrenergic inhibition of adenylate cyclase: GTP-binding proteins as macromolecular messengers. *Adv Exp Med Biol* **1983,** *161*, 91-111.

38. Lefkowitz, R. J.; Caron, M. G., Adrenergic receptors: molecular mechanisms of clinically relevant regulation. *Clinical research* **1985,** *33* (3), 395-406.

39. Howlett, A. C., Pharmacology of cannabinoid receptors. *Annu Rev Pharmacol Toxicol* **1995,** *35*, 607-34.

40. Pertwee, R. G., Pharmacology of cannabinoid CB1 and CB2 receptors. *Pharmacol Ther* **1997,** *74* (2), 129-80.

41. Neve, K. A.; Seamans, J. K.; Trantham-Davidson, H., Dopamine receptor signaling. *J Recept Signal Transduct Res* **2004,** *24* (3), 165-205.

42. Gerber, U.; Gee, C. E.; Benquet, P., Metabotropic glutamate receptors: intracellular signaling pathways. *Curr Opin Pharmacol* **2007,** *7* (1), 56-61.

43. Fagni, L., Diversity of metabotropic glutamate receptor-interacting proteins and pathophysiological functions. *Adv Exp Med Biol* **2012,** *970*, 63-79.

44. Blank, J. L.; Ross, A. H.; Exton, J. H., Purification and characterization of two G-proteins that activate the beta 1 isozyme of phosphoinositide-specific phospholipase C. Identification as members of the Gq class. *J Biol Chem* **1991,** *266* (27), 18206-16.

45. Sternweis, P. C.; Smrcka, A. V., Regulation of phospholipase C by G proteins. *Trends Biochem Sci* **1992,** *17* (12), 502-6.

46. Sternweis, P. C.; Smrcka, A. V.; Gutowski, S., Hormone signalling via G-protein: regulation of phosphatidylinositol 4,5-bisphosphate hydrolysis by Gq. *Philosophical transactions of the Royal Society of London. Series B, Biological sciences* **1992,** *336* (1276), 35-41; discussion 41-2.

47. Langlois, D.; Ouali, R.; Berthelon, M. C.; Derrien, A.; Saez, J. M., Regulation by growth factors of angiotensin II type-1 receptor and the alpha subunit of Gq and G11 in bovine adrenal cells. *Endocrinology* **1994,** *135* (1), 480-3.

48. Schoneberg, T.; Kostenis, E.; Liu, J.; Gudermann, T.; Wess, J., Molecular aspects of vasopressin receptor function. *Adv Exp Med Biol* **1998,** *449*, 347-58.

49. Bai, H.; Wu, L. L.; Xing, D. Q.; Liu, J.; Zhao, Y. L., Angiotensin II induced upregulation of G alpha q/11, phospholipase C beta 3 and extracellular signal-regulated kinase 1/2 via angiotensin II type 1 receptor. *Chinese medical journal* **2004,** *117* (1), 88-93.

50. Ali, F.; Guglin, M.; Vaitkevicius, P.; Ghali, J. K., Therapeutic potential of vasopressin receptor antagonists. *Drugs* **2007,** *67* (6), 847-58.

51. Okuyama, A.; Nonomura, N.; Nakamura, M.; Namiki, M.; Sonoda, T., Renin-angiotensin system. *Archives of andrology* **1988,** *21* (3), 169-80.

52. Wang, D.; Tan, Y. C.; Kreitzer, G. E.; Nakai, Y.; Shan, D.; Zheng, Y.; Huang, X. Y., G proteins G12 and G13 control the dynamic turnover of growth factor-induced dorsal ruffles. *J Biol Chem* **2006,** *281* (43), 32660-7.

53. Shan, D.; Chen, L.; Wang, D.; Tan, Y. C.; Gu, J. L.; Huang, X. Y., The G protein G alpha(13) is required for growth factor-induced cell migration. *Developmental cell* **2006,** *10* (6), 707-18.

54. De Vries, L.; Zheng, B.; Fischer, T.; Elenko, E.; Farquhar, M. G., The regulator of G protein signaling family. *Annu Rev Pharmacol Toxicol* **2000,** *40*, 235-71.

55. Hurst, J. H.; Hooks, S. B., Regulator of G-protein signaling (RGS) proteins in cancer biology. *Biochem Pharmacol* **2009,** *78* (10), 1289-97.

56. Zhang, P.; Mende, U., Regulators of G-protein signaling in the heart and their potential as therapeutic targets. *Circ Res* **2011,** *109* (3), 320-33.

57. Snow, B. E.; Krumins, A. M.; Brothers, G. M.; Lee, S. F.; Wall, M. A.; Chung, S.; Mangion, J.; Arya, S.; Gilman, A. G.; Siderovski, D. P., A G protein gamma subunit-like domain shared between RGS11 and other RGS proteins specifies binding to Gbeta5 subunits. *Proc Natl Acad Sci U S A* **1998,** *95* (22), 13307-12.

58. Ponting, C. P.; Bork, P., Pleckstrin's repeat performance: a novel domain in G-protein signaling? *Trends Biochem Sci* **1996,** *21* (7), 245-6.

59. Snow, B. E.; Betts, L.; Mangion, J.; Sondek, J.; Siderovski, D. P., Fidelity of G protein beta-subunit association by the G protein gamma-subunit-like domains of RGS6, RGS7, and RGS11. *Proc Natl Acad Sci U S A* **1999,** *96* (11), 6489-94.

60. Makino, E. R.; Handy, J. W.; Li, T.; Arshavsky, V. Y., The GTPase activating factor for transducin in rod photoreceptors is the complex between RGS9 and type 5 G protein beta subunit. *Proc Natl Acad Sci U S A* **1999,** *96* (5), 1947-52.

61. Levay, K.; Cabrera, J. L.; Satpaev, D. K.; Slepak, V. Z., Gbeta5 prevents the RGS7-Galphao interaction through binding to a distinct Ggamma-like domain found in RGS7 and other RGS proteins. *Proc Natl Acad Sci U S A* **1999,** *96* (5), 2503-7.

62. Hoffman, G. A.; Garrison, T. R.; Dohlman, H. G., Endoproteolytic processing of Sst2, a multidomain regulator of G protein signaling in yeast. *J Biol Chem* **2000,** *275* (48), 37533-41.

63. Snow, B. E.; Hall, R. A.; Krumins, A. M.; Brothers, G. M.; Bouchard, D.; Brothers, C. A.; Chung, S.; Mangion, J.; Gilman, A. G.; Lefkowitz, R. J.; Siderovski, D. P., GTPase activating specificity of RGS12 and binding specificity of an alternatively spliced PDZ (PSD-95/Dlg/ZO-1) domain. *J Biol Chem* **1998,** *273* (28), 17749-55.

64. Schiff, M. L.; Siderovski, D. P.; Jordan, J. D.; Brothers, G.; Snow, B.; De Vries, L.; Ortiz, D. F.; Diverse-Pierluissi, M., Tyrosine-kinase-dependent recruitment of RGS12 to the N-type calcium channel. *Nature* **2000,** *408* (6813), 723-7.

65. Ponting, C. P., Raf-like Ras/Rap-binding domains in RGS12- and still-life-like signalling proteins. *Journal of molecular medicine* **1999,** *77* (10), 695-8.

66. De Vries, L.; Elenko, E.; Hubler, L.; Jones, T. L.; Farquhar, M. G., GAIP is membrane-anchored by palmitoylation and interacts with the activated (GTP-bound) form of G alpha i subunits. *Proc Natl Acad Sci U S A* **1996,** *93* (26), 15203-8.

67. Glick, J. L.; Meigs, T. E.; Miron, A.; Casey, P. J., RGSZ1, a Gz-selective regulator of G protein signaling whose action is sensitive to the phosphorylation state of Gzalpha. *J Biol Chem* **1998,** *273* (40), 26008-13.

68. Jordan, J. D.; Carey, K. D.; Stork, P. J.; Iyengar, R., Modulation of rap activity by direct interaction of Galpha(o) with Rap1 GTPase-activating protein. *J Biol Chem* **1999,** *274* (31), 21507-10.

69. Barker, S. A.; Wang, J.; Sierra, D. A.; Ross, E. M., RGSZ1 and Ret RGS: two of several splice variants from the gene RGS20. *Genomics* **2001,** *78* (3), 223-9.

70. Nunn, C.; Mao, H.; Chidiac, P.; Albert, P. R., RGS17/RGSZ2 and the RZ/A family of regulators of G-protein signaling. *Semin Cell Dev Biol* **2006,** *17* (3), 390-9.

71. Mao, H.; Zhao, Q.; Daigle, M.; Ghahremani, M. H.; Chidiac, P.; Albert, P. R., RGS17/RGSZ2, a novel regulator of Gi/o, Gz, and Gq signaling. *J Biol Chem* **2004,** *279* (25), 26314-22.

72. James, M. A.; Lu, Y.; Liu, Y.; Vikis, H. G.; You, M., RGS17, an overexpressed gene in human lung and prostate cancer, induces tumor cell proliferation through the cyclic AMP-PKA-CREB pathway. *Cancer Res* **2009,** *69* (5), 2108-16.

73. You, M.; Wang, D.; Liu, P.; Vikis, H.; James, M.; Lu, Y.; Wang, Y.; Wang, M.; Chen, Q.; Jia, D.; Liu, Y.; Wen, W.; Yang, P.; Sun, Z.; Pinney, S. M.; Zheng, W.; Shu, X. O.; Long, J.; Gao, Y. T.; Xiang, Y. B.; Chow, W. H.; Rothman, N.; Petersen, G. M.; de Andrade, M.; Wu, Y.; Cunningham, J. M.; Wiest, J. S.; Fain, P. R.; Schwartz, A. G.; Girard, L.; Gazdar, A.; Gaba, C.; Rothschild, H.; Mandal, D.; Coons, T.; Lee, J.; Kupert, E.; Seminara, D.; Minna, J.; Bailey-Wilson, J. E.; Amos, C. I.; Anderson, M. W., Fine mapping of chromosome 6q23-25 region in familial lung cancer families reveals RGS17 as a likely candidate gene. *Clin Cancer Res* **2009,** *15* (8), 2666-74.

74. Feigin, M. E.; Malbon, C. C., RGS19 regulates Wnt-beta-catenin signaling through inactivation of Galpha(o). *Journal of cell science* **2007,** *120* (Pt 19), 3404-14.

75. Kirikoshi, H.; Katoh, M., Expression of human GIPC1 in normal tissues, cancer cell lines, and primary tumors. *Int J Mol Med* **2002,** *9* (5), 509-13.

76. Riker, A. I.; Enkemann, S. A.; Fodstad, O.; Liu, S.; Ren, S.; Morris, C.; Xi, Y.; Howell, P.; Metge, B.; Samant, R. S.; Shevde, L. A.; Li, W.; Eschrich, S.; Daud, A.; Ju, J.; Matta, J., The gene expression profiles of primary and metastatic melanoma yields a transition point of tumor progression and metastasis. *BMC Med Genomics* **2008,** *1*, 13.

77. Liu, C. J.; Liu, T. Y.; Kuo, L. T.; Cheng, H. W.; Chu, T. H.; Chang, K. W.; Lin, S. C., Differential gene expression signature between primary and metastatic head and neck squamous cell carcinoma. *The Journal of pathology* **2008,** *214* (4), 489-97.

78. Koga, H.; Imada, K.; Ueda, M.; Hishizawa, M.; Uchiyama, T., Identification of differentially expressed molecules in adult T-cell leukemia cells proliferating in vivo. *Cancer Sci* **2004,** *95* (5), 411-7.

79. Wong, Y. F.; Cheung, T. H.; Tsao, G. S.; Lo, K. W.; Yim, S. F.; Wang, V. W.; Heung, M. M.; Chan, S. C.; Chan, L. K.; Ho, T. W.; Wong, K. W.; Li, C.; Guo, Y.; Chung, T. K.; Smith, D. I., Genome-wide gene expression profiling of cervical cancer in Hong Kong women by oligonucleotide microarray. *Int J Cancer* **2006,** *118* (10), 2461-9.

80. Zhu, Y.; Hollmen, J.; Raty, R.; Aalto, Y.; Nagy, B.; Elonen, E.; Kere, J.; Mannila, H.; Franssila, K.; Knuutila, S., Investigatory and analytical approaches to differential gene expression profiling in mantle cell lymphoma. *British journal of haematology* **2002,** *119* (4), 905-15.

81. Smalley, M. J.; Iravani, M.; Leao, M.; Grigoriadis, A.; Kendrick, H.; Dexter, T.; Fenwick, K.; Regan, J. L.; Britt, K.; McDonald, S.; Lord, C. J.; Mackay, A.; Ashworth, A., Regulator of G-protein signalling 2 mRNA is differentially expressed in mammary epithelial subpopulations and over-expressed in the majority of breast cancers. *Breast Cancer Res* **2007,** *9* (6), R85.

82. Kannangai, R.; Vivekanandan, P.; Martinez-Murillo, F.; Choti, M.; Torbenson, M., Fibrolamellar carcinomas show overexpression of genes in the RAS, MAPK, PIK3, and xenobiotic degradation pathways. *Human pathology* **2007,** *38* (4), 639-44.

83. Cao, X.; Qin, J.; Xie, Y.; Khan, O.; Dowd, F.; Scofield, M.; Lin, M. F.; Tu, Y., Regulator of G-protein signaling 2 (RGS2) inhibits androgen-independent activation of androgen receptor in prostate cancer cells. *Oncogene* **2006,** *25* (26), 3719-34.

84. Schwable, J.; Choudhary, C.; Thiede, C.; Tickenbrock, L.; Sargin, B.; Steur, C.; Rehage, M.; Rudat, A.; Brandts, C.; Berdel, W. E.; Muller-Tidow, C.; Serve, H., RGS2 is an important target gene of Flt3-ITD mutations in AML and functions in myeloid differentiation and leukemic transformation. *Blood* **2005,** *105* (5), 2107-14.

85. Ooe, A.; Kato, K.; Noguchi, S., Possible involvement of CCT5, RGS3, and YKT6 genes up-regulated in p53-mutated tumors in resistance to docetaxel in human breast cancers. *Breast cancer research and treatment* **2007,** *101* (3), 305-15.

86. Tatenhorst, L.; Senner, V.; Puttmann, S.; Paulus, W., Regulators of G-protein signaling 3 and 4 (RGS3, RGS4) are associated with glioma cell motility. *Journal of neuropathology and experimental neurology* **2004,** *63* (3), 210-22.

87. Takahashi, H.; Nemoto, T.; Yoshida, T.; Honda, H.; Hasegawa, T., Cancer diagnosis marker extraction for soft tissue sarcomas based on gene expression profiling data by using projective adaptive resonance theory (PART) filtering method. *BMC Bioinformatics* **2006,** *7*, 399.

88. Nikolova, D. N.; Zembutsu, H.; Sechanov, T.; Vidinov, K.; Kee, L. S.; Ivanova, R.; Becheva, E.; Kocova, M.; Toncheva, D.; Nakamura, Y., Genome-wide gene expression profiles of thyroid carcinoma: Identification of molecular targets for treatment of thyroid carcinoma. *Oncology reports* **2008,** *20* (1), 105-21.

89. Chen, X.; Higgins, J.; Cheung, S. T.; Li, R.; Mason, V.; Montgomery, K.; Fan, S. T.; van de Rijn, M.; So, S., Novel endothelial cell markers in hepatocellular carcinoma. *Modern pathology : an official journal of the United States and Canadian Academy of Pathology, Inc* **2004,** *17* (10), 1198-210.

90. Boss, C. N.; Grunebach, F.; Brauer, K.; Hantschel, M.; Mirakaj, V.; Weinschenk, T.; Stevanovic, S.; Rammensee, H. G.; Brossart, P., Identification and characterization of T-cell epitopes deduced from RGS5, a novel broadly expressed tumor antigen. *Clin Cancer Res* **2007,** *13* (11), 3347-55.

91. Islam, T. C.; Asplund, A. C.; Lindvall, J. M.; Nygren, L.; Liden, J.; Kimby, E.; Christensson, B.; Smith, C. I.; Sander, B., High level of cannabinoid receptor 1, absence of regulator of G protein signalling 13 and differential expression of Cyclin D1 in mantle cell lymphoma. *Leukemia* **2003,** *17* (9), 1880-90.

92. Chng, W. J.; Remstein, E. D.; Fonseca, R.; Bergsagel, P. L.; Vrana, J. A.; Kurtin, P. J.; Dogan, A., Gene expression profiling of pulmonary mucosa-associated lymphoid tissue lymphoma identifies new biologic insights with potential diagnostic and therapeutic applications. *Blood* **2009,** *113* (3), 635-45.

93. Davidsson, J.; Andersson, A.; Paulsson, K.; Heidenblad, M.; Isaksson, M.; Borg, A.; Heldrup, J.; Behrendtz, M.; Panagopoulos, I.; Fioretos, T.; Johansson, B., Tiling resolution array comparative genomic hybridization, expression and methylation analyses of dup(1q) in Burkitt lymphomas and pediatric high hyperdiploid acute lymphoblastic leukemias reveal clustered near-centromeric breakpoints and overexpression of genes in 1q22-32.3. *Hum Mol Genet* **2007,** *16* (18), 2215-25.

94. Fevre-Montange, M.; Champier, J.; Szathmari, A.; Wierinckx, A.; Mottolese, C.; Guyotat, J.; Figarella-Branger, D.; Jouvet, A.; Lachuer, J., Microarray analysis reveals differential gene expression patterns in tumors of the pineal region. *Journal of neuropathology and experimental neurology* **2006,** *65* (7), 675-84.

95. Buckbinder, L.; Velasco-Miguel, S.; Chen, Y.; Xu, N.; Talbott, R.; Gelbert, L.; Gao, J.; Seizinger, B. R.; Gutkind, J. S.; Kley, N., The p53 tumor suppressor targets a novel regulator of G protein signaling. *Proc Natl Acad Sci U S A* **1997,** *94* (15), 7868-72.

96. Berman, D. M.; Wang, Y.; Liu, Z.; Dong, Q.; Burke, L. A.; Liotta, L. A.; Fisher, R.; Wu, X., A functional polymorphism in RGS6 modulates the risk of bladder cancer. *Cancer Res* **2004,** *64* (18), 6820-6.

97. Martinez-Cardus, A.; Martinez-Balibrea, E.; Bandres, E.; Malumbres, R.; Gines, A.; Manzano, J. L.; Taron, M.; Garcia-Foncillas, J.; Abad, A., Pharmacogenomic approach for the identification of novel determinants of acquired resistance to oxaliplatin in colorectal cancer. *Mol Cancer Ther* **2009,** *8* (1), 194-202.

98. Pan, K. F.; Liu, W. G.; Zhang, L.; You, W. C.; Lu, Y. Y., Mutations in components of the Wnt signaling pathway in gastric cancer. *World journal of gastroenterology : WJG* **2008,** *14* (10), 1570-4.

99. Ishizaki, Y.; Ikeda, S.; Fujimori, M.; Shimizu, Y.; Kurihara, T.; Itamoto, T.; Kikuchi, A.; Okajima, M.; Asahara, T., Immunohistochemical analysis and mutational analyses of beta-catenin, Axin family and APC genes in hepatocellular carcinomas. *Int J Oncol* **2004,** *24* (5), 1077-83.

100. Tokumoto, N.; Ikeda, S.; Ishizaki, Y.; Kurihara, T.; Ozaki, S.; Iseki, M.; Shimizu, Y.; Itamoto, T.; Arihiro, K.; Okajima, M.; Asahara, T., Immunohistochemical and mutational analyses of Wnt signaling components and target genes in intrahepatic cholangiocarcinomas. *Int J Oncol* **2005,** *27* (4), 973-80.

101. Daa, T.; Kashima, K.; Kaku, N.; Suzuki, M.; Yokoyama, S., Mutations in components of the Wnt signaling pathway in adenoid cystic carcinoma. *Modern pathology : an official journal of the United States and Canadian Academy of Pathology, Inc* **2004,** *17* (12), 1475-82.

102. Baeza, N.; Masuoka, J.; Kleihues, P.; Ohgaki, H., AXIN1 mutations but not deletions in cerebellar medulloblastomas. *Oncogene* **2003,** *22* (4), 632-6.

103. Iwai, S.; Katagiri, W.; Kong, C.; Amekawa, S.; Nakazawa, M.; Yura, Y., Mutations of the APC, beta-catenin, and axin 1 genes and cytoplasmic accumulation of beta-catenin in oral squamous cell carcinoma. *Journal of cancer research and clinical oncology* **2005,** *131* (12), 773-82.

104. Jin, L. H.; Shao, Q. J.; Luo, W.; Ye, Z. Y.; Li, Q.; Lin, S. C., Detection of point mutations of the Axin1 gene in colorectal cancers. *Int J Cancer* **2003,** *107* (5), 696-9.

105. Pospisil, H.; Herrmann, A.; Butherus, K.; Pirson, S.; Reich, J. G.; Kemmner, W., Verification of predicted alternatively spliced Wnt genes reveals two new splice variants (CTNNB1 and LRP5) and altered Axin-1 expression during tumour progression. *BMC genomics* **2006,** *7*, 148.

106. Xu, H. T.; Wang, L.; Lin, D.; Liu, Y.; Liu, N.; Yuan, X. M.; Wang, E. H., Abnormal beta-catenin and reduced axin expression are associated with poor differentiation and progression in non-small cell lung cancer. *American journal of clinical pathology* **2006,** *125* (4), 534-41.

107. Steg, A.; Wang, W.; Blanquicett, C.; Grunda, J. M.; Eltoum, I. A.; Wang, K.; Buchsbaum, D. J.; Vickers, S. M.; Russo, S.; Diasio, R. B.; Frost, A. R.; LoBuglio, A. F.; Grizzle, W. E.; Johnson, M. R., Multiple gene expression analyses in paraffin-embedded tissues by TaqMan low-density array: Application to hedgehog and Wnt pathway analysis in ovarian endometrioid adenocarcinoma. *The Journal of molecular diagnostics : JMD* **2006,** *8* (1), 76-83.

108. Roh, M. S.; Hong, S. H.; Jeong, J. S.; Kwon, H. C.; Kim, M. C.; Cho, S. H.; Yoon, J. H.; Hwang, T. H., Gene expression profiling of breast cancers with emphasis of beta-catenin regulation. *Journal of Korean medical science* **2004,** *19* (2), 275-82.

109. Dahmen, R. P.; Koch, A.; Denkhaus, D.; Tonn, J. C.; Sorensen, N.; Berthold, F.; Behrens, J.; Birchmeier, W.; Wiestler, O. D.; Pietsch, T., Deletions of AXIN1, a component of the WNT/wingless pathway, in sporadic medulloblastomas. *Cancer Res* **2001,** *61* (19), 7039-43.

110. Siegel, R.; Ma, J.; Zou, Z.; Jemal, A., Cancer statistics, 2014. *CA Cancer J Clin* **2014,** *64* (1), 9-29.

111. Mackie, D. I.; Roman, D. L., Development of a novel high-throughput screen and identification of small-molecule inhibitors of the Galpha-RGS17 protein-protein interaction using AlphaScreen. *J Biomol Screen* **2011,** *16* (8), 869-77.

112. Ross, E. M.; Wilkie, T. M., GTPase-activating proteins for heterotrimeric G proteins: regulators of G protein signaling (RGS) and RGS-like proteins. *Annu Rev Biochem* **2000,** *69*, 795-827.

113. McCoy, K. L.; Hepler, J. R., Chapter 3 regulators of g protein signaling proteins as central components of g protein-coupled receptor signaling complexes. *Prog Mol Biol Transl Sci* **2009,** *86*, 49-74.

114. Larminie, C.; Murdock, P.; Walhin, J. P.; Duckworth, M.; Blumer, K. J.; Scheideler, M. A.; Garnier, M., Selective expression of regulators of G-protein signaling (RGS) in the human central nervous system. *Brain Res Mol Brain Res* **2004,** *122* (1), 24-34.

115. Technikova-Dobrova, Z.; Sardanelli, A. M.; Speranza, F.; Scacco, S.; Signorile, A.; Lorusso, V.; Papa, S., Cyclic adenosine monophosphate-dependent phosphorylation of mammalian mitochondrial proteins: enzyme and substrate characterization and functional role. *Biochemistry* **2001,** *40* (46), 13941-7.

116. Kim, C.; Vigil, D.; Anand, G.; Taylor, S. S., Structure and dynamics of PKA signaling proteins. *Eur J Cell Biol* **2006,** *85* (7), 651-4.

117. Taylor, S. S.; Kim, C.; Vigil, D.; Haste, N. M.; Yang, J.; Wu, J.; Anand, G. S., Dynamics of signaling by PKA. *Biochim Biophys Acta* **2005,** *1754* (1-2), 25-37.

118. Shaywitz, A. J.; Greenberg, M. E., CREB: a stimulus-induced transcription factor activated by a diverse array of extracellular signals. *Annu Rev Biochem* **1999,** *68*, 821-61.

119. Mayr, B.; Montminy, M., Transcriptional regulation by the phosphorylation-dependent factor CREB. *Nat Rev Mol Cell Biol* **2001,** *2* (8), 599-609.

120. Lonze, B. E.; Ginty, D. D., Function and regulation of CREB family transcription factors in the nervous system. *Neuron* **2002,** *35* (4), 605-23.

121. Choi, Y. J.; Kim, S. Y.; Oh, J. M.; Juhnn, Y. S., Stimulatory heterotrimeric G protein augments gamma ray-induced apoptosis by up-regulation of Bak expression via CREB and AP-1 in H1299 human lung cancer cells. *Exp Mol Med* **2009,** *41* (8), 592-600.

122. Rosenberg, D.; Groussin, L.; Jullian, E.; Perlemoine, K.; Bertagna, X.; Bertherat, J., Role of the PKA-regulated transcription factor CREB in development and tumorigenesis of endocrine tissues. *Ann N Y Acad Sci* **2002,** *968*, 65-74.

123. Cekanova, M.; Majidy, M.; Masi, T.; Al-Wadei, H. A.; Schuller, H. M., Overexpressed Raf-1 and phosphorylated cyclic adenosine 3'-5'-monophosphatate response element-binding protein are early markers for lung adenocarcinoma. *Cancer* **2007,** *109* (6), 1164-73.

124. Uehara, Y.; Mochizuki, M.; Matsuno, K.; Haino, T.; Asai, A., Novel high-throughput screening system for identifying STAT3-SH2 antagonists. *Biochem Biophys Res Commun* **2009,** *380* (3), 627-31.

125. Yi, F.; Zhu, P.; Southall, N.; Inglese, J.; Austin, C. P.; Zheng, W.; Regan, L., An AlphaScreen-based high-throughput screen to identify inhibitors of Hsp90-cochaperone interaction. *J Biomol Screen* **2009,** *14* (3), 273-81.

126. Roman, D. L.; Ota, S.; Neubig, R. R., Polyplexed flow cytometry protein interaction assay: a novel high-throughput screening paradigm for RGS protein inhibitors. *J Biomol Screen* **2009,** *14* (6), 610-9.

127. Roman, D. L.; Talbot, J. N.; Roof, R. A.; Sunahara, R. K.; Traynor, J. R.; Neubig, R. R., Identification of small-molecule inhibitors of RGS4 using a high-throughput flow cytometry protein interaction assay. *Mol Pharmacol* **2007,** *71* (1), 169-75.

128. Roof, R. A.; Sobczyk-Kojiro, K.; Turbiak, A. J.; Roman, D. L.; Pogozheva, I. D.; Blazer, L. L.; Neubig, R. R.; Mosberg, H. I., Novel peptide ligands of RGS4 from a focused one-bead, one-compound library. *Chem Biol Drug Des* **2008,** *72* (2), 111-9.

129. Lee, E.; Linder, M. E.; Gilman, A. G., Expression of G-protein alpha subunits in Escherichia coli. *Methods Enzymol* **1994,** *237*, 146-64.

130. Phillips, K.; de la Pena, A. H., The combined use of the Thermofluor assay and ThermoQ analytical software for the determination of protein stability and buffer optimization as an aid in protein crystallization. *Current protocols in molecular biology / edited by Frederick M. Ausubel ... [et al.]* **2011,** *Chapter 10*, Unit10 28.

131. Zhang, J. H.; Chung, T. D.; Oldenburg, K. R., A Simple Statistical Parameter for Use in Evaluation and Validation of High Throughput Screening Assays. *J Biomol Screen* **1999,** *4* (2), 67-73.

132. Neubig, R. R., Regulators of G protein signaling (RGS proteins): novel central nervous system drug targets. *J Pept Res* **2002,** *60* (6), 312-6.

133. Neubig, R. R.; Siderovski, D. P., Regulators of G-protein signalling as new central nervous system drug targets. *Nat Rev Drug Discov* **2002,** *1* (3), 187-97.

134. Sjogren, B.; Neubig, R. R., Thinking outside of the "RGS box": new approaches to therapeutic targeting of regulators of G protein signaling. *Mol Pharmacol* **2010,** *78* (4), 550-7.

135. Young, K. H.; Wang, Y.; Bender, C.; Ajit, S.; Ramirez, F.; Gilbert, A.; Nieuwenhuijsen, B. W., Yeast-based screening for inhibitors of RGS proteins. *Methods Enzymol* **2004,** *389*, 277-301.

136. Sternweis, P. C.; Northup, J. K.; Smigel, M. D.; Gilman, A. G., The regulatory component of adenylate cyclase. Purification and properties. *J Biol Chem* **1981,** *256* (22), 11517-26.

137. Blazer, L. L.; Roman, D. L.; Chung, A.; Larsen, M. J.; Greedy, B. M.; Husbands, S. M.; Neubig, R. R., Reversible, allosteric small-molecule inhibitors of regulator of G protein signaling proteins. *Mol Pharmacol* **2010,** *78* (3), 524-33.

138. Shoichet, B. K., Screening in a spirit haunted world. *Drug Discov Today* **2006,** *11* (13-14), 607-15.

139. Bolton, J. L.; Trush, M. A.; Penning, T. M.; Dryhurst, G.; Monks, T. J., Role of quinones in toxicology. *Chemical research in toxicology* **2000,** *13* (3), 135-60.

140. Wei, Y.; Lin, Y.; Zhang, A. Q.; Guo, L. H.; Cao, J., Evaluation of the noncovalent binding interactions between polycyclic aromatic hydrocarbon metabolites and human p53 cDNA. *The Science of the total environment* **2010,** *408* (24), 6285-90.

141. Lynn, J. M., Sulfonamide toxicity. *California medicine* **1949,** *70* (1), 48-56.

142. Monroy, C. A.; Mackie, D. I.; Roman, D. L., A high throughput screen for RGS proteins using steady state monitoring of free phosphate formation. *PLoS One* **2013,** *8* (4), e62247.

143. Higashijima, T.; Ferguson, K. M.; Sternweis, P. C.; Smigel, M. D.; Gilman, A. G., Effects of Mg2+ and the beta gamma-subunit complex on the interactions of guanine nucleotides with G proteins. *J Biol Chem* **1987,** *262* (2), 762-6.

144. Eeles, R. A.; Olama, A. A.; Benlloch, S.; Saunders, E. J.; Leongamornlert, D. A.; Tymrakiewicz, M.; Ghoussaini, M.; Luccarini, C.; Dennis, J.; Jugurnauth-Little, S.; Dadaev, T.; Neal, D. E.; Hamdy, F. C.; Donovan, J. L.; Muir, K.; Giles, G. G.; Severi, G.; Wiklund, F.; Gronberg, H.; Haiman, C. A.; Schumacher, F.; Henderson, B. E.; Le Marchand, L.; Lindstrom, S.; Kraft, P.; Hunter, D. J.; Gapstur, S.; Chanock, S. J.; Berndt, S. I.; Albanes, D.; Andriole, G.; Schleutker, J.; Weischer, M.; Canzian, F.; Riboli, E.; Key, T. J.; Travis, R. C.; Campa, D.; Ingles, S. A.; John, E. M.; Hayes, R. B.; Pharoah, P. D.; Pashayan, N.; Khaw, K. T.; Stanford, J. L.; Ostrander, E. A.; Signorello, L. B.; Thibodeau, S. N.; Schaid, D.; Maier, C.; Vogel, W.; Kibel, A. S.; Cybulski, C.; Lubinski, J.; Cannon-Albright, L.; Brenner, H.; Park, J. Y.; Kaneva, R.; Batra, J.; Spurdle, A. B.; Clements, J. A.; Teixeira, M. R.; Dicks, E.; Lee, A.; Dunning, A. M.; Baynes, C.; Conroy, D.; Maranian, M. J.; Ahmed, S.; Govindasami, K.; Guy, M.; Wilkinson, R. A.; Sawyer, E. J.; Morgan, A.; Dearnaley, D. P.; Horwich, A.; Huddart, R. A.; Khoo, V. S.; Parker, C. C.; Van As, N. J.; Woodhouse, C. J.; Thompson, A.; Dudderidge, T.; Ogden, C.; Cooper, C. S.; Lophatananon, A.; Cox, A.; Southey, M. C.; Hopper, J. L.; English, D. R.; Aly, M.; Adolfsson, J.; Xu, J.; Zheng, S. L.; Yeager, M.; Kaaks, R.; Diver, W. R.; Gaudet, M. M.; Stern, M. C.; Corral, R.; Joshi, A. D.; Shahabi, A.; Wahlfors, T.; Tammela, T. L.; Auvinen, A.; Virtamo, J.; Klarskov, P.; Nordestgaard, B. G.; Roder, M.

A.; Nielsen, S. F.; Bojesen, S. E.; Siddiq, A.; Fitzgerald, L. M.; Kolb, S.; Kwon, E. M.; Karyadi, D. M.; Blot, W. J.; Zheng, W.; Cai, Q.; McDonnell, S. K.; Rinckleb, A. E.; Drake, B.; Colditz, G.; Wokolorczyk, D.; Stephenson, R. A.; Teerlink, C.; Muller, H.; Rothenbacher, D.; Sellers, T. A.; Lin, H. Y.; Slavov, C.; Mitev, V.; Lose, F.; Srinivasan, S.; Maia, S.; Paulo, P.; Lange, E.; Cooney, K. A.; Antoniou, A. C.; Vincent, D.; Bacot, F.; Tessier, D. C.; Initiative, C. O.-C. R. U. G.-E.; Australian Prostate Cancer, B.; Oncology, U. K. G. P. C. S. C. B. A. o. U. S. S. o.; Collaborators, U. K. P. S.; Consortium, P.; Kote-Jarai, Z.; Easton, D. F., Identification of 23 new prostate cancer susceptibility loci using the iCOGS custom genotyping array. *Nat Genet* **2013,** *45* (4), 385-91, 391e1-2.

145. Lavinder, J. J.; Hari, S. B.; Sullivan, B. J.; Magliery, T. J., High-throughput thermal scanning: a general, rapid dye-binding thermal shift screen for protein engineering. *J Am Chem Soc* **2009,** *131* (11), 3794-5.

146. Blazer, L. L.; Zhang, H.; Casey, E. M.; Husbands, S. M.; Neubig, R. R., A nanomolar-potency small molecule inhibitor of regulator of G-protein signaling proteins. *Biochemistry* **2011,** *50* (15), 3181-92.

147. Traynor, J. R.; Terzi, D.; Caldarone, B. J.; Zachariou, V., RGS9-2: probing an intracellular modulator of behavior as a drug target. *Trends Pharmacol Sci* **2009,** *30* (3), 105-11.

148. Blazer, L. L.; Neubig, R. R., Small molecule protein-protein interaction inhibitors as CNS therapeutic agents: current progress and future hurdles. *Neuropsychopharmacology* **2009,** *34* (1), 126-41.

149. Garzon, J.; Rodriguez-Munoz, M.; Lopez-Fando, A.; Sanchez-Blazquez, P., The RGSZ2 protein exists in a complex with mu-opioid receptors and regulates the desensitizing capacity of Gz proteins. *Neuropsychopharmacology* **2005,** *30* (9), 1632-48.

150. Fox, S. B.; Brown, P.; Han, C.; Ashe, S.; Leek, R. D.; Harris, A. L.; Banham, A. H., Expression of the forkhead transcription factor FOXP1 is associated with estrogen receptor alpha and improved survival in primary human breast carcinomas. *Clin Cancer Res* **2004,** *10* (10), 3521-7.

151. Taylor, B. S.; Schultz, N.; Hieronymus, H.; Gopalan, A.; Xiao, Y.; Carver, B. S.; Arora, V. K.; Kaushik, P.; Cerami, E.; Reva, B.; Antipin, Y.; Mitsiades, N.; Landers, T.; Dolgalev, I.; Major, J. E.; Wilson, M.; Socci, N. D.; Lash, A. E.; Heguy, A.; Eastham, J. A.; Scher, H. I.; Reuter, V. E.; Scardino, P. T.; Sander, C.; Sawyers, C. L.; Gerald, W. L., Integrative genomic profiling of human prostate cancer. *Cancer cell* **2010,** *18* (1), 11-22.

152. Teufel, A.; Wong, E. A.; Mukhopadhyay, M.; Malik, N.; Westphal, H., FoxP4, a novel forkhead transcription factor. *Biochim Biophys Acta* **2003,** *1627* (2-3), 147-52.

153. Campbell, A. J.; Lyne, L.; Brown, P. J.; Launchbury, R. J.; Bignone, P.; Chi, J.; Roncador, G.; Lawrie, C. H.; Gatter, K. C.; Kusec, R.; Banham, A. H., Aberrant expression of the neuronal transcription factor FOXP2 in neoplastic plasma cells. *British journal of haematology* **2010,** *149* (2), 221-30.

154. Stumm, L.; Burkhardt, L.; Steurer, S.; Simon, R.; Adam, M.; Becker, A.; Sauter, G.; Minner, S.; Schlomm, T.; Sirma, H.; Michl, U., Strong expression of the neuronal transcription factor FOXP2 is linked to an increased risk of early PSA recurrence in ERG fusion-negative cancers. *Journal of clinical pathology* **2013,** *66* (7), 563-8.

155. Drobnjak, M.; Osman, I.; Scher, H. I.; Fazzari, M.; Cordon-Cardo, C., Overexpression of cyclin D1 is associated with metastatic prostate cancer to bone. *Clin Cancer Res* **2000,** *6* (5), 1891-5.

156. Gautschi, O.; Ratschiller, D.; Gugger, M.; Betticher, D. C.; Heighway, J., Cyclin D1 in non-small cell lung cancer: a key driver of malignant transformation. *Lung cancer* **2007,** *55* (1), 1-14.

157. Santarius, T.; Shipley, J.; Brewer, D.; Stratton, M. R.; Cooper, C. S., A census of amplified and overexpressed human cancer genes. *Nat Rev Cancer* **2010,** *10* (1), 59-64.

158. Li, R.; An, S. J.; Chen, Z. H.; Zhang, G. C.; Zhu, J. Q.; Nie, Q.; Xie, Z.; Guo, A. L.; Mok, T. S.; Wu, Y. L., Expression of cyclin D1 splice variants is differentially associated with outcome in non-small cell lung cancer patients. *Human pathology* **2008,** *39* (12), 1792-801.

159. Agus, D. B.; Cordon-Cardo, C.; Fox, W.; Drobnjak, M.; Koff, A.; Golde, D. W.; Scher, H. I., Prostate cancer cell cycle regulators: response to androgen withdrawal and development of androgen independence. *Journal of the National Cancer Institute* **1999,** *91* (21), 1869-76.

160. Li, R.; Wang, H.; Bekele, B. N.; Yin, Z.; Caraway, N. P.; Katz, R. L.; Stass, S. A.; Jiang, F., Identification of putative oncogenes in lung adenocarcinoma by a comprehensive functional genomic approach. *Oncogene* **2006,** *25* (18), 2628-35.

161. Fu, Z.; Tindall, D. J., FOXOs, cancer and regulation of apoptosis. *Oncogene* **2008,** *27* (16), 2312-9.

162. Su, B.; Gao, L.; Baranowski, C.; Gillard, B.; Wang, J.; Ransom, R.; Ko, H. K.; Gelman, I. H., A Genome-Wide RNAi Screen Identifies FOXO4 as a Metastasis-Suppressor through Counteracting PI3K/AKT Signal Pathway in Prostate Cancer. *PLoS One* **2014,** *9* (7), e101411.

163. Xu, M. M.; Mao, G. X.; Liu, J.; Li, J. C.; Huang, H.; Liu, Y. F.; Liu, J. H., Low expression of the FoxO4 gene may contribute to the phenomenon of EMT in non-small cell lung cancer. *Asian Pacific journal of cancer prevention : APJCP* **2014,** *15* (9), 4013-8.

164. Dai, Y.; Desano, J.; Tang, W.; Meng, X.; Meng, Y.; Burstein, E.; Lawrence, T. S.; Xu, L., Natural proteasome inhibitor celastrol suppresses androgen-independent prostate cancer progression by modulating apoptotic proteins and NF-kappaB. *PLoS One* **2010,** *5* (12), e14153.

165. Ryu, Y. B.; Park, S. J.; Kim, Y. M.; Lee, J. Y.; Seo, W. D.; Chang, J. S.; Park, K. H.; Rho, M. C.; Lee, W. S., SARS-CoV 3CLpro inhibitory effects of quinone-methide triterpenes from Tripterygium regelii. *Bioorg Med Chem Lett* **2010,** *20* (6), 1873-6.

166. Zhu, H.; Liu, X. W.; Cai, T. Y.; Cao, J.; Tu, C. X.; Lu, W.; He, Q. J.; Yang, B., Celastrol acts as a potent antimetastatic agent targeting beta1 integrin and inhibiting cell-extracellular matrix adhesion, in part via the p38 mitogen-activated protein kinase pathway. *J Pharmacol Exp Ther* **2010,** *334* (2), 489-99.

167. Yang, H. S.; Kim, J. Y.; Lee, J. H.; Lee, B. W.; Park, K. H.; Shim, K. H.; Lee, M. K.; Seo, K. I., Celastrol isolated from Tripterygium regelii induces apoptosis through both caspase-dependent and -independent pathways in human breast cancer cells. *Food and chemical toxicology : an international journal published for the British Industrial Biological Research Association* **2011,** *49* (2), 527-32.

168. Lee, J. H.; Choi, K. J.; Seo, W. D.; Jang, S. Y.; Kim, M.; Lee, B. W.; Kim, J. Y.; Kang, S.; Park, K. H.; Lee, Y. S.; Bae, S., Enhancement of radiation sensitivity in lung cancer cells by celastrol is mediated by inhibition of Hsp90. *Int J Mol Med* **2011,** *27* (3), 441-6.

169. Barlow, C. A.; Kitiphongspattana, K.; Siddiqui, N.; Roe, M. W.; Mossman, B. T.; Lounsbury, K. M., Protein kinase A-mediated CREB phosphorylation is an oxidant-induced survival pathway in alveolar type II cells. *Apoptosis : an international journal on programmed cell death* **2008,** *13* (5), 681-92.

170. Schie, I. W.; Huser, T., Label-free analysis of cellular biochemistry by Raman spectroscopy and microscopy. *Comprehensive Physiology* **2013,** *3* (2), 941-56.

171. Hart, C. P., Finding the target after screening the phenotype. *Drug Discov Today* **2005,** *10* (7), 513-9.

172. Swinney, D. C.; Anthony, J., How were new medicines discovered? *Nat Rev Drug Discov* **2011,** *10* (7), 507-19.

173. Fang, Y.; Ferrie, A. M.; Fontaine, N. H.; Mauro, J.; Balakrishnan, J., Resonant waveguide grating biosensor for living cell sensing. *Biophys J* **2006,** *91* (5), 1925-40.

174. Blake, R. A., Cellular screening assays using fluorescence microscopy. *Curr Opin Pharmacol* **2001,** *1* (5), 533-9.

175. Abraham, V. C.; Taylor, D. L.; Haskins, J. R., High content screening applied to large-scale cell biology. *Trends Biotechnol* **2004,** *22* (1), 15-22.

176. Rocheville, M.; Martin, J.; Jerman, J.; Kostenis, E., Mining the potential of label-free biosensors for seven-transmembrane receptor drug discovery. *Prog Mol Biol Transl Sci* **2013,** *115*, 123-42.

177. Xi, B.; Yu, N.; Wang, X.; Xu, X.; Abassi, Y. A., The application of cell-based label-free technology in drug discovery. *Biotechnology journal* **2008,** *3* (4), 484-95.

178. Fang, Y., Label-free drug discovery. *Frontiers in pharmacology* **2014,** *5*, 52.

179. Fang, Y.; Li, G.; Ferrie, A. M., Non-invasive optical biosensor for assaying endogenous G protein-coupled receptors in adherent cells. *Journal of pharmacological and toxicological methods* **2007,** *55* (3), 314-22.

180. Zilbershtein, A.; Bein, A.; Lirtsman, V.; Schwartz, B.; Golosovsky, M.; Davidov, D., Surface plasmon resonance-based infrared biosensor for cell studies with simultaneous control. *Journal of biomedical optics* **2014,** *19* (11), 111608.

181. Leatherbarrow, R. J.; Edwards, P. R., Analysis of molecular recognition using optical biosensors. *Curr Opin Chem Biol* **1999,** *3* (5), 544-7.

182. Cooper, M. A., Optical biosensors in drug discovery. *Nat Rev Drug Discov* **2002,** *1* (7), 515-28.

183. Fang, Y., Label-Free Receptor Assays. *Drug discovery today. Technologies* **2011,** *7* (1), e5-e11.

184. Fang, Y.; Ferrie, A. M., Label-free optical biosensor for ligand-directed functional selectivity acting on beta(2) adrenoceptor in living cells. *FEBS Lett* **2008,** *582* (5), 558-64.

185. Fang, Y.; Ferrie, A. M.; Fontaine, N. H.; Yuen, P. K., Characteristics of dynamic mass redistribution of epidermal growth factor receptor signaling in living cells measured with label-free optical biosensors. *Anal Chem* **2005,** *77* (17), 5720-5.

186. Benians, A.; Nobles, M.; Tinker, A., Participation of RGS8 in the ternary complex of agonist, receptor and G-protein. *Biochemical Society transactions* **2004,** *32* (Pt 6), 1045-7.

187. Parra, S.; Huang, X.; Charbeneau, R. A.; Wade, S. M.; Kaur, K.; Rorabaugh, B. R.; Neubig, R. R., Conditional disruption of interactions between Galphai2 and regulator of G protein signaling (RGS) proteins protects the heart from ischemic injury. *BMC pharmacology & toxicology* **2014,** *15*, 29.

188. Neubig, R. R., And the winner is ... RGS4! *Circ Res* **2008,** *103* (5), 444-6.

189. Soundararajan, M.; Willard, F. S.; Kimple, A. J.; Turnbull, A. P.; Ball, L. J.; Schoch, G. A.; Gileadi, C.; Fedorov, O. Y.; Dowler, E. F.; Higman, V. A.; Hutsell, S. Q.; Sundstrom, M.; Doyle, D. A.; Siderovski, D. P., Structural diversity in the RGS domain and its interaction with heterotrimeric G protein alpha-subunits. *Proc Natl Acad Sci U S A* **2008,** *105* (17), 6457-62.

190. Jaen, C.; Doupnik, C. A., RGS3 and RGS4 differentially associate with G protein-coupled receptor-Kir3 channel signaling complexes revealing two modes of RGS modulation. Precoupling and collision coupling. *J Biol Chem* **2006,** *281* (45), 34549-60.

191. Garzon, J.; Rodriguez-Munoz, M.; Vicente-Sanchez, A.; Garcia-Lopez, M. A.; Martinez-Murillo, R.; Fischer, T.; Sanchez-Blazquez, P., SUMO-SIM interactions regulate the activity of RGSZ2 proteins. *PLoS One* **2011,** *6* (12), e28557.

192. Rodriguez-Munoz, M.; Bermudez, D.; Sanchez-Blazquez, P.; Garzon, J., Sumoylated RGS-Rz proteins act as scaffolds for Mu-opioid receptors and G-protein complexes in mouse brain. *Neuropsychopharmacology* **2007,** *32* (4), 842-50.

193. Drews, J., Drug discovery: a historical perspective. *Science* **2000,** *287* (5460), 1960-4.

194. Ma, H.; Horiuchi, K. Y., Chemical microarray: a new tool for drug screening and discovery. *Drug Discov Today* **2006,** *11* (13-14), 661-8.

195. Henrich, C. J.; Beutler, J. A., Matching the power of high throughput screening to the chemical diversity of natural products. *Natural product reports* **2013,** *30* (10), 1284-98.

196. Mayr, L. M.; Fuerst, P., The future of high-throughput screening. *J Biomol Screen* **2008,** *13* (6), 443-8.